EXPERIMENTAL STUDY

OF THE

PHASE TRANSITION

IN

KD_2PO_4

GEORGE LANGE PAUL

Ph. D.

University of Edinburgh

July, 1969

Acknowledgements

The author is most grateful for the help extended to him during his candidature for the degree. The work was undertaken during the tenure of a Royal Society Rutherford Scholarship, the extremely generous support of which is acknowledged. The support of the Science Research Council for the experimental work is also acknowledged. Thanks are due to Atomic Energy of Canada Limited and the Atomic Energy Authority for permission to work at their establishments. Personal thanks are also extended by the author to the many people without whose assistance the work could not have been completed:

Professor W. Cochran for his supervision, enthusiasm and considerable assistance,

Dr. R.A. Cowley and others at A.E.C.L. for their interest, help and technical assistance,

Many friends in Edinburgh for most rewarding discussions and their help with problems,

His wife for everything and their child for being dormant.

Abstract

The ferroelectric phase transition in KD_2PO_4 has been studied using coherent neutron inelastic scattering. The low frequency phonon dispersion relations were determined in the two principal symmetry directions. The results were fitted to a central force rigid ion model which gave good agreement with the acoustic branches and the lowest frequency optic branches. Group theory was used to simplify all calculations. None of the phonon modes was temperature dependent and therefore the ferroelectric transition was not caused by a soft mode. Quasi-elastic critical scattering was observed, the intensity of which increased as the transition temperature was approached. The scattering extended throughout each Brillouin zone and was peaked at reciprocal lattice points. The variation of the intensity in the scattering plane showed that the displacements of the atoms in the ferroelectric fluctuations were similar to those relating the paraelectric and ferroelectric phases. The distribution of the intensity around each reciprocal lattice point showed the effect of the macroscopic field associated with the ferroelectric fluctuations. A simple Ising model with next nearest neighbour and Coulomb interactions described the results well. A microscopic model for KDP type crystals is proposed. The model neglects all dynamic effects, describes the experimental results and shows that the interaction of the phonons with the ferroelectric fluctuations is of more importance

than previously thought. The model also predicts the shape of ferroelectric critical scattering in other ferroelectric and antiferroelectric KDP type crystals.

Table of Contents

Experimental Study of the Phase Transition in KD_2PO_4

1. Introduction

A ferroelectric transition is one of the phase transitions which may occur in crystals. It is a transition in which a high temperature paraelectric phase, having no electric polarisation, becomes, at lower temperatures, a ferroelectric phase, exhibiting a reversible spontaneous polarisation. The temperature at which the transition occurs is called the Curie temperature.

Ferroelectric crystals are divided into the two types, displacive and order-disorder. The former class is characterised by small displacements. That is to say, the difference between the crystal structure of the two phases may be described by small displacements of some or all of the atoms. Order-disorder ferroelectrics are characterised by large displacements of atoms or molecules. In displacive ferroelectrics it is believed that the energy of a particular normal mode of vibration in the paraelectric phase approaches zero as a function of temperature (Cochran, 1960). There is an unstable, or soft, normal mode called in this case a ferroelectric mode. In order-disorder ferroelectrics the atoms or molecules become ordered below the transition temperature on only one of the high temperature equilibrium sites. It has been found that the formalism of the Ising model is suitable for describing these ferroelectrics (Yamada and Yamada, 1967).

Crystals of potassium dihydrogen phosphate KH_2PO_4 (abbreviated

KDP) and some isomorphous crystals become ferroelectric. They display the characteristics of both displacive and order-disorder types, small displacements of the potassium and phosphorus atoms along the ferroelectric axis and large displacements of the protons between the two possible sites along a line almost perpendicular to the ferroelectric axis (Bacon and Pease, 1953, 1955). Crystals of the isomorphous $NH_4H_2PO_4$(ADP) are however antiferroelectric. The crystal structure below the transition temperature has not been determined.

The early theories of the phase-transition and the properties of KDP type crystals have been adequately reviewed by Megaw (1957) and Jona and Shirane (1962). Some of the theoretical and recent experimental work on these crystals which is of interest in introducing the present research will be mentioned here.

Paraelectric KDP crystals have the tetragonal piezoelectric non-polar space group $I\bar{4}2d$, the tetrad axis becoming the ferroelectric axis in the low temperature phase, whose space group is the polar $Fdd2$. The structure and group theory of KDP are discussed in appendix 1.

The first theories of KDP crystals considered the energies of possible configurations of the four protons surrounding one PO_4 group. Initially only short range interactions between configurations with two protons close to a PO_4 group were considered (Slater, 1941). Later modifications

(Takagi, 1948; Grindlay et al., 1959; Senko, 1961 Silsbee et al., 1964) considered the remaining configurations and in order to explain the isotope effect on the transition, or Curie temperature, included long range dipole-dipole interactions. Parameters fitted to the isotope effect on one property were used to predict that on another property. Upon deuteration the Curie temperature T_c = 123°K (KDP) becomes 222°K (KD_2PO_4, or DKDP) (Sliker and Burlage, 1963).

Pirenne (1949, 1955) however, chose to think of the proton moving in an anharmonic potential well in order to explain the isotope effect quantum mechanically. Silsbee et al (1964) using the Slater-Takagi theory described the isotope effect in terms of the distance of the proton or deuteron from the centre of the bond.

A totally different approach was used by Cochran (1961). In order to account for the behaviour of the dielectric constant in the same way as for true displacive ferroelectrics, a low frequency ferroelectric phonon mode in KDP type crystals was proposed. Unlike the other theories this description could elegantly account qualitatively for the antiferroelectric transition in ADP. The dielectric susceptibility measurements of Hill and Ichiki (1963) however can only be described by a Gaussian distribution of relaxation times in a Debye formula rather than a single relaxation time for a unique excitation. The form of the dielectric susceptibility may be generalised to any distribution of relaxation times

to describe other ferroelectrics (Matsubara and Yoshimitsu, 1967). The distribution of relaxation times may, however, be specimen dependent and it may therefore be valid to propose a single mode in order to describe the dielectric susceptibility.

Infra-red spectra of hydrogen-bonded ferroelectrics led Blinc (1960) to use Pirenne's model for the case of a double minimum potential. He developed the idea of protons tunnelling in the potential well. This tunnelling description was developed (Blinc and Ribaric, 1963; Blinc and Svetina, 1965, 1966; Tokunaga, 1966) to include short and long range proton-proton interactions as well as proton-lattice interactions. These latter interactions are obviously necessary in any theory describing principally the proton order-disorder, as the protons themselves contribute very little to the spontaneous polarisation.

A more easy-to-see-what's-going-on fictitious spin $\frac{1}{2}$ notation was introduced by de Gennes (1963) who was then able to show the form of the collective excitations in the system. De Gennes stated that his model could produce an antiferroelectric transition, arising in the same way as Cochran's transition. Kobayashi (1968) is the only recent author who has mentioned this point, but his reasoning is regarded as being incorrect (chapter 6). De Gennes predicted that the neutron scattering from DKDP would be quasielastic due to the low tunnelling frequency and that from KDP a broad spectrum centred around zero frequency would be

observed. Several authors (Brout et al., 1966; Villain and Stamenkovic, 1966; Tokunaga and Matsubara, 1966) then showed that the collective excitations are soft modes in the same sense as the ferroelectric phonon modes, so that some low frequency excitation is expected near T_c in the paraelectric phase. The effect of proton-lattice interaction on this excitation has been discussed by Villain and Stamenkovic (1966), Novakovic (1967) and recently by Kobayashi (1968).

Conclusive evidence on dynamic tunnelling has been hard to obtain. The experimental pressure dependence of T_c (Samara, 1967; Umebayashi et al., 1967) was claimed as evidence, but it could also be explained by a shift of proton position (Silsbee et al., 1964). Magnetic resonance experiments, however, indicated that the protons and deuterons do in fact jump along the hydrogen bonds in the paraelectric phase at frequencies greater than 10^5Hz (for deuterons) (Schmidt and Uehling, 1962; Bjorkstam, 1967; Blinc et al., 1967). The units of energy used here will normally be THz (10^{12}c/s). Early calculations of tunnelling frequencies (Baker, 1956; 1.5THz, KDP; 0.03THz, DKDP) indicated that even the KDP excitations would not be accessible in the usual infra-red frequency range. Martin and Stone (1963) however showed that there was some very heavily damped excitation appearing in both KDP and ADP below 50cm^{-1} (1.5THz). More precise infra-red work (Barker and Tinkham, 1963) showed that in KDP the low frequency excitation was overdamped and that it accounted for the high c-axis dielectric constant.

The a-axis measurements, however, did not show the low frequency excitation necessary to explain the a-axis dielectric constant.

Neutron spectroscopic measurements on KDP have been of the incoherent scattering using mainly time of flight techniques (Imry et al., 1967; Blinc et al., 1967; Schenk et al., 1968), although Plesser and Stiller (1968) used a triple axis instrument to investigate incoherent elastic scattering. From these experiments the only firm conclusion is that there is some temperature dependent inelastic scattering at frequencies less than 1.5THz for KDP.

The nature of the transition was determined to be second order for KDP and first order for DKDP from specific heat measurements (Reese and May 1967, 1968), in agreement with the conclusions from measurement of the anomalous elastic constant (KDP, Brody and Cummins, 1968; DKDP, Litov and Uehling, 1968). These latter measurements on DKDP show that the transition is almost second order (measurements to $0.05^{\circ}K$ below T_c) rather than decidedly first order as implied by Bjorkstam's (1967) more coarsely temperature controlled measurements (coexistence of magnetic resonance spectra of both phases within $T_c \pm 0.5^{\circ}K$).

The present experimental work was designed to study the ferroelectric transition in KDP and in particular to find the ferroelectric mode in KDP and to determine its nature. It was decided to make use of coherent neutron scattering experiments and in order to avoid excessive

incoherent scattering the crystal used was DKDP. Some later experiments were performed on KDP.

The experimental work and results are described in the next chapter. The work includes the measurement of the dispersion relations of several low frequency phonon branches in the two principal symmetry directions, as well as a study of the very low frequency (quasi-elastic) critical scattering associated with the transition. Chapter three deals with the models used to describe the phonon dispersion relations and with associated calculations to fit the experimental data. The group theoretical techniques used in the calculations are described in the first appendix. Attempts at fitting the critical scattering to various models are discussed in chapter four and chapter five presents a microscopic model of KDP type crystals.

The final chapter includes a discussion of the model and how well it applies to DKDP. It is shown that the model may also be used to describe the recent results of Meister et al. (1969) on DADP and furthermore from the dielectric constants of the crystal the model predicts the shape of additional neutron scattering in DADP.

In the second appendix are described experiments performed in an attempt to find a soft mode in a cubic displacive ferroelectric, work which was performed before that on KDP.

2. Experimental Results

2.1 Experimental details

Three single crystals supplied by Isomet Corp. U.S.A. were used in the experiments. The 9.5 g. KDP crystal was approximately cubic with a volume of 3.8 cm.^{3}. The first DKDP crystal obtained, weighing 17.6 g., was approximately cubic with a volume of 7.2 cm.^{3} and the second DKDP crystal (63.5 g.) was a cylinder, 5 cm. long and 2.5 cm. diameter whose axis was the c-axis of the crystal. It was claimed that the DKDP crystals were of high purity. The room temperature unit cell dimensions used for the crystals were $a = b = 7.453$ Å, $c = 6.975$ Å (KDP) and $a = b = 7.468$ Å, $c = 6.974$ Å (DKDP).

X-ray Laue photographs together with neutron elastic scattering experiments performed at A.E.R.E. Harwell showed the orientations of the KDP and small DKDP crystals. The crystal faces were approximately perpendicular to the unit cell axes. A comparison of the integrated intensities (I) of the 004 reflection from both crystals using the relation (Bacon, 1962)

$$I \propto |F|^2 \, V$$

where the volumes of the crystals (V) were known and the structure factors F had been calculated, indicated that the small DKDP crystal did contain an unknown percentage of deuterium. A calibration was not done with a standard extinction free crystal and so the absolute values of the

intensities could not be calculated. The effects of extinction were therefore unknown and it is surprising that the ratio of the structure factors agreed to within 6% of the calculated value for a fully deuterated DKDP crystal. The orientation of the large DKDP crystal was determined at A.E.C.L. Chalk River. The Curie temperature for the larger DKDP crystal (chapter 4) showed that it was fully deuterated ($\pm$ 3%). The mosaic spreads of the three crystals were 0.2°, 0.15° and 0.15° full width at half maximum (FWHM) measured against the (111) planes of an aluminium monochromator of mosaic spread less than 0.1°.

Preliminary investigations and alignment of the crystals were carried out on three two-axis neutron spectrometers. All of the inelastic data was obtained on one triple axis spectrometer. The two axis spectrometers were the Badger instruments on the DIDO reactor at A.E.R.E. Harwell and one instrument on the NRX reactor at Chalk River. The angle between the neutron beam emerging from the reactor and the beam diffracted by the monochromator crystal ($2\theta_M$) was easily variable on the Chalk River equipment, but it was unnecessary to use this facility in the present work. Two axis instruments have been adequately described by Bacon (1962). The triple axis spectrometer used is at the C5 facility of the NRU reactor at Chalk River. A detailed description of this instrument has been given by Brockhouse (1961).

The constant energy and constant $\underline{Q}$ modes of operation of the

spectrometer were used in the experiments. The angle between the beam scattered by the sample and the beam diffracted by the analyser crystal ($2\theta_A$) is not easily variable on the instrument and is therefore kept constant for any series of measurements on one sample. Orientation of the crystal specimen is restricted to rotation about one (vertical) axis (ψ) and therefore within the limits of the resolution of the spectrometer the observable scattering is confined to a plane. The momenta of the neutrons which are incident on and scattered from the crystal, and then observed, are therefore confined to one plane in the reciprocal space of the crystal. Coordinates in this plane are defined by (ζ, η) in reciprocal lattice units. The angle between the incident and scattered neutron beams is ϕ. The constant energy mode involves variation of ϕ and ψ only and gives the distribution of neutrons scattered with a fixed energy transfer with a momentum transfer variable in any direction in the scattering plane. The constant $\underline{Q}$ mode requires variation of all three angles $2\theta_M$, ϕ and ψ and gives the energy distribution of neutrons scattered with a fixed momentum transfer. The angular steps usually selected are those which give constant energy step size, but in order to keep within the resolution of the instrument on one hand, and not to do unnecessary work on the other, steps of a constant $2\theta_M$ value were used in preliminary measurements over large energy ranges.

The resolution function of a triple axis spectrometer (Cooper and Nathans, 1967) is particularly complicated and must be taken into account

when designing an experiment. The main factors which limit the resolution obtainable are the time available for an experiment and therefore the neutron flux of the reactor. With the limited time and high flux available at the C5 facility the experiment was designed to use the (111) planes of both an aluminium monochromator crystal and a squeezed germanium analyser crystal. The additional degrees of freedom ($2\Theta_A$) and the collimation of the beams would enable the energy resolution to be varied. The collimation was however, unaltered throughout the measurements and is given in table 2.1. The design of the spectrometer places a maximum limit on the ϕ angle (106°) and also determines that $2\Theta_M$ lies between 28° and 63°.

The low total neutron scattering cross section of aluminium has led to its general use as a material for encasing and mounting crystals in neutron beams. All three crystals which required protection from humidity were sealed in machined aluminium cylinders with narrow walls. They were mounted on aluminium bases so that their orientations could be adjusted by approximately five degrees about horizontal axes. The crystals were mounted so that (h0ℓ) was the scattering plane. This allowed measurement of phonon dispersion relations in the two principal symmetry directions (Λ and Σ) and also allowed observation of reciprocal lattice points h0ℓ with odd Miller indexes h and ℓ. ($h + \ell$ must be even). The phase factors in the one phonon structure factor (Cochran and Cowley,

1967) show that if the crystal were composed only of two simple body centred tetragonal lattices, related to each other by c/2, then near these odd reciprocal lattice points the optic modes would produce strong scattering. These points would not be seen in the (hhℓ) plane. The notation (ζ, η) for the scattering plane refers to the a* (ζ) and c* (η) directions. The reciprocal lattice points hkℓ are written (h, ℓ) in this notation, where the Miller indexes h, k and ℓ are integers.

For low temperature experiments the mounted and aligned crystals were placed in 8" diameter aluminium cryostats designed for liquid nitrogen use. The crystal was surrounded by an aluminium radiation shield of approximately 5" diameter. Control and monitoring of the temperature was arranged using three thermocouples. One each was attached to the radiation shield, the base and the crystal. The thermocouple on the base was used to control the temperature which could be held constant to within 0.2°K for long periods. Liquid nitrogen was used as the refrigerant for the KDP crystal but as the liquid could not be insulated from the crystal, dry ice (solid CO_2) was used as the refrigerant for DKDP, which has a higher Curie temperature.

2.2 Phonon measurements

Prior to the neutron scattering experiments no work had been done on the group theory of KDP at wave vectors other than zero or on a model to predict phonon dispersion relations. Therefore apart from the simple

rules of even ℓ indexes for acoustic modes and odd ℓ indexes for optic modes, derived from the one phonon structure factor, no information was available which would assist the planning of an experiment to observe phonons in DKDP. It has been shown that group theory can by itself predict the reciprocal lattice points around which it is best to look for a phonon of particular symmetry (Elliott et al., 1967). In KDP this information would have been useful to indicate where not to look for a mode. There are, however, four different space groups sites occupied by the atoms K, P, O and H and only a model of the lattice dynamics of the crystal could produce useful predictions of structure factors for one phonon scattering. As there are atoms on general positions in the unit cell, the structure zone which contains all the scattering information is infinite in three directions. It is felt that the group theoretical techniques, while worthwhile if the time is available before an experiment, provide only a little more information than the simple rules stated above. Group theoretical techniques are, however, indispensible for the analysis of the data.

The difference between the structures of paraelectric and ferroelectric KDP gives displacements which may be interpreted as those of the ferroelectric mode. Calculations (chapter 3) of the structure factors for this mode were useful not for finding phonons but in interpreting the critical scattering described in the next section.

Preliminary measurements were made on the smaller DKDP crystal of phonons propagating in the $\underline{a}$ and $\underline{c}$ directions with frequencies up to 6THz. $2\theta_A$ was chosen as 29.5° so that the detected neutron energy (E_1, momentum $\underline{k}$) was approximately 7THz. The incident neutron energy (E_o) ranged from 7THz to 13THz corresponding to $2\theta_M$ angles of 42° to 29° in the neutron energy loss experiments performed.

$$\hbar\omega(\underline{q}) = E_o - E_1 \qquad \ldots\ldots\ldots\ldots\ldots 2.1$$

The resultant energy width of neutrons scattered incoherently and elastically from a slab of vanadium was 2.5° in $2\theta_M$ or approximately 0.75THz full width at half maximum (FWHM). This width defines the energy resolution available in the first series of experiments. The vanadium experiment serves as a check on the energy scale. The large momentum transfers

$$\underline{Q} = \underline{k} - \underline{k}_o \qquad \ldots\ldots\ldots\ldots\ldots 2.2$$

available with these high incident energies enabled reciprocal lattice vectors with $\zeta^2 + \eta^2$ less than approximately 45 to be reached for zero energy transfer ($\underline{a}^*$ and $\underline{c}^*$ differ by only 7%). Measurements were taken at 300°K around the reciprocal lattice points ($\underline{\tau}$) (002, 004, 105, 400, 402 and 501) in phonon momentum ($\underline{q} = \underline{Q} - \underline{\tau}$) steps of 0.2 reciprocal lattice units in the $\underline{c}^*$ (Λ) and $\underline{a}^*$ (Σ) directions. While it is convenient to describe $\underline{\tau}$ and $\underline{q}$ in reduced reciprocal lattice units $h0\ell$ and (ζ, η) respectively, their units in any formulae are reciprocal length

$\underline{\tau} = (\frac{2\pi h}{a},\ 0,\ \frac{2\pi \ell}{c})$ and $\underline{q} = (\frac{2\pi \zeta}{a},\ 0,\ \frac{2\pi \eta}{c})$.

The structure factor for one phonon coherent scattering includes a term $\underline{Q} \cdot \underline{e}_K(\underline{q}j)$, where $\underline{e}_K(\underline{q}j)$ is the eigenvector for the Kth atom in the mode $\underline{q}j$ (Cochran and Cowley, 1967). Therefore, for the symmetry directions Λ and Σ, when $\underline{q}$ is approximately perpendicular to $\underline{Q}$ transverse phonons scatter strongly and when $\underline{q} \parallel \underline{Q}$ longitudinal modes scatter strongly. This is certainly true when considering only the motion of the K and P atoms in the crystal, but as the oxygen atoms are on general positions in the space group their motion is not restricted by symmetry in any normal mode and so the terms longitudinal and transverse have no meaning for these atoms. For this reason scattering from the longitudinal type modes may be seen in the transverse scattering configuration and vice versa. Also scattering from the transverse modes with polarisation vectors for K and P restricted perpendicular to the scattering plane may also be seen (figure 2.7). For transverse acoustic phonons (and for transverse optic phonons with a frequency gradient) the resolution function of the spectrometer either focusses or defocusses the energy distribution of the scattered neutrons (Cooper and Nathans, 1967). An example of this focussing is given in figure 2.1 where two of the neutron groups observed at (-0.6, 4) are shown.

Neutron groups were observed in both transverse and longitudinal configurations with some duplication. The experimental results are summarised in figure 2.2 which also shows the results of preliminary model

calculations described in chapter 3. The larger DKDP crystal then became available and it was used for higher resolution measurements of the phonons. The structure factors calculated from the above model were found to be of no great value in assisting the experiment.

The resolution for the second experiment was chosen with $2\theta_A = 43^\circ$ (E_1, 3.5THz). For zero energy transfer $2\theta_M = 61.6^\circ$ and so only a very limited range (0.2THz) was available for energy gain experiments ($(2\theta_M)_{max} = 63^\circ$). The width of the vanadium scattering was again 2.5° which at this $2\theta_M$ corresponds to 0.26THz (FWHM). The momentum transfer, $\underline{Q}$, allowed corresponds to approximately $\zeta^2 + \eta^2$ less than 25. Measurements were taken at 300°K in the zones around reciprocal lattice points 002, 004, 103, 202, 204, 301, 400, 402 and 501. Results were obtained at $\underline{q}$ intervals of 0.1 reciprocal lattice units in the Λ and Σ directions. Some measurements were also taken at wave vectors half way between these values in attempts to clarify the results. The better resolution of these measurements is indicated by showing again the neutron groups at (-0.6, 4) (figure 2.3).

Not all of the neutron groups observed arise from one phonon coherent scattering processes according to the conditions of equations 2.1 and 2.2. Several types of spurious processes give rise to neutron groups labelled 'spurions'. The absence of the (222) reflection from germanium single crystals, due to space group rather than point group symmetry, prohibits

spurious scattering processes with scattered wave vector $2\underline{k}$. For example those processes with momentum transfer $2\underline{Q} = 2\underline{k} - 2\underline{k}_o$ and energy transfer $\hbar\omega(\underline{q}) = 4E_o - 4E_1$ do not occur. Other spurious processes were, however observed. One type of spurion was detected only at $\underline{q} = 0$ with a frequency of 1.5THz. These groups were the result of incoherent one phonon scattering, the energy distribution of which is a weighted frequency distribution of the normal modes of the crystal. The groups seen correspond to scattering from the transverse acoustic branch, or sheet, which is particularly flat near the zone boundary. Similar incoherent scattering has been observed in partially deuterated hexamethylenetetramine, where it was at first interpreted as a phonon branch (Powell, 1968). The one phonon incoherent scattering depends on $\underline{Q}$ only through the Debye-Waller factor and the $\underline{Q} \cdot \underline{e}_K(\underline{qj})$ term in the structure factor (Cochran and Cowley, 1967). The scattering should therefore not vary dramatically with $\underline{Q}$. It is thought that the incoherent scattering observed in DKDP at 1.5THz, which was very weak, was masked by the longitudinal acoustic modes at wave vectors greater than $\underline{q} = 0$. This incoherent scattering indicates that the crystal was not fully deuterated. No quantitative measurements of the scattering were made.

Four cases of $\underline{Q} = 3\underline{k} - 2\underline{k}_o = \underline{\tau}$, (8, 2), (-3, 9), (-3, 5), (12, 2) spurious scattering were observed. At these reciprocal lattice points the energy transfer $4E_o - 9E_1 = 0$. and so the elastic scattering from a Bragg peak falls within the resolution function. The spurion at a momentum transfer

$\underline{Q} = \underline{k} - \underline{k}_o$ then has energy $E_o - E_1 \sim 4$THz.

After removal of the spurions several phonon branches became clear in the data. In the Λ direction both acoustic branches were observed as well as one resolved optic branch and parts of other less clearly defined optic branches. In the Σ direction two acoustic branches were observed as well as the zone boundary end of the second transverse acoustic branch. Again parts of some less clearly defined optic branches were observed. The experimental results are summarised in figure 2.4 in which are also shown the results of final calculations to fit the dispersion relations (chapter 3). The observed frequencies which were not corrected for experimental resolution, their estimated standard deviations and the calculated frequencies are given in table 2.2.

The results show no low frequency phonon branch as in $SrTiO_3$ (Cowley, 1964). The lowest frequency neutron groups at the zone boundary (M_{34}), at $\underline{q} = 0$ (Γ_5) and some of the neighbouring groups (Λ_{34} and Σ_2) were measured at lower temperatures, but the distributions were unaltered (figure 2.5). The dispersion relations were clearly able to be described by a simple lattice dynamical model. It could therefore be concluded that the ferroelectric transition in DKDP was not the result of instability of a normal mode.

The high $\underline{c}$-axis dielectric constant in DKDP indicated that there must

be some low frequency temperature dependent excitation in the crystal. A set of constant Q scans at various Q values with energy transfers from 1THz to -0.02THz (energy gain) was therefore carried out. No low frequency excitation was found, but on cooling the crystal to 253°K, the intensity of the elastic scattering, which had the natural width of 0.26THz and which had been assumed to be due to incoherent elastic scattering, increased in a q dependent manner. Incoherent elastic scattering is only Q (and not q) dependent through the Debye-Waller factor and should not be temperature dependent, so that the elastic scattering observed was not totally incoherent.

2.3 Critical scattering

The anomalous elastic scattering was investigated on the triple axis spectrometer with the better resolution mentioned above, using constant energy scans with zero energy transfer. The scans were in one quadrant of the (ζ, η) plane along lines parallel to a* and c*, 0.15 units away from reciprocal lattice points in order to avoid first order Bragg scattering. As the energy of the scattered neutrons was so low multiple order (4th and 5th) Bragg scattering could occur and caused some spurious peaks.

The distribution of neutrons observed throughout the (ζ, η) plane was most prominent near reciprocal lattice points and was therefore not due entirely to incoherent elastic scattering of neutrons. The distribution

around each reciprocal lattice point was elongated in the $\underline{a}^*$ direction with little scattering in the $\underline{c}^*$ direction (figure 2.6). The intensity distribution of the scattering as a function of $\underline{q}$ did not alter with temperature. The intensity itself, however, was found to be temperature dependent, becoming greater as the temperature approached the transition temperature and decreasing rapidly below this temperature. The scattering was therefore called critical scattering.

The intensity also differed from one reciprocal lattice point to another, but where the scattering was strong the $\underline{q}$-space distributions were always similar. In order to provide data for a model which could predict the intensity of the scattering at each reciprocal lattice point (chapter 4) estimates of the intensity at (h, l) were obtained by assuming that there is little scattering at $(h, l \pm 0.15)$ and subtracting this value from the intensity at $(h \pm 0.15, l)$ (figure 2.10). The incoherent scattering is assumed to be constant over this region and it is also assumed that there is no other scattering present, that is to say, that all the anomalous scattering arises from the $\underline{c}$-axis ferroelectric fluctuations. The intensities were recorded at 254.2°K and 233.7°K. There were no significant differences between the relative intensities. The measurements were in qualitative agreement with the scattering expected from displacements of the predicted ferroelectric mode (chapter 3).

The strongest scattering was around the reciprocal lattice point (3, 3).

Extensive measurements as a function of energy, $\underline{q}$ and temperature were taken around this point. The energy distributions at three points along the line (ζ, 3) are shown in figure 2.7 as a function of temperature. It is seen that the energy width does not become greater than the instrumental resolution (0.26THz FWHM) either as a function of $\underline{q}$ or of temperature. The scattering may therefore be termed quasielastic. The half width of the resolution function is then certainly consistent with the inverse relaxation time $1/\tau_o$ = 0.017THz derived from dielectric susceptibility measurements by Hill and Ichiki (1963) for room temperature. The results presented here give no evidence that the scattering is due to resonant excitations with a discrete energy. The scattering may arise from excitations with a discrete energy, but they would not be resonant, indeed they would be heavily damped. It may, however, be concluded that the quasielastic nature of the critical scattering indicates that there are fluctuations in the crystal associated with the ferroelectric phase transition which are on a very long time scale compared with the phonons, except for the very long wavelength acoustic modes.

Figure 2.7 also shows the scattering from the two transverse acoustic modes at (2.85, 3). The lower frequency mode is the one referred to in the previous section from which the scattering observed is mainly due to oxygen and hydrogen displacements.

The distribution of the quasielastic scattering along the line (ζ, 3)

near the reciprocal lattice point (3, 3) is shown in figure 2.8. The Q-space resolution of the results is good enough to enable the Bragg peak 303, which is shown in the left hand part of the figure, to be subtracted, yielding the data shown on the right hand side. The distribution of the quasielastic scattering along the line (ζ, 3.1) is shown in figure 2.9. Some spurious scattering has been removed to give the results shown.

The distribution of the quasielastic critical scattering in reciprocal space is shown for two temperatures in figure 2.10. The intensity contour lines show that the shape is independent of temperature. The most important characteristic of the scattering is its dumbbell shape with little scattering in the $\underline{c}^*$ direction. The critical scattering was not studied in the $\underline{a}^*$ - $\underline{b}^*$ plane.

The inverse intensity at any point near (3, 3) was found to be an approximately linear function of inverse temperature, implying that the intensity

$$I \propto \frac{T}{T - T_o}$$

where T_o is some ($\underline{q}$-dependent) constant temperature. The temperature dependence is discussed in chapter 4.

Following this work some measurements were repeated under conditions of better collimation with the (111) planes of a germanium crystal as monochromator (R. A. Cowley and W. J. L. Buyers, private

communication). The only significant difference between the results is that the better $\underline{Q}$ -space resolution enabled the Bragg peak to be subtracted more easily.

2.4 Critical scattering in KDP

With the KDP crystal available an experiment was performed on the triple axis spectrometer in order to look for inelastic incoherent critical scattering. The resolution of the spectrometer was chosen with the same collimation as previously and a $2\theta_A$ of 36° (E_1 = 4.9THz). The width of the vanadium scattering was 0.43THz FWHM at $2\theta_M = 51.2^\circ$.

Infra-red scattering results indicated that any critical scattering should be observed at frequencies less than 1.5THz. Constant energy scans from 4THz to zero energy transfer were performed at four different reciprocal lattice points (1, 5), (2, 2), (3, 3), and (5, 1), to take advantage of any $\underline{Q}$ dependence of the incoherent critical scattering. The measurements were performed 20°K and 10°K above T_c at 143°K and 133°K.

There was no significant difference between the distributions recorded at different temperatures and only slight differences between the intensity of measurements at various momentum transfers (figure 2.11). The latter differences could be qualitatively described by the $\underline{Q}$ dependence of the structure factor for incoherent one phonon scattering. The temperature dependence of the critical scattering in DKDP implies that

similar scattering in KDP should have doubled in intensity on the above temperature change. The experiment therefore shows that the incoherent scattering from the acoustic modes is much stronger than any critical scattering which may be present. The lack of $\underline{Q}$ dependence in the shape of the scattering shows that the inelastic scattering arises from modes which do not involve large displacements of the protons in one direction, as would be expected from the ferroelectric displacements.

These preliminary investigations showed that a neutron inelastic scattering investigation of the ferroelectric phase transition in KDP would be more difficult than the study of DKDP described in this chapter. The ferroelectric mode scattering has recently been observed in KDP by Raman scattering, but this unfortunately does not yield information on the $\underline{q}$-dependence of the mode (Kaminow and Damen, 1968).

Table 2.1

C5 Spectrometer experimental settings

Full width at half maximum of the collimation and mosaic spreads are given in degrees.

Horizontal Collimation

α_0	Before Monochromator		0.8
α_1	Monochromator	- Specimen	0.75
α_2	Specimen	- Analyser	0.67
α_3	Analyser	- Detector	4.0

Vertical Collimation

β_0	Before Monochromator		1.0
β_1	Monochromator	- Specimen	2.0
β_2	Specimen	- Analyser	6.0
β_3	Analyser	- Detector	6.0

Crystal Mosaic Spread

η_M	Monochromator	Al(111)	0.48
η_A	Analyser	Ge(111)	0.35

Table 2.2

Observed and calculated normal mode frequencies (THz) in DKDP at 300°K

Estimated standard deviations (s.d.) are given. The observed frequency marked * was not included in the least squares fit.

	Λ $(0,\eta)$							
	Λ_1				Λ_2			
η	obs.	s.d.	calc. Γ_4	calc. Γ_4	obs.	s.d.	calc. Γ_3	calc. Γ_3
0.0	-	-	0	5.64	3.17	0.08	3.05	4.57
0.1	0.68	0.02	0.66	5.59	3.25	0.07	3.09	4.53
0.2	1.35	0.02	1.30	5.45	3.22	0.03	3.20	4.43
0.3	2.00	0.03	-	-	-	-	-	-
0.4	2.55	0.04	2.43	4.96	-	-	3.35	4.26
0.5	2.98	0.03	-	-	-	-	-	-
0.55	3.07	0.04	-	-	-	-	-	-
0.6	3.10	0.04	3.09	4.47	-	-	2.90	4.51
0.7	2.93	0.04	-	-	2.65	0.08	-	-
0.75	2.82	0.03	-	-	-	-	-	-
0.8	2.64	0.04	2.78	4.59	2.37	0.03	2.36	4.78
0.9	2.40	0.02	-	-	2.24	0.04	-	-
1.0	2.23	0.02	2.30	4.81	2.23	0.02	2.30	4.81
			M_5	M_5			M_5	M_5

Table 2.2 (continued)

$\Lambda \quad (0, \eta)$

Λ_{34}

η	obs.	s.d.	calc. Γ_5	obs.	s.d.	calc. Γ_5	calc. Γ_5	calc. Γ_5
0.0	-	-	0	2.85	0.04	2.75	5.17	5.64
0.1	0.34	0.02	0.36	2.81	0.06	2.73	5.17	5.63
0.2	0.67	0.02	0.72	2.75	0.03	2.66	5.19	5.62
0.3	0.98	0.02	-	2.59	0.03	-	-	-
0.4	1.26	0.03	1.36	2.50	0.07	2.48	5.25	5.56
0.5	1.50	0.03	-	2.35	0.07	-	-	-
0.6	1.68	0.03	1.65	2.40	0.05	2.50	5.26	5.49
0.7	1.58	0.04	-	2.55	0.04	-	-	-
0.75	-	-	-	2.65	0.03	-	-	-
0.8	1.45	0.03	1.51	2.75	0.04	2.84	5.18	5.47
0.9	1.40	0.03	-	2.90	0.04	-	-	-
1.0	1.40	0.02	1.41	2.91	0.05	3.01	5.11	5.48
			M_{34}			M_{12}	M_{34}	M_{12}

Table 2.2 (continued)

$\Sigma \quad (\zeta, 0)$

Σ_1

ζ	obs.	s.d.	calc.	obs.	s.d.	calc.	obs.	s.d.	calc.	calc.	calc.	calc.
			Γ_5			Γ_5			Γ_3	Γ_3	Γ_5	Γ_5
0.0	-	-	0	2.85	0.04	2.75	3.17	0.08	3.05	4.57	5.64	5.71
0.1	0.71	0.02	0.72	2.85	0.04	2.75	-	-	3.05	4.56	5.62	5.68
0.2	1.38	0.03	1.40	2.87	0.04	2.76	-	-	3.08	4.54	5.55	5.64
0.3	2.06	0.04	-	2.85	0.05	-	-	-	-	-	-	-
0.35	2.40	0.05	-	2.89	0.06	-	-	-	-	-	-	-
0.4	2.55	0.06	2.34	2.84*	0.05	2.78	-	-	3.35	4.45	5.23	5.58
0.45	2.61	0.05	-	2.81	0.05	-	-	-	-	-	-	-
0.5	2.48	0.04	-	2.72	0.04	-	-	-	-	-	-	-
0.6	2.38	0.03	2.43	-	-	2.89	-	-	3.60	4.63	4.99	5.53
0.7	2.28	0.04	-	-	-	-	-	-	-	-	-	-
0.8	2.14*	0.02	2.34	2.77*	0.05	2.98	2.98*	0.07	3.22	4.83	5.25	5.49
0.9	2.22	0.02	-	2.87	0.07	-	2.98	0.06	-	-	-	-
1.0	2.23	0.02	2.30	2.91	0.05	3.01	2.91	0.05	3.01	4.81	5.48	5.48
			M_5			M_{12}			M_{12}	M_5	M_{12}	M_{12}

Table 2.2 (continued)

$\Sigma \quad (\zeta, 0)$

Σ_2

ζ	obs.	s.d.	calc.	obs.	s.d.	calc.	obs.	s.d.	calc.	calc.	calc.	calc.
			Γ_5			Γ_4			Γ_5	Γ_4	Γ_5	Γ_5
0.0	-	-	0	-	-	0	2.85	0.04	2.75	5.04	5.17	5.64
0.1	0.22	0.02	0.26	0.32	0.02	0.30	2.95	0.05	2.81	5.04	5.16	5.57
0.2	0.46	0.02	0.50	0.62	0.02	0.60	-	-	2.97	5.05	5.15	5.39
0.3	0.65	0.02	-	0.92	0.02	-	-	-	-	-	-	-
0.4	0.86	0.02	0.89	1.22	0.02	1.14	-	-	3.46	4.69	5.08	5.16
0.5	-	-	-	1.50	0.02	-	-	-	-	-	-	-
0.6	1.16	0.03	1.18	1.74	0.02	1.57	-	-	3.41	4.30	5.11	5.14
0.7	1.28	0.04	-	1.95	0.02	-	-	-	-	-	-	-
0.8	1.38	0.04	1.35	1.74	0.05	1.70	-	-	2.52	4.65	5.12	5.13
0.9	1.39	0.04	-	1.46	0.04	-	-	-	-	-	-	-
1.0	1.40	0.02	1.41	1.40	0.02	1.41	2.23	0.02	2.30	4.81	5.11	5.11
			M_{34}			M_{34}			M_5	M_5	M_{34}	M_{34}

Table 2.2 (continued)

Unassigned frequencies

	$\Sigma(\zeta,0)$						$\Lambda(0,\zeta)$					
ζ	obs.	s.d.	obs.	s.d.	obs.	s.d.	obs.	s.d.	obs.	s.d.	obs.	s.d.
0.1	4.57	0.06					4.18	0.10				
0.2	4.61	0.06	5.08	0.09			3.40	0.03				
0.3	3.20	0.05	4.56	0.06			3.40	0.04	4.30	0.10		
0.35	3.36	0.08										
0.4	3.39	0.07	4.54	0.05			3.43	0.03	4.40	0.10		
0.5	3.20	0.04	3.56	0.07	4.65	0.05	3.50	0.04	4.27	0.05		
0.55							3.48	0.04				
0.6	3.00	0.05	3.32	0.05	3.70	0.03	3.48	0.07				
	4.58	0.05										
0.7	3.00	0.06	3.32	0.04	3.94	0.04	3.35	0.05	3.79	0.06	4.12	0.10
	4.47	0.05										
0.75	2.02	0.04										
0.8	3.35	0.04	4.09	0.04	4.50	0.04	3.35	0.04	3.93	0.08	4.27	0.05
0.9	3.40	0.05	4.28	0.05	4.50	0.07	3.40	0.04	4.23	0.06	4.35	0.06
1.0	3.40	0.04	4.40	0.05			3.40	0.04	4.40	0.05		

Figure 2.1

Scattering diagram in reciprocal space and the neutron groups observed in the constant $\underline{q}$ mode at (-0.6, 4) from the small DKDP crystal. The monitor count was 4×10^6 neutrons for each point. The acoustic mode at 1.8THz has been focussed by the resolution function.

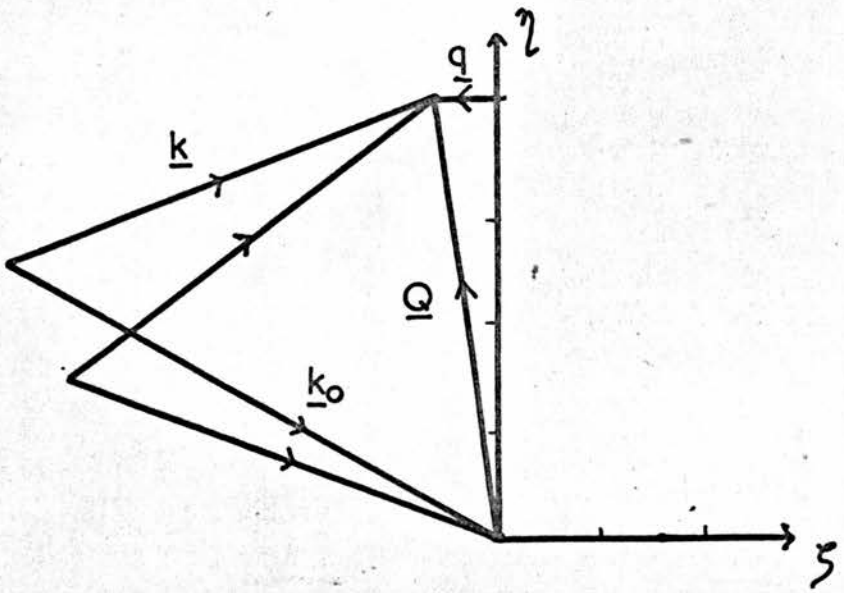
q
ζ
k
Q
k₀
ξ

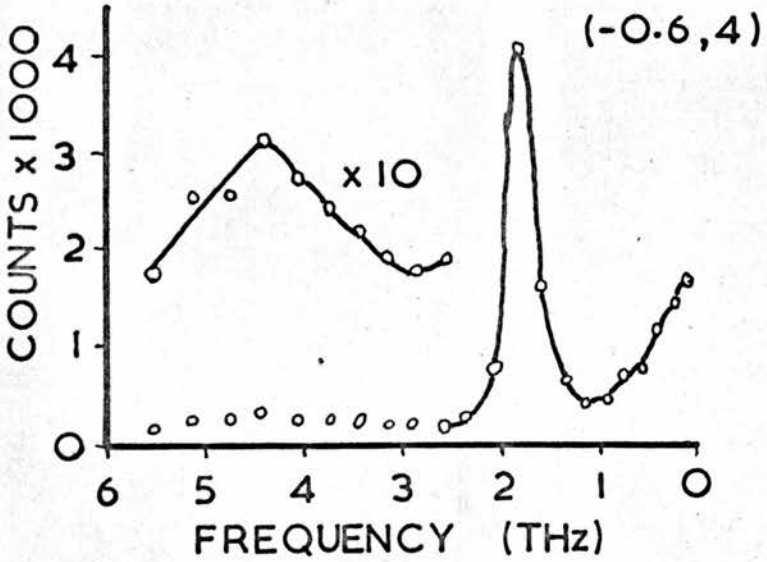
(-0.6,4)
x 10
COUNTS x 1000
0
1
2
3
4
6
5
4
3
2
1
0
FREQUENCY (THz)

Figure 2.2

Preliminary results for the dispersion relations of DKDP at 300°K as measured on the small DKDP crystal. The solid lines represent a least squares fit to the acoustic modes only using a simple lattice dynamical model described in chapter 3.

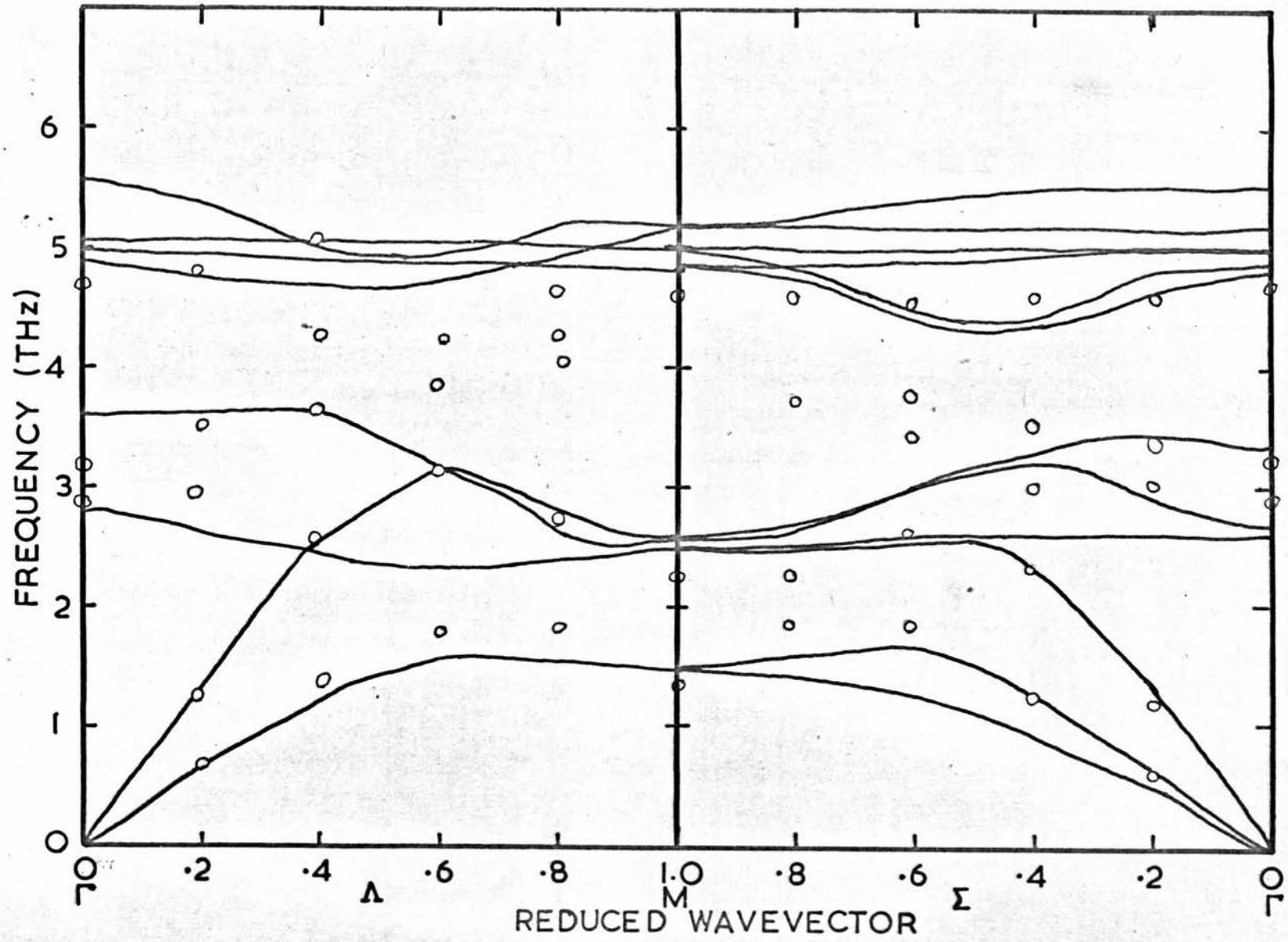
FREQUENCY (THz)
0
1
2
3
4
5
6
Γ
0
·2
·4
Λ
·6
·8
M
1.0
·8
·6
Σ
·4
·2
Γ
0
REDUCED WAVEVECTOR

Figure 2.3

The neutron groups at (-0.6, 4) from the large DKDP crystal. The experimental resolution is different to that for the groups shown in Figure 2.1. The monitor count was 10^6 neutrons and the large crystal is 3.5 times the volume of the small crystal.

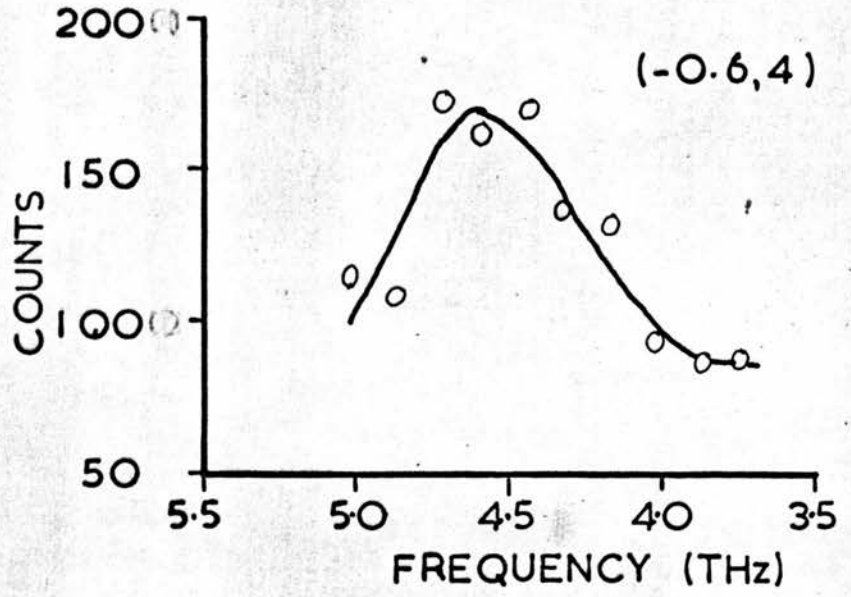
200
150
100
50
COUNTS
(-0.6,4)
5·5
5·0
4·5
4·0
3·5
FREQUENCY (THz)

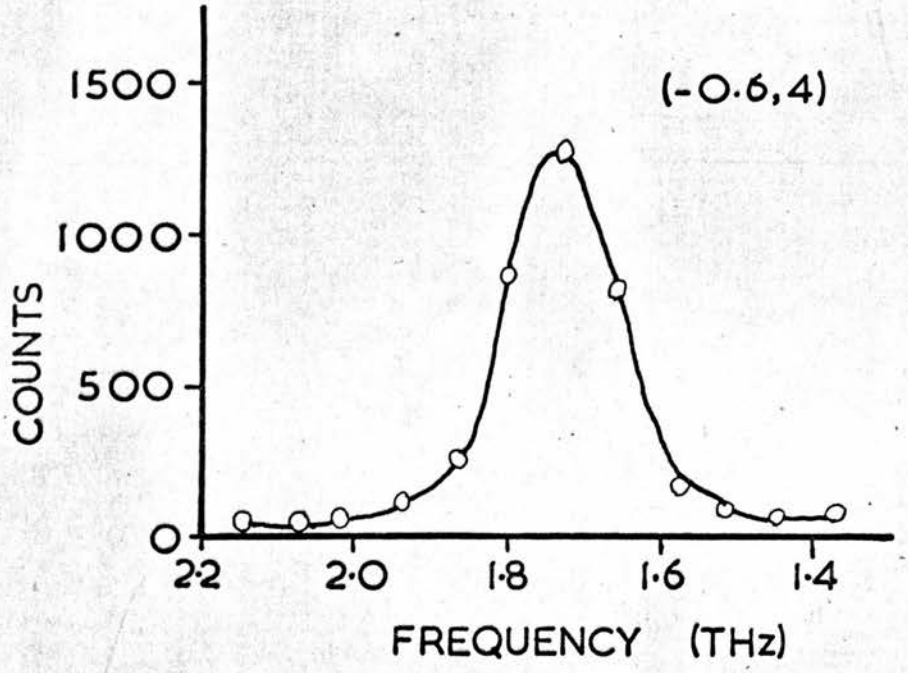
1500
1000
500
0
COUNTS
(-0.6,4)
2·2
2·0
1·8
1·6
1·4
FREQUENCY (THz)

Figure 2.4

Phonon dispersion relations of DKDP at 300°K. The measured values and the errors are given in table 2.2. The solid lines represent a best least squares fit to the data as described in chapter 3.

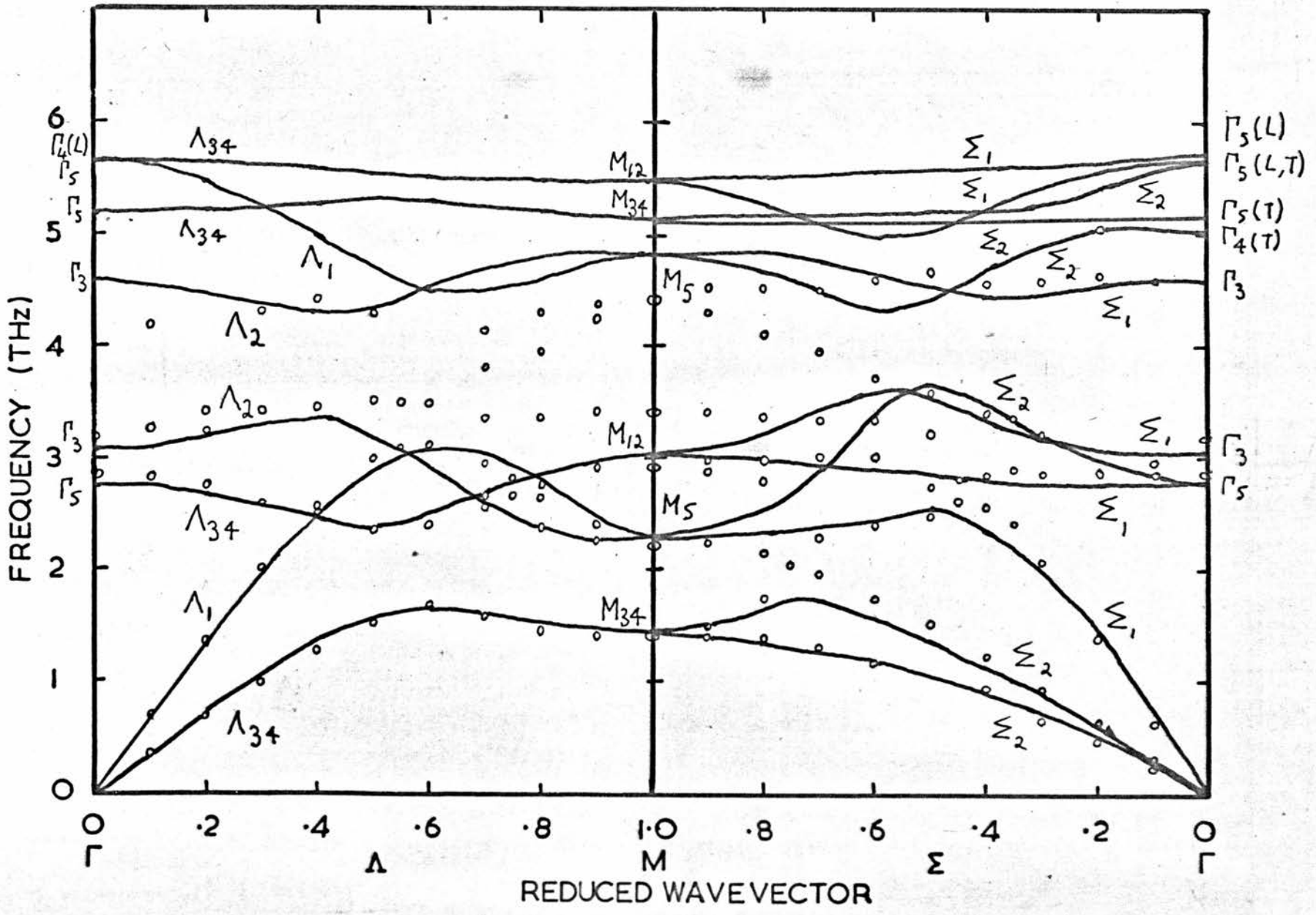
FREQUENCY (THz)
0
1
2
3
4
5
6
Γ1(L)
Γ5
Γ5
Γ3
Γ3
Γ5
Λ34
Λ34
Λ1
Λ2
Λ2
Λ34
Λ1
Λ34
M12
M34
M5
M12
M5
M34
Σ1
Σ1
Σ2
Σ2
Σ2
Σ1
Σ2
Σ1
Σ1
Σ2
Σ2
Γ5(L)
Γ5(L,T)
Γ5(T)
Γ4(T)
Γ3
Γ3
Γ5
0
·2
·4
·6
·8
1·0
·8
·6
·4
·2
0
Γ
Λ
M
Σ
Γ
REDUCED WAVEVECTOR

Figure 2.5

Temperature dependence of normal modes in DKDP. The neutron groups of lowest frequency, Γ_5 at (2, 2) and M_{34} at (3, 2) are shown at several temperatures. The distributions could not be claimed to be temperature dependent.

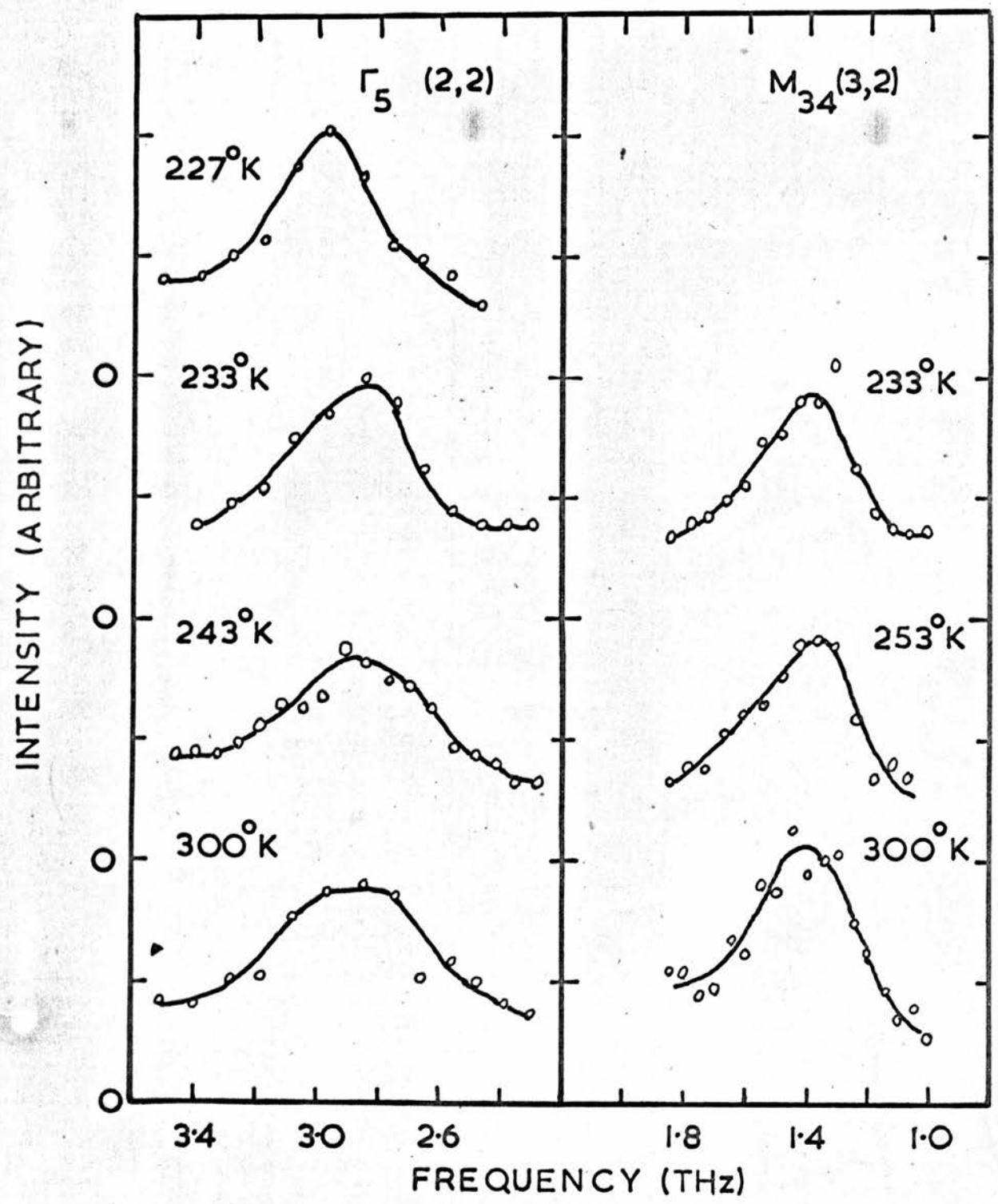
Γ_5 (2,2)
M_{34}(3,2)
227°K
233°K
243°K
300°K
233°K
253°K
300°K
INTENSITY (ARBITRARY)
3·4
3·0
2·6
1·8
1·4
1·0
FREQUENCY (THz)

Figure 2.6

Constant energy scans with zero energy transfer along the line (ζ, 3.2) near the reciprocal lattice point (3, 3). The monitor count was 10^6 neutrons. The peak at $\zeta = 2.4$ may be due to 5th order Bragg scattering. The shape of the scattering indicates that it is not incoherent and the temperature dependence shows that it is associated with the ferroelectric transition. The nearest reciprocal lattice points along the line (ζ, 3) are (1, 3) and (5, 3).

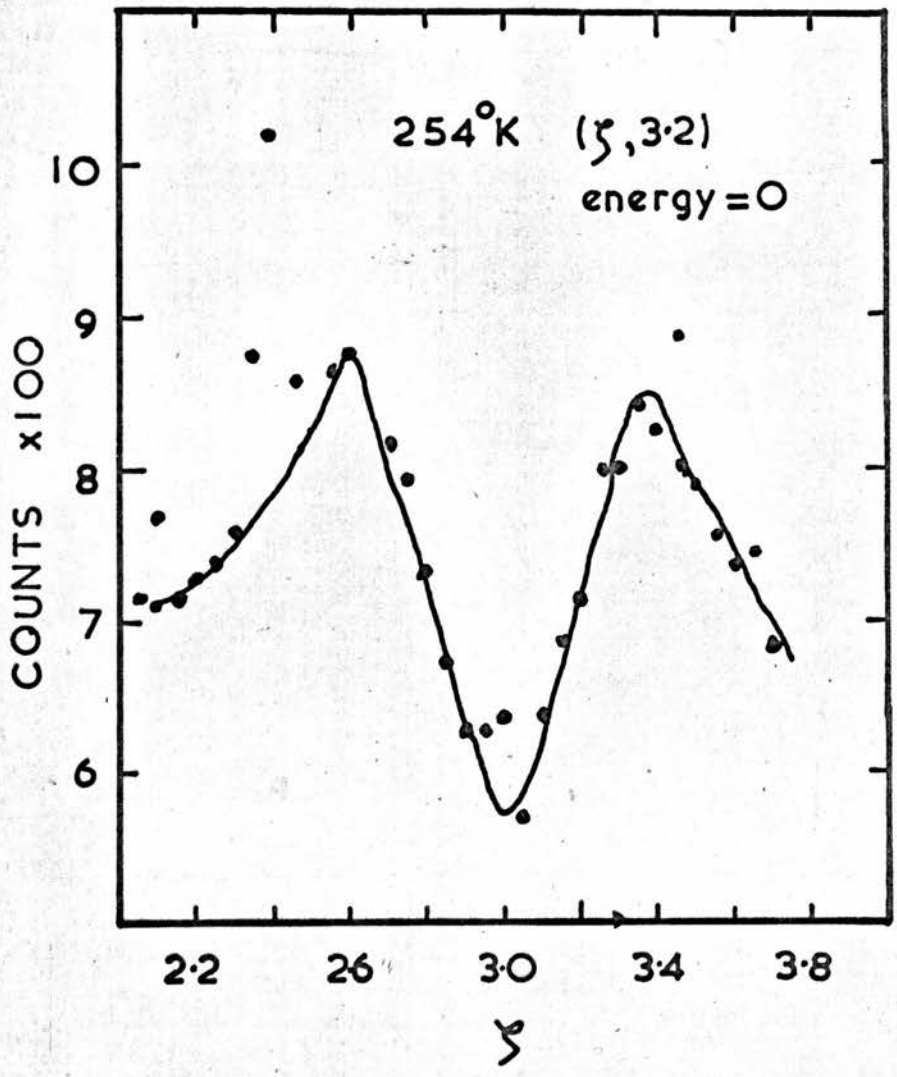
254°K (ζ, 3·2)
energy = 0
COUNTS x100
10
9
8
7
6
2·2
2·6
3·0
3·4
3·8
ζ

Figure 2.7

Energy distributions of the critical scattering at the points (2.85, 3), (2.7, 3) and (2.57, 3) at four temperatures. The monitor count was 10^6 neutrons. The width of every distribution is that of the instrumental resolution. The neutron groups corresponding to the two transverse acoustic modes are seen in the (2.85, 3) picture. The scattering is stronger as $\underline{q}$ approaches zero.

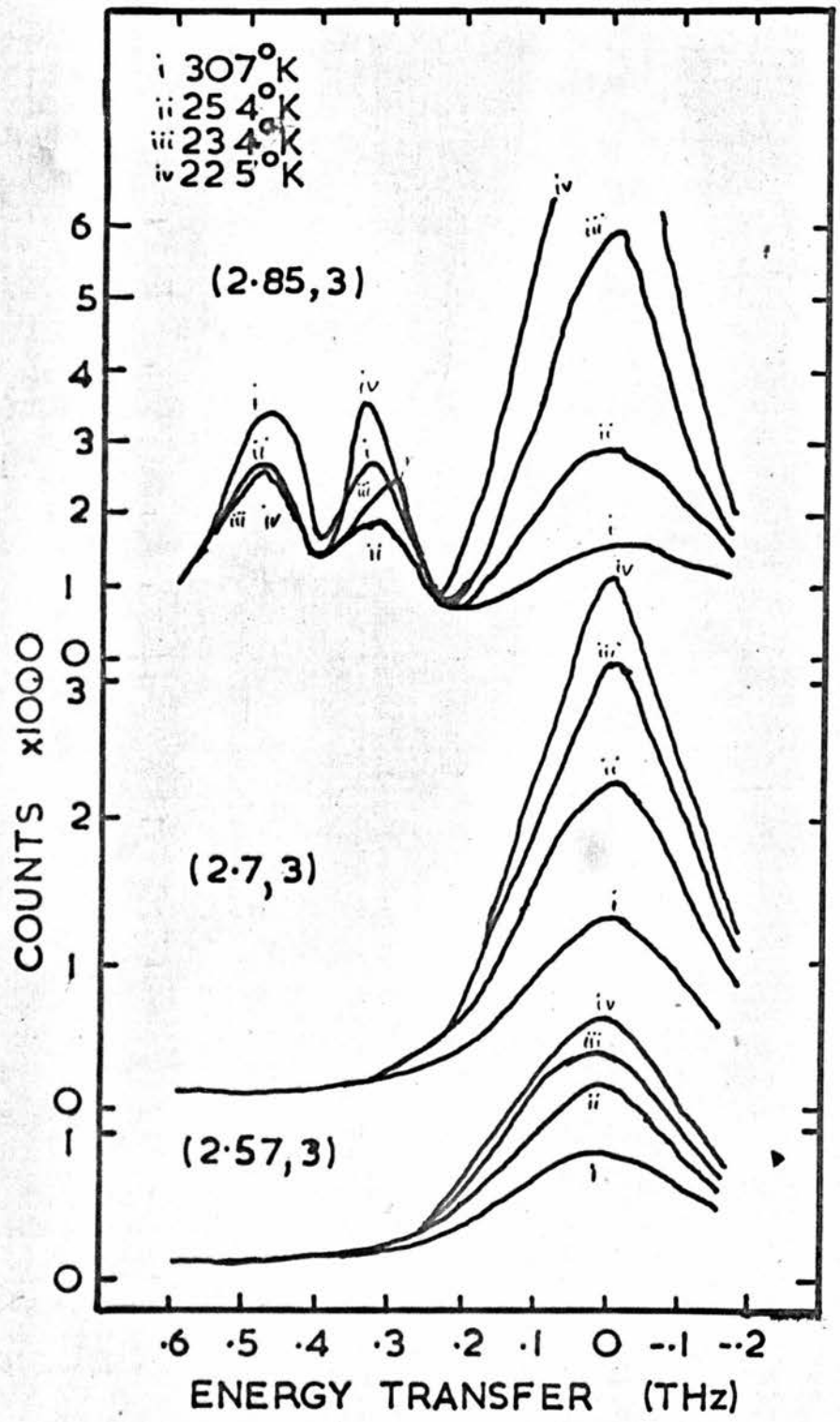
i 307°K
ii 254°K
iii 234°K
iv 225°K
(2·85,3)
(2·7,3)
(2·57,3)
COUNTS x1000
ENERGY TRANSFER (THz)
·6 ·5 ·4 ·3 ·2 ·1 0 -·1 -·2

Figure 2.8

The intensity of the quasielastic critical scattering along the line (ζ,3). The width of the Bragg peak is shown in the left hand side of the figure. The Bragg peak has been subtracted from the distributions shown on the right hand side, which illustrate the temperature dependence of the critical scattering.

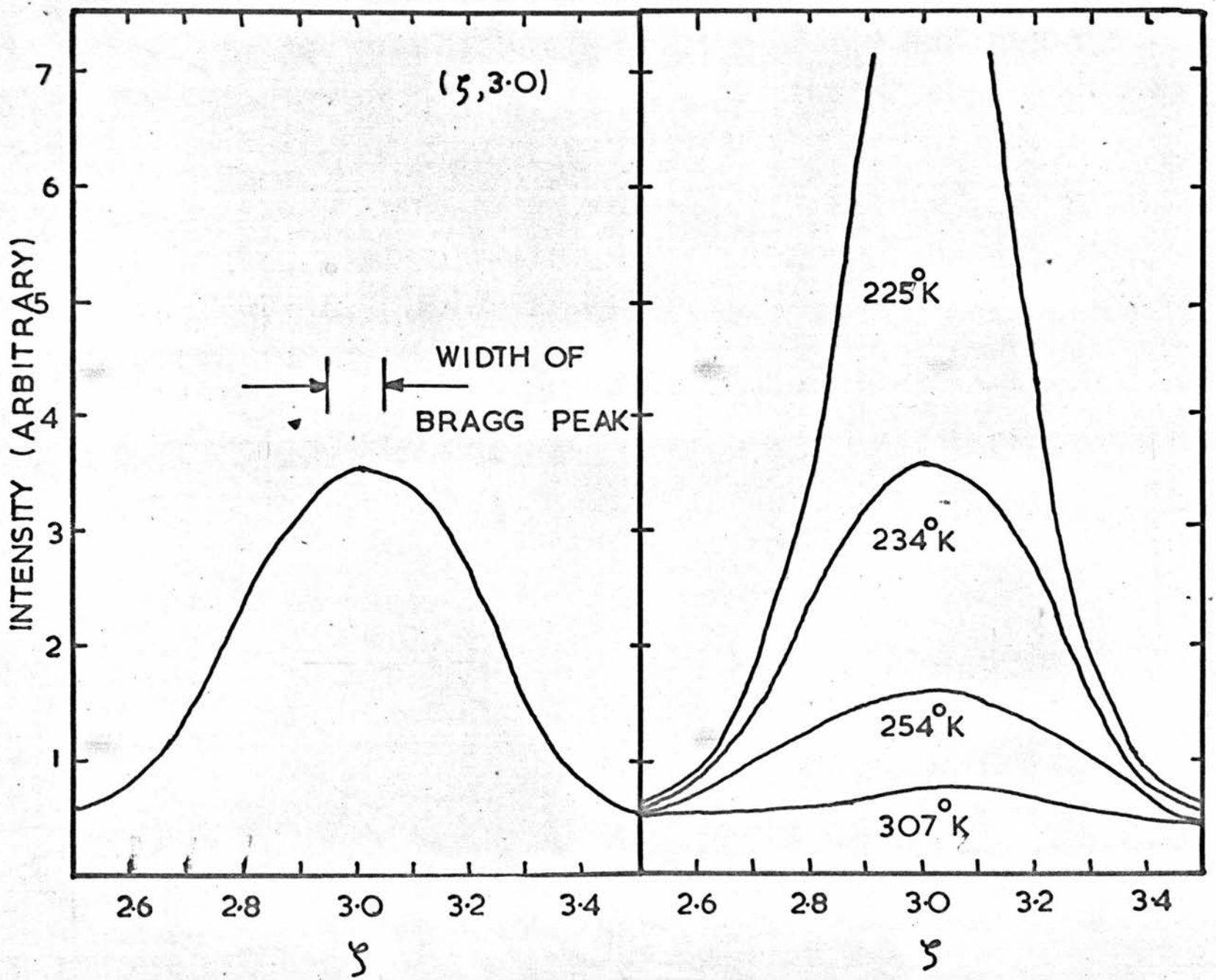
(5,3·0)
INTENSITY (ARBITRARY)
WIDTH OF
BRAGG PEAK
225°K
234°K
254°K
307°K
7
6
5
4
3
2
1
2·6
2·8
3·0
3·2
3·4
ζ
ζ

Figure 2.9

The intensity of the quasielastic critical scattering along the line (ζ , 3.1).

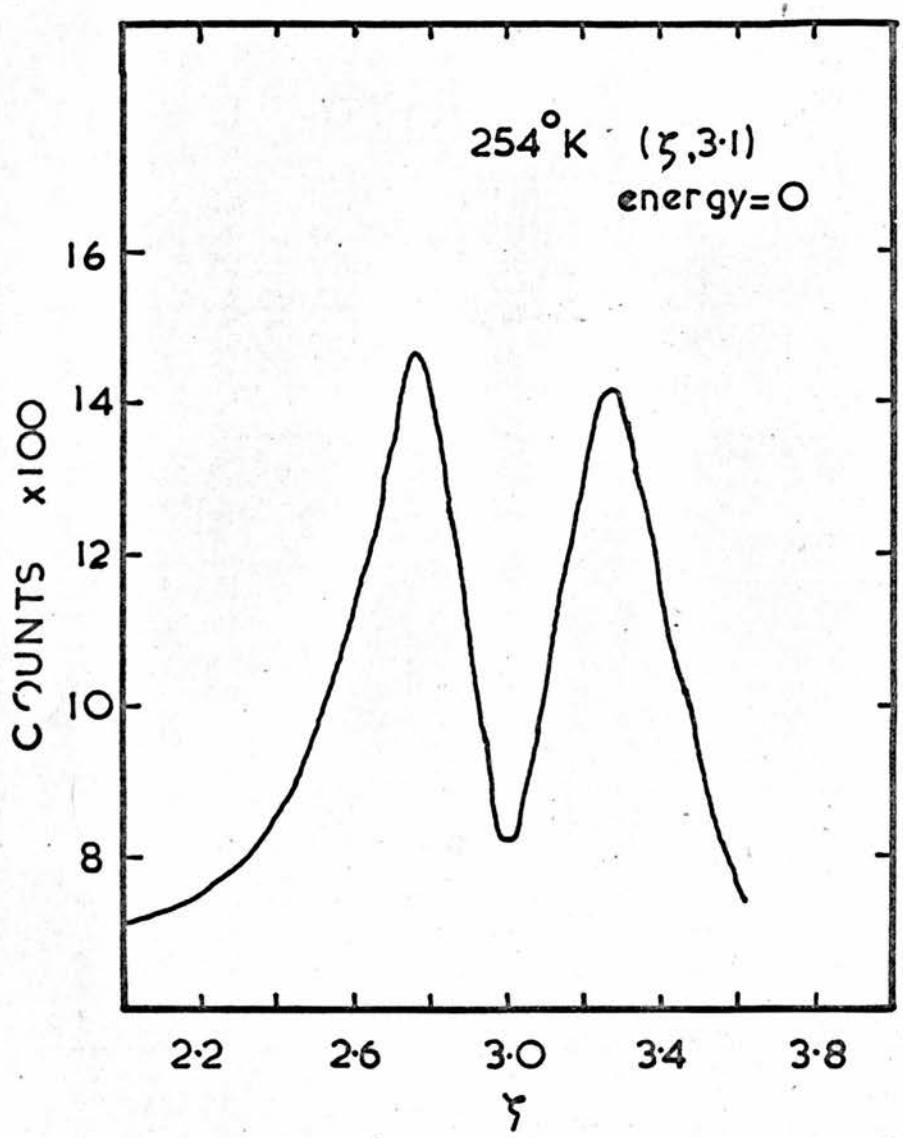
254°K (ζ,3·1)
energy=0
COUNTS x100
16
14
12
10
8
2·2
2·6
3·0
3·4
3·8
ζ

Figure 2.10

Distribution of the quasielastic critical scattering in the (ζ, η) plane around the reciprocal lattice point (3, 3). The contours are not equally spaced as can be seen by comparing figure 2.8.

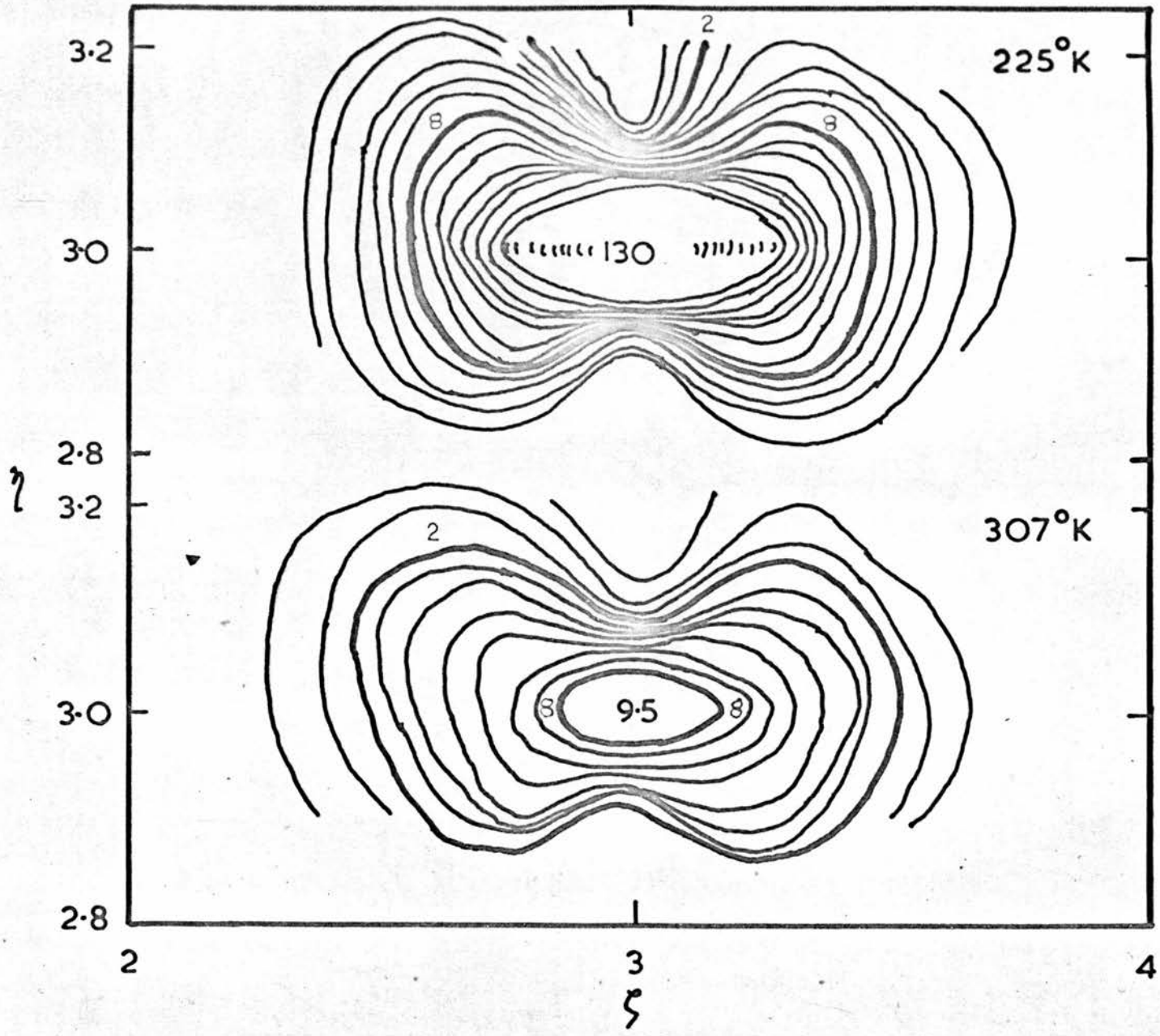
3·2
3·0
2·8
η
3·2
3·0
2·8
2
3
4
ζ
225°K
307°K
2
8
8
130
2
8
8
9·5

Figure 2.11

The energy distribution of neutrons scattered incoherently from KDP at 133°K with momentum transfers (3, 3) and (2, 2). The monitor count is 3×10^6 neutrons. The distribution at 143°K is not significantly different.

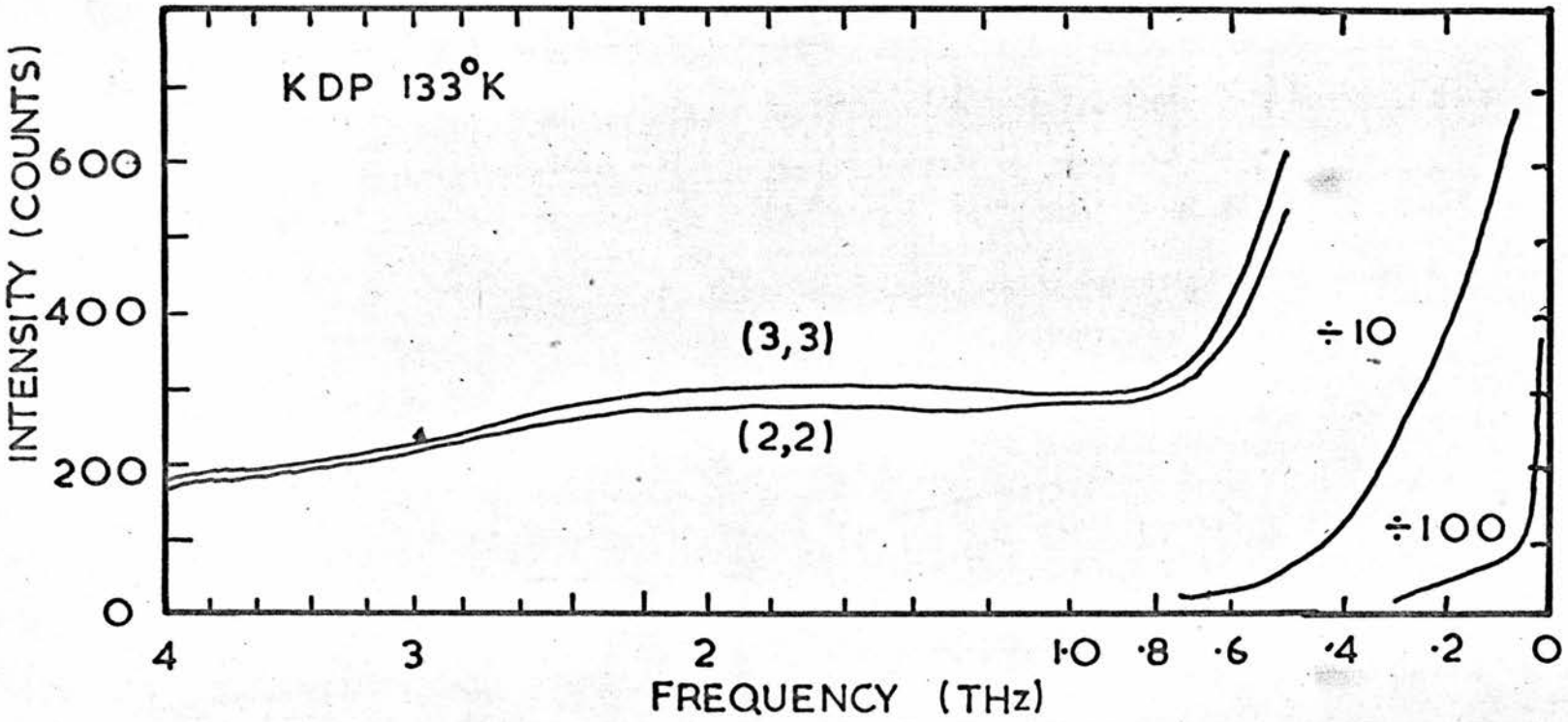
KDP 133°K
INTENSITY (COUNTS)
600
400
200
0
(3,3)
(2,2)
÷10
÷100
4
3
2
1·0
·8
·6
·4
·2
0
FREQUENCY (THz)

3. Calculations

3.1 Preliminary calculations

Before performing any experiments it was desirable to know around which reciprocal lattice points the scattering from the ferroelectric displacements would be strongest. The displacements were calculated from the difference between the structures of the ferroelectric phases with opposite polarisation. The z displacements were calculated by assuming that the centre of mass of the crystal does not move. The atomic coordinates and the displacements are given in table 3.1. The displacements between the structures of the paraelectric and ferroelectric phases as determined by neutron diffraction (Bacon and Pease, 1955) do not have the Γ_4 symmetry expected of the ferroelectric displacements (appendix 1), as the oxygen atom displacements are not exactly related by symmetry.

The structure factor used was that for one phonon scattering (Cochran and Cowley, 1967) at reciprocal lattice points ($\underline{\tau}$ or $hk\ell$)

$$F(\underline{\tau}) = \sum_k b_k(\underline{\tau})\, \underline{\tau}.\underline{u}(k) \exp(i\underline{\tau}.\underline{R}(k))$$

where the atoms k at $\underline{R}(k)$ have displacements $\underline{u}(k)$ and scattering lengths

$$b_k(\underline{\tau}) = b_k \exp(-0.25\,[B_1(k)(h^2+k^2)/a^2 + B_3(k)\ell^2/c^2])$$

including the Debye-Waller factors $B_i(k)$ of Bacon and Pease (1953) for the paraelectric phase. The Debye-Waller factors for the protons were

divided by the deuteron mass for conversion. The error involved in this assumption is not likely to effect any conclusion to be drawn from the calculation, indeed the temperature factors could be omitted without loss of confidence. In view of the relatively large displacements, however, an expression involving $\sin(\underline{\tau}.\underline{u})$ instead of $\underline{\tau}.\underline{u}$ would have been better for the deuterium atoms (chapter 4). The squared structure factors are given in table 3.2. The structure factors at 002, 200 and 400 are zero by symmetry. The difference between F_2 and F_3 shows at which reciprocal lattice points the scattering from motion along the hydrogen bond is important.

3.2 Phonon model calculations

All the models developed use the harmonic and adiabatic approximations described by Cochran and Cowley (1967). The potential energy in the crystal is written (omitting the constant term)

$$\phi = \tfrac{1}{2} \sum_{\substack{ll' \\ kk'}} \phi_{\alpha\beta}\left(\begin{matrix} ll' \\ kk' \end{matrix}\right) u_\alpha(lk)\, u_\beta(l'k')$$

The frequencies $\omega(\underline{q}j)$ and displacements of the atoms $\underline{e}(k\underline{q}j)/\sqrt{m_k}$ for each phonon $\underline{q}j$ and obtained from the dynamical matrix D

$$\sqrt{m_k m_{k'}}\; D_{\alpha\beta}\left(\begin{matrix} \underline{q} \\ kk' \end{matrix}\right) = \sum_{l'} \phi_{\alpha\beta}\left(\begin{matrix} ll' \\ kk' \end{matrix}\right) \exp(i\underline{q}.(\underline{R}(l'k') - \underline{R}(lk)))$$

$$\omega^2(\underline{q}j)\, e_\alpha(k\underline{q}j) = \sum_{k'} D_{\alpha\beta}\left(\begin{matrix} \underline{q} \\ kk' \end{matrix}\right) e_\beta(k'\underline{q}j)$$

The description of the forces acting in the crystal was limited to short range axially symmetric central forces and Coulomb forces between atoms. Although Coulomb forces were included and it would not have been difficult to construct a shell model description of the lattice it was thought that the final model was complicated enough without the introduction of further parameters.

The Coulomb coefficients were calculated using the expressions given by Born and Huang (1954) by a computer program written by Mrs. S. Cowley of A.E.C.L. The first calculations were for four atoms (2KP) and the second for twelve atoms ($2KPO_4$). The wave vectors used were in 0.2 reciprocal lattice unit steps in the Λ and Σ directions from the zone centre to the zone boundary, plus the wave vector 0.1 in each direction. For the zone centre the two wave vectors $aq_x/2\pi$ and $cq_z/2\pi = 0.00001$ were used, as the Coulomb coefficients can only be calculated in the limit $\underline{q} \rightarrow 0$. The sums in real and reciprocal space extended to 4 and 5 lattice units in each of the three orthogonal directions respectively.

The short range forces used were assumed to be derived from a potential $\phi(|\underline{r}|)$. They are therefore axially symmetric central forces given by the expression (Lehman et al., 1962)

$$-\phi_{\alpha\beta}\begin{pmatrix} \ell\ell' \\ kk' \end{pmatrix} = \frac{e^2}{2v}\left(\frac{A_{kk'} - B_{kk'}}{|\underline{r}|^2} r_\alpha r_\beta + B_{kk'}\delta_{\alpha\beta}\right) \quad \ldots\ldots\ldots\ldots 3.1$$

where $\underline{r} = \underline{R}(\ell'k') - \underline{R}(\ell k)$, v is the unit cell volume and e is the electron

charge, so that $A_{kk'}$ and $B_{kk'}$ are dimensionless, nearest neighbour force constants.

As every atom in the crystal is required to be in an equilibrium position and the crystal is required to be stress free, the potential function ϕ must be a minimum with respect to the coordinates of the atoms included in the calculation and with respect to the cell dimensions $\underline{a}$ and $\underline{c}$ (Born and Huang, 1954). For a crystal in which there are only short range axially symmetric central forces the equilibrium condition requires some relations to exist between the force constants $B_{kk'}$. When Coulomb forces are involved, however, the derivative of the Madelung energy (Born and Huang, 1954) is required. Although the Madelung constant is independent of the dimensions of the lattice it does depend on the atomic position. The derivative of the Madelung constant with respect to the hydrogen and oxygen coordinates is therefore required. This calculation was not performed and so the two, five or eight possible relationships (depending on the number of atoms in the model) between the products of the charges taken two at a time and the force constants $B_{kk'}$ were not obtained. A comparison of these conditions with the parameters fitted to the phonon dispersion relations would indicate the validity of the axially symmetric central force rigid ion model. The effect of omitting the equilibrium condition is that the acoustic gradients corresponding to the elastic constants c_{44} in the Λ and Σ directions do not have the correct ratio.

The elastic constants for DKDP are (Shuvalov et al., 1966) c_{11}, c_{12}, c_{13}, c_{33}, c_{44}, c_{66} (0.693, -0.078, 0.122, 0.545, 0.1265, 0.0594) x 10^{12} dynes/cm.^{2} (x 0.1 TN/m.^{2}). The corresponding acoustic gradients for the Λ and Σ directions are c_{33}, c_{44}; 6.66, 3.21THz and c_{11}, c_{44}, c_{66}; 6.96, 2.98, 2.04THz per reciprocal lattice unit respectively(see p.58).

The first model (2KP) was set up before the experimental work had commenced and was intended to indicate the frequencies of the optic modes by fitting the values of the elastic constants. The lattice was assumed to consist only of the potassium and phosphorus atoms. The oxygen atoms were completely disregarded, that is the PO_4 group was not taken as a rigid body. With the 2K and 2P atoms there would be 12 phonons for each $\underline{q}$ and these lattice modes would not include the expected low frequency rotational modes of the PO_4 group. Short range forces to nearest neighbours only were considered and the Coulomb forces were included with a charge of $\pm$ Z on each atom. The short range interactions were $(A_1, B_1)P - K$, $\underline{R}(P) - \underline{R}(K) = 0, 0, \frac{1}{2}$; $(A_2, B_2)P - P$, $0, \frac{1}{2}, \frac{1}{4}$ etc.; $(A_3, B_3)P - K$, $\frac{1}{2}, 0, \frac{1}{4}$ etc.

The elastic constants are given by the expression

$$c_{\alpha\gamma,\beta\lambda} = [\alpha\beta,\gamma\lambda] + [\beta\gamma,\alpha\lambda] - [\beta\lambda,\alpha\gamma] + (\alpha\gamma,\beta\lambda)$$

where the brackets are defined in terms of the long wavelength expansion of the dynamical matrix in a Taylor series (Born and Huang, 1954). For DKDP, using the symmetry relations and the relation imposed by the

equilibrium condition on the square brackets,

$$c_{11} = [11,11] + (11,11)$$

$$c_{12} = 2[12,12] - [11,22] + (11,22)$$

$$c_{13} = 2[13,13] - [11,33] + (11,33)$$

$$c_{33} = [33,33] + (33,33)$$

$$c_{44} = [22,33] + (23,23)$$

$$c_{66} = [11,22] + (12,12)$$

The square brackets involve only the second order term in the expansion of the dynamical matrix. The round brackets are a product of three terms, the inverse of the constant term and the first order term twice. These latter brackets are therefore fairly complicated, but are zero by symmetry for a crystal in which every atom is at a centre of symmetry. This is not the case for DKDP so that they must be determined.

In order to find the form of the elastic constants the expressions for the brackets were worked out omitting the force constants A_3 and B_3. The short range force parts of the square brackets were given by the expressions

$$[12,12] = 0$$

$$[11,22] = \frac{e^2}{2v} \quad \frac{2B_2}{c}$$

$$[11,11] = \frac{e^2}{2v} \quad \frac{2(4a^2 A_2 + c^2 B_2)}{c(4a^2 + c^2)}$$

and other similar expressions, where a and c are the unit cell dimensions.

The Coulomb sums calculated at reduced wavevectors 0.00001, 0.02 and 0.05 in the [100], [001], [110] and [101] directions enabled the Coulomb contributions to the elastic constants to be determined using the expressions given by Born and Huang (1954) for the long wavelength expansion of the Coulomb part of the dynamical matrix minus the macroscopic field term. The square brackets all contained a term proportional to Z^2 which was added to the short range part and they were therefore fairly simple. The round brackets, however, due to the inverse matrix had a complicated form which meant that the elastic constants could not be used to determine the parameters. The short range and Coulomb contributions to the first order term in the Taylor series expansion of the dynamical matrix on the present model showed that the brackets (33, 33), (12, 12) and (11, 33) were zero. The elastic constants c_{13}, c_{33} and c_{66} therefore had simple expressions, but the three were not enough to determine the four force constants and one charge.

Some expressions for the elastic constants in terms of only short range force constants for K-O and P-O interactions were derived by Evrard (1962). He used the resultant force constants to calculate the frequencies of the lattice vibrations of a rigid body PO_4 group model in the long wavelength limit. The ten frequencies obtained (Γ_1, Γ_2, $2\,\Gamma_3$, Γ_4, $5\,\Gamma_5$) (plus the two acoustic modes) were all between 4.2 and 8.4THz. These frequencies do not agree with the calculations on the

model described later which includes the Coulomb forces in the lattice.

Attempts were made to fit the simple model with force constants 1, 2 and 3 plus the ionic charge to the results of the preliminary phonon measurements described in section 2.2. The charges on the phosphorus and potassium ions were set equal to -1 and +1 respectively and a poor fit to the results was obtained by guessing values for the parameters to fit the acoustic gradients. When all seven parameters were varied in a least squares fit to the acoustic branches in the Λ and Σ directions, the ionic charge dropped from 1 to 0.2 (table 3.3). The results are shown in figure 2.2. As the results before the least squares were only fitted well at wave vectors less than 0.6, the drastic change in the ionic charge could be the result of an attempt to fit the zone boundary ends of the branches. It is not chemically reasonable that the potassium ion has a charge of 0.2 and so it may be concluded that either the model needs improving or that a false minimum was obtained in the least squares fit.

It seemed useful to consider a more realistic model in which all the atoms except the hydrogen atoms were included. Short range forces of the form equation 3.1 were included between (figure A1.1) K-O in the phosphate group $\pm c/2$ from K(A_1, B_1); O-O along the hydrogen bond (A_2, B_2); K-O, $\frac{1}{2}$, 0, $\frac{1}{4}$ etc. (A_3, B_3); and P-O (A_4, B_4). The Coulomb sums were calculated at the same reduced wavevectors as for the 2KP model so that charges on the K, P and O atoms could be considered. The

dynamical matrix for this model ($2KPO_4$) was 36 x 36 dimensional, but with the help of group theory this was reduced at most to 18 x 18 (table A1.5).

A model in which the long range Coulomb forces between K, P and O ions as well as short range K-O and P-O forces were included was used in an attempt to describe the phase transition in KDP (Grindlay and ter Haar, 1959). It was found that the parameters could not fit the data used, the susceptibility, transition temperature and Curie constant. The present model was designed to describe the phonon dispersion relations in the lattice and, based on the results of the 2KP model, it seemed sure of some success. The phase transition is considered in chapters 4 and 5.

The parameters A_4 and B_4 (P-O) could certainly not be fitted from the low frequency phonon data alone. It was intended to fit the parameters to the high frequency Raman and infra-red spectroscopic data on KDP and DKDP. The approximate frequencies of vibration of the free PO_4 ion were used to assign irreducible representations to the spectra. The irreducible representations to which the vibrations of a tetrahedron of four atoms in the point group $\bar{4}3m$ belong are Γ_1, Γ_3 and Γ_5. (The character table may be found in any book on group theory. Γ_3 is two dimensional and Γ_5 is three dimensional.) The frequencies are labelled ν_1, ν_2 and ν_4. When the tetrahedron is restricted to only $\bar{4}2m$ symmetry the representations are $2\,\Gamma_1(\nu_1 + \nu_2)$, $\Gamma_3(\nu_2)$, $\Gamma_4(\nu_4)$ and $\Gamma_5(\nu_4)$

(table A1.2). The rotations of the tetrahedron in $\bar{4}2m$ transform as Γ_2 and Γ_5 and the translations as Γ_4 and Γ_5. Now using the concept of product spaces discussed by Montgomery (1969), the vibration space for one tetrahedron is S_V, and it may be decomposed as above. This space corresponds to Montgomery's Euclidean space and is applied to the cell space which contains one tetrahedron at the origin and another at $(0, \frac{1}{2}, \frac{1}{4})$ in the space group $I\bar{4}2d$. This cell space therefore transforms in the same way as S_P (table A1.5), $\Gamma_1 + \Gamma_2$, and so the vibrations of the 4 oxygen atoms in KPO_4 transform as the product of the two spaces: $3\,\Gamma_1(\nu_1 + \nu_2 + \overline{\text{rot.}})$, $3\,\Gamma_2(\bar{\nu}_1 + \bar{\nu}_2 + \text{rot.})$, $3\,\Gamma_3(\nu_2 + \bar{\nu}_3 + \bar{\nu}_4)$, $3\,\Gamma_4(\bar{\nu}_2 + \nu_3 + \nu_4)$, and $6\,\Gamma_5(\nu_3 + \nu_4 + \text{rot.} + \bar{\nu}_3 + \bar{\nu}_4 + \overline{\text{rot.}})$ where rot. is a rotational mode and ν_3 comes from the translation of the oxygen atoms with respect to the rest of the lattice. $\bar{\nu}_i$ means that the two tetrahedra are vibrating in antiphase with approximately the same frequency as a free ν_i vibration.

For two later models the hydrogen atoms were also considered. The hydrogen vibrations in the lattice are classified as either stretching (ν) or bending (δ, γ) and each type of vibration occurs once in each irreducible representation.

The spectroscopic data were obtained mainly from Stekhanov and Popova (1966), Barker and Tinkham (1963), Blinc and Hadzi (1958) and Imry et al. (1965). The differences between the spectra of KDP and

DKDP enabled the proton and deuteron vibrations to be detected. Despite the closeness of other frequencies in the spectra some of these differences were surprisingly close to the $1/\sqrt{m}$ factor required. The assignments for DKDP of those frequencies selected from the spectroscopic data as reasonable values are given in table 3.4 together with the values calculated in the model described below. Data for DADP including the vibrations of the ND_4 tetrahedron are given in table 3.5, also with values calculated in another model described below.

The eigenvectors obtained from the early attempts to use the KPO_4 model showed that the oxygen atoms do indeed have displacements quite different from the phosphorus atoms in their PO_4 group. That this should be so is seen from the closeness of the frequency of the ν_2 type vibration (11THz) to the highest previously fitted 'lattice' mode (6THz).

Before the KPO_4 model was fitted to the phonon results two other models $2KD_4PO_4$ and $2ND_4D_4PO_4$ were investigated to see the effect of the deuterons in DKDP and DADP on the phonon spectrum. The ammonium ion ND_4 replaces the potassium ion for DADP and in both models the four other deuterium atoms are placed in the two equilibrium positions in each hydrogen bond. The coordinates for DADP were taken from the data of Tenzer et al. (1958) on ADP. The $q_z \rightarrow 0$ calculations only were performed for the two models so that the longitudinal Γ_4 modes only were obtained. The polarisation of the data was unknown, but it was

assumed that this point was unimportant for the purpose of roughly fitting the force constants. The Coulomb forces were included with all deuterons having zero charge and short range forces of the form equation 3.1 were used between the deuterium atoms and their neighbours: short and long O-D interactions in the hydrogen bond; and for DADP, one N-D interaction and two D-O terms corresponding to the two for K-O.

The parameters used in the calculation were close to those which gave a poor fit to the phonons for the $2KPO_4$ model. The remaining parameters were fitted to the frequencies by noting the eigenvectors, determining the derivatives of the frequencies with respect to each parameter and applying appropriate shifts. The ionic charges were assumed to be +5 and +1 for the phosphorus and potassium ions respectively, making the oxygen atoms -1.5 units. This assumption gives reasonable agreement with the spontaneous polarisation (Jona and Shirane, 1962). The parameters obtained are listed in table 3.6 and the results are in tables 3.4 and 3.5. The parameters (A_6, B_6) describing the long O-D contact in the hydrogen bond could not be fitted to the observations. A value was assumed for each, although they could probably have been set to zero without effecting the results greatly. The benefit of group theory was evident in the DADP model where the dynamical matrix 84 x 84 was reduced to square matrixes of size 9, 9, 11, 11 and 22. When the parameters were adjusted to give a poor fit to the low frequency modes, the

eigenvectors for these modes showed that the deuterons in the hydrogen bonds and those on the ND_4 ion do not have displacements very different from their nearest O or N atoms. The deuterons could therefore be neglected in any model calculations. This implies that the low frequency dispersion relations for KDP and DKDP will be identical and will also be very similar to the dispersion relations for ADP and DADP. The eigenvectors also showed that the characters of the modes whose frequencies are close (in one irreducible representation) are not well defined. The assignments given in tables 3.4 and 3.5 are therefore not unique.

3.3 Least squares fitting of phonon dispersion relations

Considerable difficulty was experienced in fitting the $2KPO_4$ model to the experimental results for the low frequency phonons in the Λ and Σ directions. Reasonable qualitative agreement with the phonons could be obtained by altering the parameters to their apparent best values. The least squares procedure to fit only the acoustic branches showed that the parameter space was not at all regular. The main problem in the fitting procedure stemmed from the fact that for each frequency $\omega(\underline{q}j)$ there is an eigenvector $\underline{e}(k\underline{q}j)$ defined for every atom k. Upon changing the parameters from one set of values to another it was found that at any wavevector the eigenvectors might alter dramatically (within the one irreducible representation) while the frequency would remain unchanged.

The least squares program was adapted from a general least squares program which had been translated by G. S. Pawley. The function minimised was the sum of the weighted squares of the differences between the observed and calculated squared frequencies

$$\sum_{\underline{q}j} W(\underline{q}j)(\omega_o^2(\underline{q}j) - \omega_c^2(\underline{q}j))^2 .$$

The weights $W(\underline{q}j)$ used were the inverse squares of the estimated standard deviation of the squared frequency.

$$W(\underline{q}j) = (2\,\omega_o(\underline{q}j)\,\sigma(\omega_o(\underline{q}j)))^{-2}$$

where $\sigma(\omega_o(\underline{q}j))$ is the estimated standard deviation of the observed frequency.

Group theory was of considerable use in classifying the observed frequencies. The calculations were performed at those wavevectors at which the Coulomb coefficients were known. The calculated frequencies were sorted numerically within each irreducible representation and this allowed unambiguous assignment of the frequencies of the acoustic branches in both the Λ and Σ directions, as well as of the lowest frequency Λ_{34} optic branch.

The P-O force constant of the $2KD_4PO_4$ model (table 3.6) was used in attempts to fit only the acoustic branches by varying the other parameters. It was found that the derivatives of the frequencies with respect to some parameters changed sign when other parameters were varied. This

implies that the parameters are correlated. It was also found that the elements of the correlation matrix could change sign with a change in parameters.

The least squares minimum fit to the neutron inelastic scattering data of table 2.2 is shown in figure 2.4. The parameters, which were refined in pairs in order to save time and in order to avoid correlations, are given in table 3.7. The correlations found in the last cycles of least squares were -0.32 (A_1:A_3), -0.33 (B_1:B_3), -0.28 (A_2:B_2), -0.24 (A_4:B_4) and 0.47 (Z_P:Z_K). The final parameter shifts were all less than 20% of the standard deviations, except for A_2 and B_2 whose final shifts were less than 2% of the parameter values. The parameters therefore do define a least squares minimum. The χ value which is equal to the square root of the minimised function divided by the number of observations was 1.6 for both Λ and Σ data, although the refinement showed that slightly better fits could be obtained for the data taken separately. 23 observations were used in the Λ data from Γ to M. 17 observations were used in the Σ data between reduced wavevectors of 0.1 and 0.8. The significance of the χ value is that it is a measure of the reliability of the estimated standard deviations.

The P-O force constants of the $2KD_4PO_4$ model had been fitted assuming ionic charges of +5, +1 and -1.5 for the P, K and O atoms respectively, but as the refinement progressed it became clear that the

final ionic charges would be considerably less than these formal values. The parameters A_4 and B_4 were refined to their final values with the ionic charges less than 0.2 standard deviations from their final values. The data used for the final refinement of these parameters was the same as that for the $2KD_4PO_4$ model and is shown with the calculated values in table 3.9. The calculated values of the transverse Γ_4 and longitudinal Γ_5 modes are also shown for comparison. The final χ value for the 18 data was 1.9, using standard deviations of 1THz for all frequencies. The four values marked * in table 3.9 do not have the required symmetry at Γ. The modes transform as either Γ_1 instead of Γ_4 or Γ_2 instead of Γ_3 and vice versa. However, as the parameters A_4 and B_4 had been refined from values close to those for the $2KD_4PO_4$ model, the final values represent the best values that can be reasonably obtained. Although some of the low frequency O-D modes in the $2KD_4PO_4$ model (table 3.4) are close to the phosphate group frequencies it is doubtful whether exclusion of these atoms in the $2KPO_4$ model would effect the phosphate group frequencies greatly.

It was obvious throughout the fitting that the simple axially symmetric central force, rigid ion model being used could not fit even the low frequency branches exactly. The observations at frequencies above 3.2 THz were therefore not included in the fitting. The branches included in the fitting were all of the acoustic branches, Λ_1, Λ_{34}, Σ_1, and 2 Σ_2,

the lowest frequency Λ_{34} branch and parts of the lowest frequency Λ_2 and Σ_1 branches.

The final parameters give reasonable agreement between the acoustic branch gradients as calculated at a reduced wavevector of 0.1 (6.57, 3.63, 7.19, 3.01 and 2.56THz) and the elastic constant values (6.66, 3.21, 6.96, 2.98 and 2.04THz) for the Λ_1, Λ_{34}, Σ_1 and $2\,\Sigma_2$ branches, or c_{33}, c_{44}, c_{11}, c_{44} and c_{66}, except for the Λ_{34} (c_{44}) and Σ_2 (c_{66}) values. The ratio of the c_{44} branch gradients is 0.83 which must be compared with the c/a ratio of 0.93. The force constants (B_i) and the ionic charges given in table 3.7 therefore do not yield a crystal in equilibrium. This disagreement may be seen, to some extent, as a failing of the model.

The only major differences between the neutron inelastic scattering data and the calculations are for the Σ_1 and higher Σ_2 acoustic branches. The observation at (0.75, 0) of a neutron group whose frequency appeared to be 2.02THz must, in view of the symmetries of the branches in this region, be interpreted as a superposition of two neutron groups whose energies lie between 1.9 and 2.1THz. The experimental results do indicate, however, that the two Σ_2 branches should have very similar energies near (0.75, 0), implying that two branches with the same symmetry but different characters wish to cross one another. Such a situation was not obtained with the model. It is thought that short range forces to other than nearest neighbours would not produce the desired

crossing, but that a shell model might produce a better fit. One other not unreasonable difference is that the second lowest M_{34} mode has too high a calculated frequency.

Of the remaining data in table 2.2 to which irreducible representations have not been assigned, it appears that the data near the zone boundary in the Λ direction at approximately 4THz could be from a Λ_1 branch. This then implies that the agreement of the flat Σ_1 branch at approximately 4.5THz with some data might not be meaningful. The neutron groups observed at approximately 3.4THz in both Λ and Σ directions may be the result of incoherent scattering from the sheet including the Λ_2 and Λ_1 branches compatible with the Γ_3 mode whose calculated frequency is 3.05THz.

The differences between the longitudinal (L) and transverse (T) Γ_4 and Γ_5 modes are of some interest. The L and T Γ_5 modes come from Σ_1 and Λ_{34} respectively, while the L and T Γ_4 modes come from Λ_1 and Σ_2 (table A1.4 for compatibilities). The frequencies are listed in table 3.8. A longitudinal mode cannot have a lower frequency than its transverse partner, and the difference between the squares of the frequencies is proportional to the square of the electric polarisation produced by the mode. It may therefore be said that there is very little polarisation associated with the modes whose frequencies are (Γ_4) 13.30THz and (Γ_5) 2.75, 5.64, 13.15, 13.38, 14.64THz. The

The 5.64THz L and T Γ_5 modes may be included here because their eigenvectors show that they have the same character and that they polarise the crystal very little. The eigenvectors also pair together the L and T 5.71 and 5.17THz Γ_5 modes whose polarisation is five times the magnitude of that for the 5.64THz modes. The frequencies calculated for the 5.64THz modes are, to one more significant figure, (L) 5.635 and (T) 5.638THz. These values do not follow the rule that a longitudinal phonon must have a higher frequency than its transverse partner. The fact that the 5.71 -5.17THz mode has the same symmetry as the 5.64THz mode means, however, that this result is allowed. When it is remembered that the ferroelectric displacements have Γ_4 symmetry, it is interesting to note that the model associates a large electric polarisation with the lowest frequency Γ_4 mode, (T) 5.04THz and (L) 5.64THz.

The values of the short range force constants in table 3.7 are of no real significance. It should, however, be mentioned that if the parameters represent a repulsive potential $|\underline{r}|^{-k}$, then the ratio A/B is expected to be -(k-1). The forces described by the simple model used are therefore not due to purely repulsive potentials.

The ionic charges (Z_k) which were determined are of considerably more interest. When the z-components of the ferroelectric displacements ($u_z(k)$) are considered, the spontaneous polarisation in the crystal may be determined

$$P_s = (v)^{-1} \sum_k Z_k u_z(k)$$

For the charges of table 3.7, $P_s = 1.68 \mu C/cm.^2$, while for the formal ionic charges +5, +1, -2 and +1 for the P, K, O and D atoms, $P_s = 5.42 \mu C/cm.^2$ which compares well with Bantle's (1942) measurement of $4.83 \mu C/cm.^2$. This discrepancy casts some doubt on the value of the model. Further doubt is cast on the model by the result that some of the sets of parameters, which were far from the least squares minimum values, produced dispersion relations which were qualitatively acceptable descriptions of the results. One of these sets of parameters had ionic charges of 4.2, 0.6 and -1.2 for the P, K and O atoms. The regions of poor fit were for the second Σ_2 acoustic branch and for the zone boundary ends of the lowest Λ_1, Λ_2 and Σ_1 branches. Another set of parameters with ionic charges of 5.2, 1.3 and -1.6 gave a better fit in the Σ direction. However, it was from these values that the final least squares minimum results were obtained.

These points show the difficulty in using the least squares procedure on a problem with highly correlated parameters, and of probably more importance in this case, a problem which is not only non-linear, but impossible to linearise. It is not known whether the minimum found in the parameter space is unique, or whether another minimum exists with more reasonable ionic charges, or indeed, with any other ionic charges.

A considerable amount of work would be required to investigate this point.

On the other hand the discussion may be interpreted as indicating the inadequacy of the model to describe the results. In this case it could be suggested that a better model be used. It is not obvious that next nearest neighbour forces would be of great assistance. Certainly the four protons at each equilibrium site of both hydrogen bonds could be introduced, if only to improve the O-O force constant, but it is felt that major improvement could only be obtained by introducing a shell model.

The results presented may be claimed to produce a least squares minimum fit to the observed data. It may therefore be stated that the simple axially symmetric central force, rigid ion model is able to describe the phonon dispersion relations in DKDP.

Table 3.1

Ferroelectric displacements

	coordinate			displacement x 10^2 (fractional units)		
	x	y	z	x	y	z
P	0	0	0	0	0	-1.0
K	0	0	0.5	0	0	0.6
O	0.149	0.0827	0.126	-0.620	-0.089	0.1
D	0.147	0.250	0.125	0	-2.605	0.25

Table 3.2

Squared structure factors for ferroelectric mode (h0ℓ) zone

reflection	$\|F_1\|^2$	$\|F_2\|^2$	$\|F_3\|^2$
004	175.73	70.44	70.44
101	30.30	26.17	2.58
103	1.92	0.07	45.66
105	363.86	299.84	126.23
202	0.03	0.54	0.54
204	4.69	27.23	27.23
301	461.17	436.37	1.59
303	435.44	509.19	12.83
402	6.58	0.10	0.10

The structure factor F_1 uses the displacements of table 3.1. F_2 has the deuterium z displacement set to zero and F_3 has no deuterium contribution.

Table 3.3

2KP model parameters

parameter	before least squares	after least squares
A_1	31	26.3
B_1	-1	3.4
A_2	13	13.1
B_2	13	4.8
A_3	46	34.2
B_3	-3.5	1.2
Z	1.0	0.2

Table 3.4

Selected observed frequencies (THz), assignments and calculated values for DKDP

Γ_1			Γ_2			Γ_3		
	obs.	calc.		obs.	calc.		obs.	calc.
ν	61.5	61.6	ν	61.5	63.4	ν	61.5	61.6
δ	36.0	36.5	δ	36.0	36.1	δ	36.0	37.6
γ	27.4	33.1	γ	27.4	33.2	γ	27.4	33.7
ν_1	27.5	27.5	$\bar{\nu}_1$	27.5	27.7	$\bar{\nu}_4$	33.8	32.5
$\overline{\text{rot}}$	20.0	19.3	rot	20.0	14.7	$\bar{\nu}_3$	17.1	21.9
ν_2	11.8	13.8	$\bar{\nu}_2$	11.8	11.2	ν_2	11.8	16.9

Γ_4			Γ_5			Γ_6		
	obs.	calc.		obs.	calc.		obs.	calc.
ν	61.5	63.4	ν	59.7	63.4	$\bar{\nu}_4$	33.5	32.7
δ	36.0	40.0	ν	53.1	61.7	ν_4	31.4	31.7
γ	27.4	33.3	δ	41.1	38.0	$\overline{\text{rot}}$	21.3	21.4
ν_4	32.7	32.6	δ	41.1	37.2	rot	15.6	18.2
ν_3	14.7	20.8	γ	28.5	34.1	$\bar{\nu}_3$	15.0	14.9
$\bar{\nu}_2$	11.4	12.5	γ	28.5	33.2	ν_3	13.5	12.2

Table 3.5

Selected observed frequencies (THz), assignments and calculated values for DADP

Γ_1			Γ_2			Γ_3		
	obs.	calc.		obs.*	calc.		obs.	calc.
ν_1	67.0	65.9	$\bar{\nu}_1$	67.0	65.9	$\bar{\nu}_4$	67.5	67.7
$\overline{\text{rot}}$	52.5	41.1	rot	52.5	41.2	$\bar{\nu}_3$	34.6	42.0
ν_2	38.4	35.8	$\bar{\nu}_2$	38.4	35.7	ν_2	38.4	36.2
ν	52.5	52.1	ν	52.5	53.8	ν	52.5	52.2
δ	34.6	33.4	δ	34.6	32.9	δ	34.6	30.9
γ	27.2	30.3	γ	27.2	30.4	γ	27.2	29.7
ν_1	27.2	25.7	$\bar{\nu}_1$	27.7	25.7	$\bar{\nu}_4$	33.9	34.7
$\overline{\text{rot}}$	26.4	17.4	rot	26.4	14.3	$\bar{\nu}_3$	17.1	19.7
ν_2	11.9	13.3	$\bar{\nu}_2$	11.9	10.6	ν_2	11.9	15.7

4			5			5		
	obs.	calc.		obs.	calc.		obs.	calc.
ν_4	67.5	67.7	$\bar{\nu}_4$	70.5	69.4	δ	38.4	34.3
ν_3	34.6	36.0	ν_4	70.5	66.6	γ	26.4	31.3
$\bar{\nu}_2$	38.4	42.0	$\overline{\text{rot}}$	52.5	47.0	γ	26.4	30.4
ν	52.5	53.8	rot	52.5	39.0	$\bar{\nu}_4$	33.0	29.9
δ	34.6	30.6	$\bar{\nu}_3$	34.6	35.8	ν_4	33.0	29.3
γ	27.2	29.8	ν_3	34.6	34.7	$\overline{\text{rot}}$	26.4	18.9
ν_4	33.0	36.9	ν	67.5	53.8	rot	26.4	16.4
ν_3	18.1	19.0	ν	58.5	52.2	$\bar{\nu}_3$	18.1	14.3
$\bar{\nu}_2$	11.9	11.9	δ	38.4	35.2	ν_3	18.1	12.0

Table 3.6

Parameters to fit high frequency modes

		$2KD_4PO_4$		$2ND_4D_4PO_4$	
		A	B	A	B
K-O	1	22	-1	22	-1
O-O	2	9	9	9	9
K-O	3	33	-3.5	33	-3.5
P-O	4	1650	-50	1800	-50
O-D	5	570	125	520	140
O-D	6	100	80	100	80
N-D	7	-	-	980	280
	Z_P	5		5	
	Z_K	1		1	
	Z_O	-1.5		-1.5	

Table 3.7

Best least squares parameters - $2KPO_4$

		A			B		
K-O	1	16.54	±	0.68	-0.94	±	0.14
O-O	2	15.21	±	0.82	5.67	±	0.22
K-O	3	43.0	±	2.6	-0.16	±	0.11
P-O	4	997	±	56	209	±	23
Z_P		1.73	±	0.31			
Z_K		0.893	±	0.030			
Z_O		-0.656	±	0.078			

Table 3.8

Longitudinal and transverse frequencies at Γ (THz)

($2KPO_4$ model)

Γ_4

L	T
5.64	5.04
13.30	13.30
17.34	17.07
34.01	33.48

Γ_5

L	T
2.75	2.75
5.64	5.17
5.71	5.64
13.15	13.15
13.38	13.38
17.01	16.80
17.58	17.51
33.86	33.73
34.28	33.88

Table 3.9

Least squares values of high frequency modes ($2KPO_4$ model)

Compare with $2KD_4PO_4$ model (table 3.4). The frequencies are in THz. The transverse Γ_4 and longitudinal Γ_5 calculated frequencies are shown for comparison.

Λ_1		$\Gamma_4(T)$	Λ_2	
obs.	calc.	calc.	obs.	calc.
11.4	13.3	13.3	11.8	13.0
11.8	13.3		11.8	13.6
14.7	14.0		17.1	14.4
20.0	17.3	17.1	20.0	17.5
17.5	25.2		27.5	25.1
32.7	34.0	33.5	33.8	33.5

Λ_{34}		$\Gamma_5(L)$
obs.	calc.	calc.
13.5	13.2	13.2
15.0	13.4	13.4
15.6	16.8	17.0
21.3	17.5	17.6
31.4	33.7	33.9
33.5	33.9	34.3

4. Analysis of Critical Scattering

4.1 The Ising model

The scattering described in section 2.3 is clearly connected with the ferroelectric transition in DKDP. It is similar in nature to the critical scattering observed near both the order-disorder transition in β-brass (Als-Nielsen and Dietrich, 1967) and the antiferroelectric transitions in $NaNO_2$ (Yamada and Yamada, 1966). The transitions in both of these crystals are describable by the order-disorder Ising model. However in $NaNO_2$ there is considerable dynamic character to the scattering, as shown by the dielectric constant (Yamada et al., 1968), and the dynamics of the Ising model which is discussed by Suzuki and Kubo (1968) has to be introduced. The dielectric susceptibility of DKDP has been measured as a function of frequency (Hill and Ichiki, 1963). The imaginary part of this susceptibility divided by the frequency (figure 4.1) shows that the neutron scattering from the excitations responsible for the susceptibility would be quasi-elastic, as found (figure 2.7). This relationship between the susceptibility and the power spectrum (neutron scattering in this case) which is derived from the fluctuation-dissipation theorem (Kubo, 1966) is discussed by Cochran (1969). The results for DKDP are therefore more like those of β-brass and a static Ising model will be used to describe the results.

In KDP type crystals there are four protons, each of which requires an order-disorder variable. The transition considered here is a ferroelectric one and so a simple model may consider only one fictitious spin variable ($S(\ell) = \pm 1$) for each primitive cell ℓ at $\underline{R}(\ell)$ which describes the electric polarisation P_S, along the $\underline{c}$-axis, associated with that cell. The unit cells ℓ and ℓ' interact with each other with an energy $I(\ell\,\ell')$ and the Hamiltonian for the system may be written

$$= \tfrac{1}{2} \sum_{\ell\ell'} I(\ell\,\ell')S(\ell)S(\ell')$$

$$= \tfrac{1}{2} \sum_{\underline{q}} I(\underline{q})S(-\underline{q})S(\underline{q})$$

in terms of the Fourier transforms in the N cell system

$$S(\ell) = \frac{1}{\sqrt{N}} \sum_{\underline{q}} S(\underline{q}) \exp(i\underline{q}.\underline{R}(\ell))$$

and therefore

$$I(\underline{q}) = \sum_{\ell} I(\ell\,\ell') \exp(i\underline{q}.(\underline{R}(\ell') - \underline{R}(\ell))).$$

The interaction matrix $I(\ell\,\ell')$ may be split into two parts, a short range part and a long range part from the Coulomb field in the lattice of dipoles. The Coulomb field itself is split into two parts, the macroscopic field and the inner field (Born and Huang, 1954), only the latter being regular as $\underline{q} \to 0$. The interaction matrix $I(\underline{q})$ is then written in terms of a regular part $J(\underline{q})$ and a term coming from the energy of the dipoles in the macroscopic field. Only the electric polarisation along the $\underline{c}$-axis is considered so that the macroscopic field and the dipoles, which are in a

medium of dielectric constant ϵ_L, are restricted to the $\underline{c}$-direction. The macroscopic field term in $I(\underline{q})$ for small wavevectors is $4\pi v P_S^2 \cos^2\alpha / \epsilon_L$ where α is the angle between $\underline{q}$ and the $\underline{c}^*$ axis. Then

$$I(\underline{q}) = J(\underline{q}) + 4\pi v P_S^2 \cos^2\alpha / \epsilon_L$$
$$= J(\underline{q}) + V_c \cos^2\alpha$$

The critical neutron scattering from this system arises from the displacements $\underline{u}(\underline{q}k)/\sqrt{m_k}$ of the atoms k with apparent charges Z_k at positions $\underline{R}(k)$ in the unit cell of the crystal. In the long wavelength limit the displacements produce the polarisation

$$vP_c = \sum_k Z_k \underline{u}(0k)/\sqrt{m_k}.$$

The mass factor is included here for consistency with the model in chapter 5 in which the neutron scattering function is discussed. For the simple model of this chapter the scattering function

$$\mathcal{S}(\underline{Q}) = N |F(\underline{Q})|^2 \langle S(-\underline{q})S(\underline{q})\rangle \qquad \ldots\ldots\ldots\ldots\ldots 4.1$$

where

$$F(\underline{Q}) = \sum_k b_k(\underline{Q}) \exp(i\underline{\tau}.\underline{R}(k)) \sin(\underline{Q}.\underline{u}(\underline{q}k)/\sqrt{m_k}) \qquad \ldots\ldots\ldots\ldots\ldots 4.2$$

summed over all atoms in the unit cell. The correlation function

$$\Gamma(\underline{q}) = \langle S(-\underline{q})S(\underline{q})\rangle$$
$$= (1 + \beta I(\underline{q}))^{-1}$$

in the random phase approximation (Brout, 1965) with the inverse temperature $\beta = 1/k_B T$ and k_B is Boltzmann's constant. $b_k(\underline{Q})$ is the temperature factor modified scattering length for the k th atom and $\underline{\tau} = \underline{Q} + \underline{q}$ is a reciprocal lattice vector.

4.2 The structure factor

The variation of the critical scattering intensity from one reciprocal lattice point to another should be described by $F(\underline{\tau})$ of equation 4.2. Estimates of the intensities were made by the method described in chapter 2 near ten reciprocal lattice points, at three of which (002, 200, 400) the experimental estimates were zero agreeing with the expected Γ_4 symmetry of the displacements.

The ferroelectric displacements only qualitatively fit the observations at 233.7°K as can be seen from model 1, table 4.1. A model of the eigenvectors to fit the seven intensities for the Γ_4 mode must include x, y and z displacements for the oxygen atoms, y and z displacements for the hydrogen atoms and z displacements for the phosphorus and potassium atoms. It was found that the oxygen x displacement could not be determined as it gave only very small contributions to the structure factors at the points measured. The oxygen y displacement was found to be almost as badly determined and so these parameters were omitted from the calculations. The expression used for fitting the data was that given in

section 3.1 rather than equation 4.2. The difference between the expressions did not exceed 8% for each of the parameters determined.

In table 4.1 the measured intensities and their standard deviations are given. The calculated values 1 are from $|F_1|^2$ in table 3.2 scaled by a factor of 11.8 to the 303 reflection. Assuming that the ferroelectric displacements do fit the intensities the displacements in the other models may be defined in absolute terms. Calculated values 2, 3 and 4 are from least squares fits to the data. With the standard deviations from counting statistics alone the χ value for the difference between the observed and calculated structure factors squared was 5.1, 8.4 and 8.4 for calculations 2, 3 and 4.

The displacements determined in the calculations are listed in table 4.2 with their standard deviations. The final shifts in the parameters did not exceed 4% of their standard deviations, so that each model represented a least squares minimum fit. The ferroelectric displacements from table 3.1 are also included for comparison. The oxygen atom displacements are omitted completely in calculations 3 and 4. As the displacements are defined in absolute terms, assuming that model 1 produces a reasonable fit, the spontaneous polarisation arising from each model may be calculated. The polarisation was calculated using the formal charges +5, +1, -2 and +1 for the P, K, O and D atoms, $P_s^{(1)}$, and also using the ionic charges determined in the least squares fit to the

phonon dispersion relations, $P_s^{(2)}$. The results are given in table 4. 2. The least squares charges give unsatisfactory results, except for case 4. The formal charges give unsatisfactory results altogether, except for the ferroelectric displacements calculated from the crystal structure.

An interesting feature of the analysis is that two different sets of potassium and phosphorus displacements together with the one deuterium displacement yield exactly the same calculated intensities (models 3 and 4). This implies that more data is required to find which is the true least squares minimum. The results of calculation 2 in which all the z-displacements are positive indicates again that more data is required. It may, however, be concluded from table 4. 2 that the y displacement of the deuterium atom (along the hydrogen bond) plays an important role in the ferroelectric critical scattering.

An interesting alternative method of interpreting the intensities is based on the Patterson synthesis of X-ray crystallography. The sum

$$P'(\underline{r}) = \sum_{\underline{\tau}} |F(\underline{\tau})|^2 \cos(\underline{\tau}.\underline{r})$$

was computed, where $|F(\underline{\tau})|^2$ were taken as the observed intensities. The crystallographic Patterson function is a self convolution function of the scattering density. The function $P'(\underline{r})$ is a weighted self convolution function of the scattering density (Cochran, 1968), in which the weights are a function of the eigenvectors for the mode involved. $h0\ell$ data only

were used and the resultant projection of $P'(\underline{r})$ on the (010) plane is shown in figure 4.2. The coordinates marked on the map are delta functions in the self convolution of the scattering density, disregarding oxygen atoms, and placing deuterium atoms at the centre of their bonds. The map is obviously dominated by the 303 intensity. Even when the symmetry information for the Γ_4 mode was considered it was impossible to derive any information from the map. Further measurements throughout reciprocal space would be required before either this method or a fitting procedure could produce meaningful eigenvectors. A similar lack of data was also evident in the analysis of the quasielastic scattering from DADP (Meister et al., 1969), although there were 29 h0ℓ observations available. The symmetry of the M_{34} antiferroelectric mode in this case would be of some assistance, together with a knowledge of the superpositions occurring in the self convolution function.

4.3 q-space distribution and temperature dependence

The extensive measurements of the critical scattering near the reciprocal lattice point 303 were described in section 2.3. The $\underline{q}$-space distribution of the scattering arises from both terms in equation 4.1, the correlation function $\Gamma(\underline{q})$ and the structure factor $F(\underline{Q})$. As the critical scattering arises from a ferroelectric mode the eigenvectors $\underline{u}(\underline{q}k)$ for $\underline{q} \rightarrow 0$ are not independent of the direction of $\underline{q}$ as discussed in chapter 5. This effect will be neglected here and no model will be put forward for the

eigenvectors. It therefore remains to fit the observed data to the correlation function $\Gamma(\underline{q})$ and to find $I(\underline{q})$ and $|F(\underline{Q})|^2$ from the fitting.

The resolution of the data was good enough to enable the Bragg peak to be subtracted. A Gaussian resolution function was fitted to the Bragg peak and this enabled the deconvolution of the data along the line $(\zeta, 3)$. The intensities most effected by the deconvolution were at wave vectors greater than 0.6, where errors due to counting statistics and background were greatest. The instrumental resolution thus had no great effect on the data. This conclusion was confirmed by measurements at higher resolution which yielded data not significantly different from that analysed here (R.A. Cowley and W.J.L. Buyers, private communication).

The background scattering was assumed to be constant over the whole zone around (3,3). The incoherent elastic scattering is expected to be almost constant within this region. There are, however, four protons in the primitive cell and there are therefore four fictitious spin modes, as described in chapter 5. Two of these modes at $\underline{q} = 0$ will give rise to $\underline{a}$-axis ferroelectric fluctuations. As there are no low frequency phonons in DKDP, the moderately high dielectric constant (60) in the $\underline{a}$-direction (Kaminow, 1965) may have a large contribution from the two degenerate fictitious spin modes which would scatter neutrons quasielastically. This scattering, although not greatly temperature dependent may be expected to have a dumbbell shape in the $\underline{a}^*$ - $\underline{c}^*$ plane near $\underline{q} = 0$ similar

to that observed for the c-axis critical scattering, but with the axes interchanged. The fourth mode also would be expected to scatter quasi-elastically as there was no evidence of it at higher energies. Although above 15°C the a-axis dielectric constant in DKDP is greater than that of the c-axis (Kaminow, 1965), the critical neutron scattering at 34°C retains the dumbbell shape observed at approximately -50°C. The neutron scattering from the a-axis fluctuations must therefore be fairly weak.

It is desired to determine the function $I(\underline{q})$, but the value of the background to be subtracted has a considerable effect on this function. The scattered intensity $S(\underline{q})$ is proportional to $\Gamma(\underline{q})$ and, with a background B may be written

$$S(\underline{q}) = \frac{A}{1 + \beta I(\underline{q})} + B \qquad \ldots\ldots\ldots\ldots\ldots 4.3$$

which may also be written

$$S(\underline{q}) = \frac{A'}{T + I(\underline{q})/k_B} + B' \; ; \; B' = A + B \; ; \; A' = -AI(\underline{q})/k_B \qquad \ldots\ldots\ldots\ldots\ldots 4.4$$

Equation 4.4 describes the relation that the inverse intensity, corrected for background B' is proportional to temperature, while equation 4.3 says that the inverse corrected intensity (-B) is proportional to inverse temperature β. The normally selected background would be B' such that it is the lowest intensity recorded in the Brillouin zone, assuming that the structure factor is not a function of $\underline{q}$. However the true background

$B = B' - A$, the difference arising from the fact that the high temperature limit of the critical scattering is not zero, as assumed when choosing B', but is A. This scattering corresponds to incoherent scattering from a completely uncorrelated order-disorder system.

For small wavevectors the correlation function $\Gamma(\underline{q})$ has the Lorentzian form $\frac{1}{K^2 + q^2}$ with an inverse correlation length K, $K^2 \propto 1 + \beta I(0)$. The pair correlation function resulting in this form for the scattering is the Ornstein-Zernike correlation function e^{-Kr}/r (Brout, 1965). The function $\Gamma(\underline{q})$ is however not isotropic due both to the Coulomb term in $I(\underline{q})$ and to the anisotropy of the lattice. The pair correlation function is then the Fourier transform of $\Gamma(\underline{q})$ and will itself be anisotropic. Qualitatively, the dumbbell shape of the scattering is then interpreted as showing large correlation along the z-axis (corresponding to considerable scattering in the $\underline{a}^* - \underline{b}^*$ plane) and much smaller correlation in the (001) plane, ~~arising from the polarisation set up by the mode~~ (corresponding to the lack of scattering along $\underline{c}^*$). The width of the scattering at 224.7°K along the line $(\zeta, 3)$ was approximately $(\zeta =)$ 0.41 or $(\underline{q} =)$ 0.37 Å^{-1} FWHM increasing to 0.52 Å^{-1} at 307.2°K. The transition temperature of the crystal was measured as 223.6°K, the temperature at which the intensity of the scattering at the point (3.15, 3) was a maximum. It was found that a Lorentzian distribution would not fit the scattering along the line $(\zeta, 3)$. The inverse background corrected

intensity at 224.7°K was fitted to a quartic function

$$(S(\underline{q}) - B)^{-1} \propto K^2 + q^2 + C^2 q^4$$

with K = 0.24 or 0.22 Å^{-1} and C = 5.4 or 6.0 Å. This expression is shown with the data in figure 4.3. The extent of the correlation along the c-axis in DKDP is made clearer when the results are compared with the true Lorentzian function found in β-brass with K = 0.06 Å, 9°K above its transition temperature (Als-Nielsen and Dietrich, 1967). The pair correlation function in DKDP along the c-axis is therefore not of the Ornstein-Zernike form and the order that does exist is of much shorter range than that in β-brass.

The most extensive measurements of the critical scattering as a function of temperature were made at (3.15,3). Of the 109 observations only 15 were more than 6°K above the transition temperature T_{tr} ($k_B T_{tr} > - I(\underline{q})$). The data were fitted to expressions 4.3 and 4.4 and it was found that B' = 620 ± 50 and B = 460 ± 70 with $-I(\underline{q})/k_B$ = 214.2 ± 0.4°K. Attempts to fit the data with a $\Gamma(\underline{q}) = (1 + \beta I(\underline{q}))^{-\gamma}$ (Brout, 1965) yielded a γ of 0.98, which could not be distinguished from 1. The random phase approximation for $\Gamma(\underline{q})$ is therefore adequate to describe the results. In all the analyses the higher temperature data were not well described. A smaller background value was required to fit these points.

Plots of inverse background corrected intensity against inverse

temperature at wavevectors along the line (ζ, 3) indicated that the data for the highest temperature measured, 307°K, required a smaller background count (assuming, of course, that expression 4.1 does describe the scattering). This disagreement could have been caused by a temperature dependent background, or by a $\underline{q}$-dependent background plus inaccuracy in subtracting the Bragg peak. The latter reason would yield large errors in the small intensity at the high temperature.

Provided that the background is not temperature dependent it may be eliminated altogether from the analysis, together with any $\underline{q}$-dependence that it may have, by the choice of one set of intensities at a particular temperature as the datum. The inverse of the difference between the intensities when plotted against the inverse of the difference between the temperatures at one particular wave vector should yield a straight line. This arises from equation 4.3, with $T(\underline{q}) = -I(\underline{q})/k_B$,

$$\frac{1}{I_1 - I_2} = \frac{T_1 - T(\underline{q})}{A\,T(\underline{q})} \left(\frac{T_1 - T(\underline{q})}{T_2 - T_1} + 1 \right)$$

The two degrees of freedom of the straight line give $T(\underline{q})(I(\underline{q}))$ and $A(N\,|F(\underline{Q})|^2)$. Unfortunately this method of analysis yielded results at (3.15, 3) of 213.3 $\pm$ 0.5°K and 573 $\pm$ 50 with the standard intensity at 307.2°K, and 217.8 $\pm$ 0.7°K and 330 $\pm$ 20 with the standard at 224.7°K. These values compare with an analysis of the same data using $B' = 620$ and equation 4.3, yielding 215.2 $\pm$ 1.0°K and 412 $\pm$ 40. The errors

given here are estimated from the plots and are conservative. The differences between the results indicate that the background may be temperature dependent, although considerably more accurate data would be required to investigate this hypothesis. The differences also indicate that the background value used is a cause for some concern. Using the data from several wavevectors, the inverse intensity not corrected for background was plotted as a function of inverse temperature. It was found that the 307°K data still required some correction for a smaller background. For the point (2.8, 3.15), the reciprocal intensity and reciprocal intensity corrected for a background of 200 were plotted against reciprocal temperature. The 307°K point was ignored in the latter plot. The resultant straight lines produced values of 139 $\pm$ 4°K for T($\underline{q}$) from both analyses and 400 $\pm$ 30 and 300 $\pm$ 30 respectively for A. The errors in the results are thus great enough to yield the same extrapolated value of inverse temperature, requiring only a different slope, or structure factor, for the different backgrounds. The background, within this range, is therefore unimportant for the determination of I($\underline{q}$). The main interest in this analysis is the function I($\underline{q}$) and, as the zero background enabled the 307°K data to be considered when attempting the linear fits, the inverse intensities were plotted without correction for background.

The experimental results were recorded along the lines (ζ, η) in 0.05 unit steps of ζ running from 2.05 to 3.7. The η values were 2.9

and 3.0 in steps of 0.05 to 3.2. The data along the lines (ζ, 3), (2.4, η), (2.6, η), (2.8, η), (2.9, η), (3.0, η) were analysed to yield I($\underline{q}$) and $N|F(\underline{Q})|^2$. Some of the plots of inverse intensity against inverse temperature are shown in figure 4.4 The resultant values of I($\underline{q}$) and $N|F(\underline{Q})|^2$ are shown in figures 4.5 and 4.6.

The structure factor remains constant throughout the region measured, with the exception of a significant anomaly at small wave vectors along the $\underline{c}^*$-axis near the centre of the Brillouin zone. This anomaly may be predicted in a microscopic model (chapter 5) and is the result of the variation of the eigenvectors of a ferroelectric mode with the direction of the wavevector.

The short range part of the interaction I($\underline{q}$) may be written to next nearest neighbours in the body centred tetragonal cell

$$J(\underline{q}) = J_0 + 8J_1 (1 - \cos(q_x a/2)\cos(q_y a/2)\cos(q_z c/2) + \\ + 2J_2(2 - \cos(q_x a) - \cos(q_y a)) + \\ + 2J_3(1 - \cos(q_z c)).$$

Using nearest neighbour (NN) interactions only the results along the line (ζ, 3) were fitted quite well, although a significant improvement was made by including next nearest neighbours (NNN). The fits which are not least squares calculations are shown in figure 4.5 and the parameters are given in table 4.3. The errors in the parameters represent the limit of

reasonable fits to the data.

The results along the lines parallel to $\underline{c}^*$ involved the Coulomb interaction V_c. Figure 4.5 shows that the data along the line (3.0, η) must be affected by the resolution function of the instrument and also by the subtraction of the Bragg peak. The accuracy of the data along the line (2.4, η), where the observed intensities were of the order of 700 counts, is better judged by the fit to the calculation rather than by the error bars. The remaining data could only give a reasonable fit to the nearest neighbour model parameters from the (ζ, 3) fit with the parameter V_c varying from one line to another. This variation was removed by using the NNN model parameters determined from the (ζ, 3) fit and using as well the parameter J_3. Both fits are shown in figures 4.6 and table 4.3.

There is no structural reason for the parameter J_3 to be greatly different from J_2. It is required to be large to fit the wide variation of V_c in the NN model. It might be thought that this variation of V_c could be reduced by introducing a background count, but the analysis of the (2.8, 3.15) data indicated that this would be of little assistance.

A next nearest neighbour model for the short range interaction can therefore describe the quasielastic scattering results quite well. Qualitatively the critical scattering itself indicates, and the analysis shows,

a ferroelectric transition with a minimum in $J(\underline{q})$ at $\underline{q} = 0$. The significance of the parameters J_1, J_2 and J_3 can not be determined as no microscopic model has been proposed. The parameter J_0 ($-222 \pm 2^{\circ}K$), on the other hand, represents the Curie temperature for the ferroelectric transition. This value is very close to the measured transition temperature of the crystal ($223.6^{\circ}K$). The difference between the free and clamped Curie temperatures and the transition temperature is discussed in chapter 6. The value of the Curie temperature is in very good agreement with the value $222 \pm 1^{\circ}K$ determined from the low frequency dielectric constant for high purity DKDP by Sliker and Burlage (1963). The neutron scattering results described in chapter 2 suggest that there may be some hydrogen in the crystal, but the analysis here shows that the crystal is of high purity and could be claimed to be fully deuterated within an error of 3%.

The critical scattering results give no evidence of any temperature dependent scattering at the zone boundary M. This is the point at which the critical scattering from DADP is strongest (Meister et al., 1969), corresponding to an antiferroelectric phase transition in which the displacements have M_{34} symmetry. Figure 5.1 shows the compatibilities, implying that strong scattering would be expected along the line (ζ, 3) from Γ(3, 3) to M (2, 3) if there were any tendency to antiferroelectricity in DKDP.

4.4 Dielectric constant

As discussed in section 4.1 the fluctuation-dissipation theorem may be used to relate the dielectric susceptibility and the power spectrum. Integration over frequency then yields the static dielectric constant in terms of the correlation function $\Gamma(\underline{q})$ for the fictitious spin model (Cochran, 1969)

$$\epsilon(0) = \epsilon_L + 4\pi v P_S^2 \beta \Gamma(0)$$

This equation shows that the Curie temperature derived from the static dielectric constant, $T_c = -J_0/k_B$ and the Curie constant

$$C = \frac{4\pi v P_S^2}{k_B} = \frac{\epsilon_L V_c}{k_B} .$$

The expression for the dielectric constant shows again that the random phase approximation for $\Gamma(\underline{q})$ is sufficient.

The values of the Curie constant and the dielectric constant due to the lattice are 4040°K (Samara, 1967) and 7.1 or 8.9 for the c- or a-axis, estimated from the mode strengths of Barker and Tinkham (1963). The values of the high frequency dielectric constant for the c- and a-directions were assumed to be 3 (as for KDP) and zero. Taking ϵ_L for the c-axis, $V_c = 568°K$. The fact that the value determined from the analysis is too low by a factor of four may mean that the model for the Coulomb inter-

actions, which is only valid for small wavevectors, has been extended too far. A more complete model such as that described in the next chapter would be required to study this point.

Table 4.1

Squared structure factors for the ferroelectric mode

reflection	observed	calculated model		
		1	2	3, 4
101	170 ± 50 (13)	353	87	116
103	490 ± 50 (22)	23	527	448
202	10 ± 40 (3)	0.4	29	112
204	1800 ± 60 (42)	55	1800	1800
301	1770 ± 60 (42)	5420	1846	2056
303	5130 ± 80 (71)	5130	5082	4679
402	480 ± 50 (22)	77	451	524

The observed values are the measured intensities with their standard deviations estimated from the counting statistics plus background, or () counting statistics alone.

Table 4.2

Calculated ferroelectric displacements

x 10^2 fractional units

atom		displacements			
		model			
		1	2	3	4
P	z	-1.0	0.66 ± 0.12	0.52 ± 0.17	-1.26 ± 0.17
K	z	0.6	0.12 ± 0.18	-0.05 ± 0.26	-2.75 ± 0.26
O	x	-0.620	0	0	0
	y	-0.089	0	0	0
	z	0.1	0.16 ± 0.08	0	0
D	y	-2.605	1.27 ± 0.05	1.30 ± 0.08	1.30 ± 0.08
	z	0.25	0.73 ± 0.10	0.85 ± 0.10	0.85 ± 0.10
$P_s^{(1)}$ (μC/cm.^{2})		5.42	-4.16	-4.90	8.36
$P_s^{(2)}$ (see p. 76)		1.68	-0.96	-0.98	5.34

P_s experiment 4.83 μC/cm.^{2}

Table 4.3

Ising model parameters (^{o}K)

model	NN	NNN
J_o	-222 ± 2	-222 ± 2
J_1	7.7 ± 0.5	9.9 ± 0.7
J_2	0	-3.5 ± 1
J_3	0	23 ± 10
V_c (2.4, η)	600 ± 100	140 ± 20
(2.6, η)	300 ± 20	
(2.8, η)	210 ± 20	
(2.9, η)	175 ± 20	
(3.0, η)	140 ± 20	

Figure 4.1

Frequency width of the critical scattering. The imaginary part of the susceptibility ($\chi''(\omega)$) is from Hill and Ichiki (1963). The neutron scattering is proportional to $\chi''(\omega)/\omega$. The energy resolution of the spectrometer in the best experiments in chapter 2 was 0.26THz (FWHM).

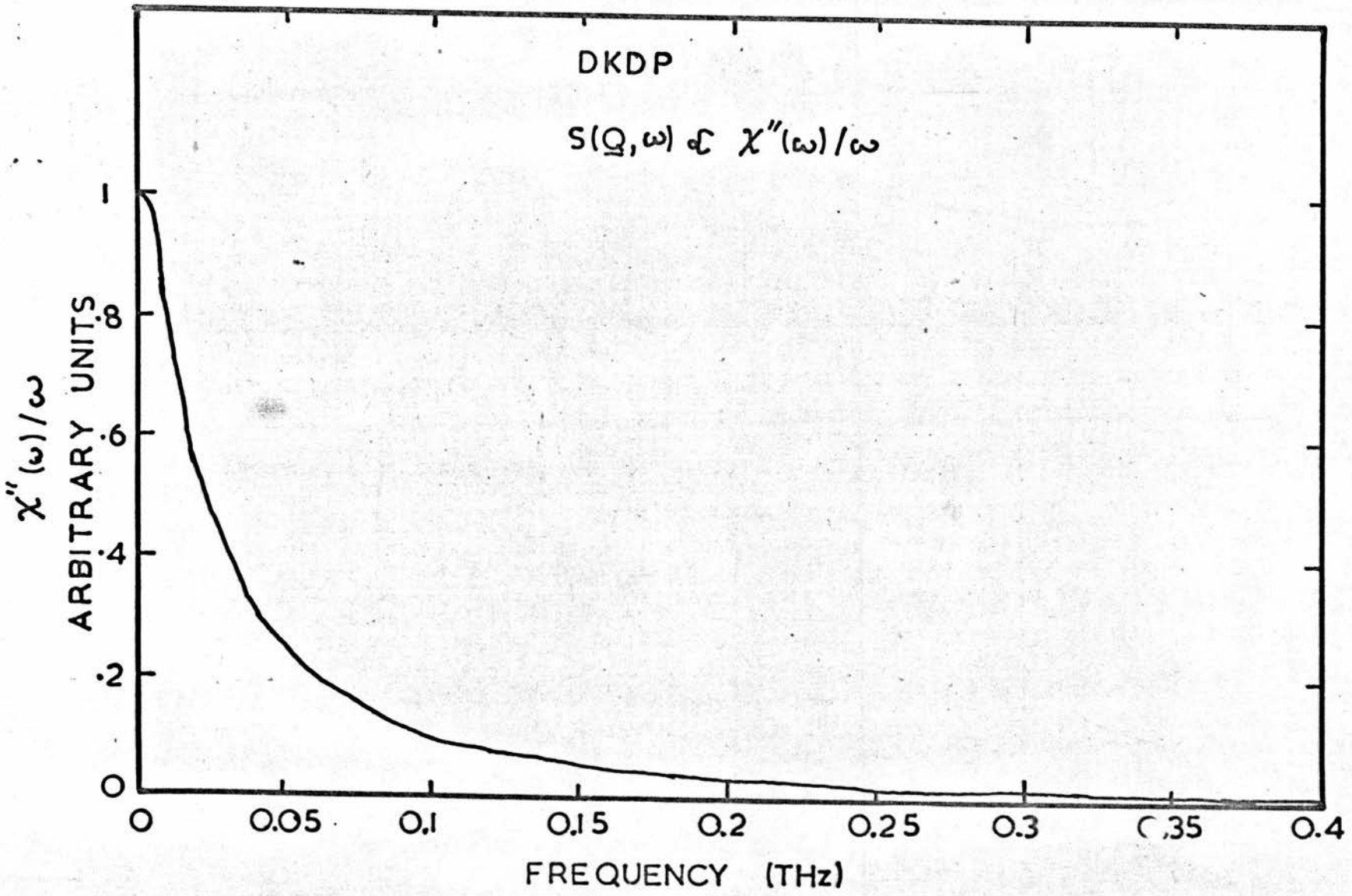
DKDP
S(Q, ω) ∝ χ″(ω)/ω
χ″(ω)/ω
ARBITRARY UNITS
1
.8
.6
.4
.2
0
0
0.05
0.1
0.15
0.2
0.25
0.3
0.35
0.4
FREQUENCY (THz)

Figure 4.2

Modified Patterson synthesis P'(r)

The (010) projection is shown, clearly dominated by the 303 intensity. The crosses mark peaks in the self convolution of the scattering density, disregarding oxygen atoms and placing deuterium atoms in the centre of their bonds. Negative contours are dashed, zero contours dotted and the full lines are positive contours.

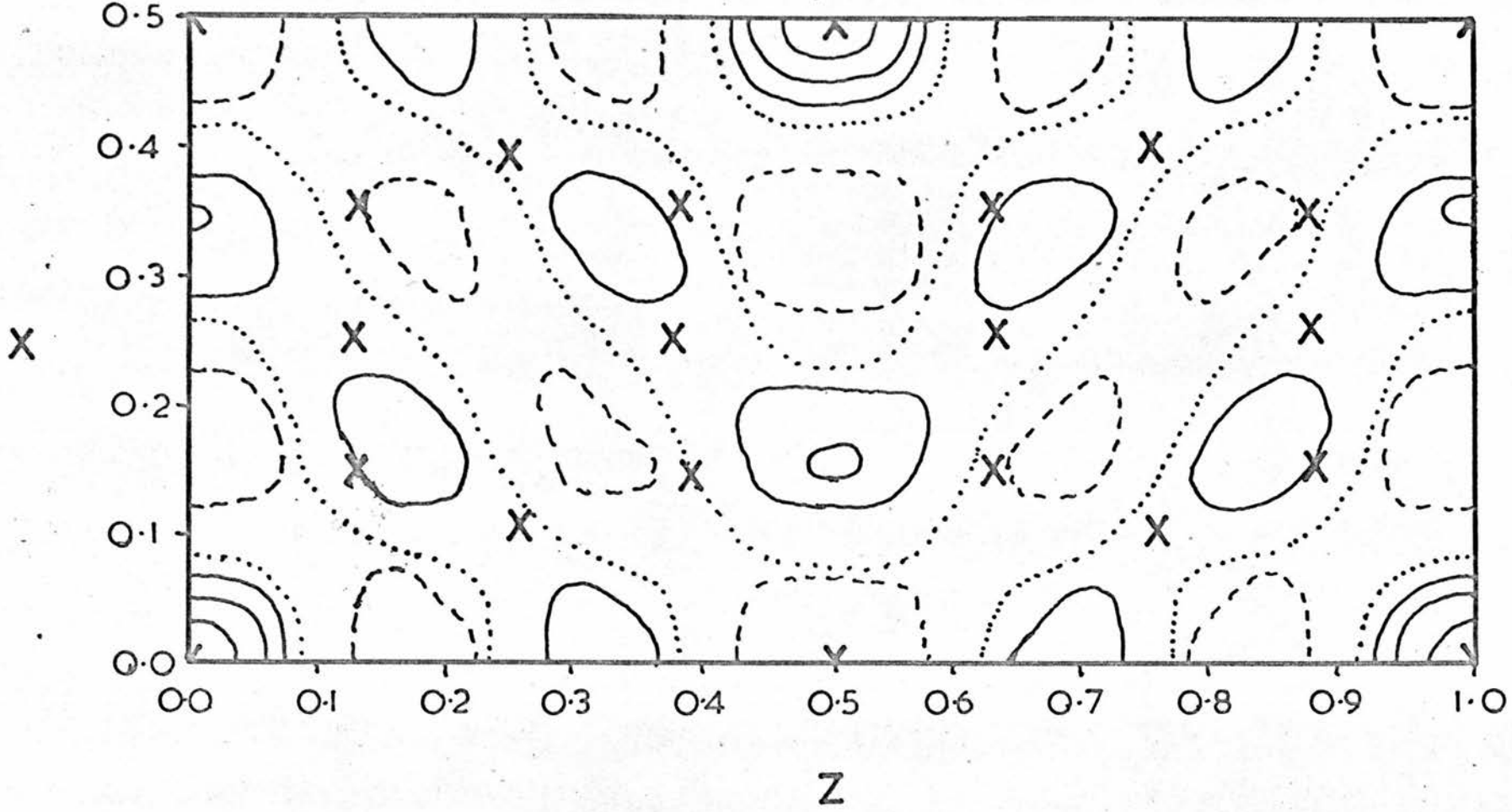
0·5
0·4
0·3
0·2
0·1
0·0
X
0·0
0·1
0·2
0·3
0·4
0·5
0·6
0·7
0·8
0·9
1·0
Z

Figure 4.3

Inverse intensity along the line (ζ , 3) at 224.7°K. The solid line shows the expression $K^2 + \zeta^2 + A^2 \zeta^4$. The intensity I has been corrected for a constant background.

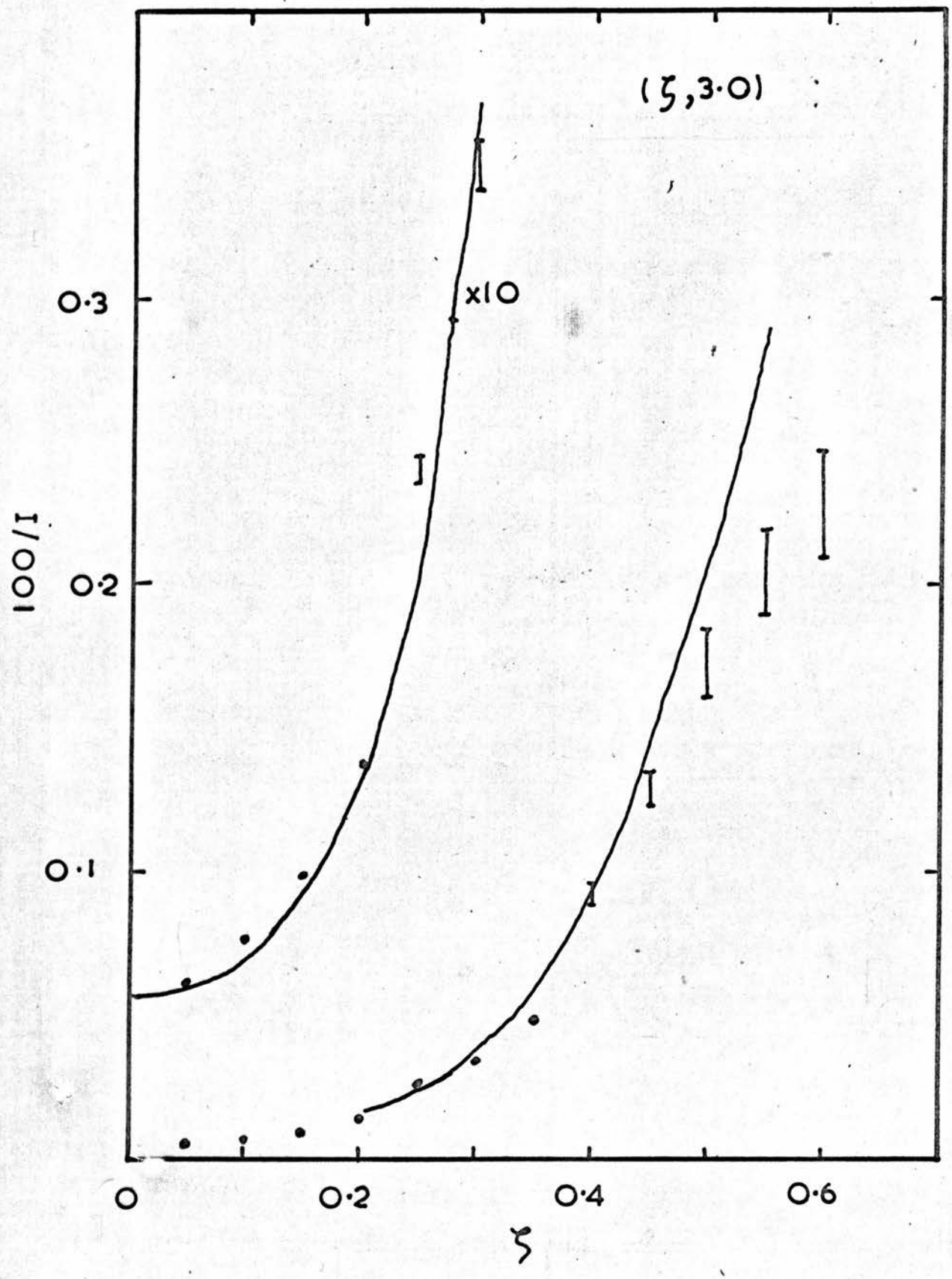
(ζ, 3·01)
x10
0·3
0·2
0·1
100/I
0
0·2
0·4
0·6
ζ

Figure 4.4

Inverse intensity as a function of inverse temperature. The accuracy of the data and the resultant linear fit are indicated at several wavevectors (ζ, η).

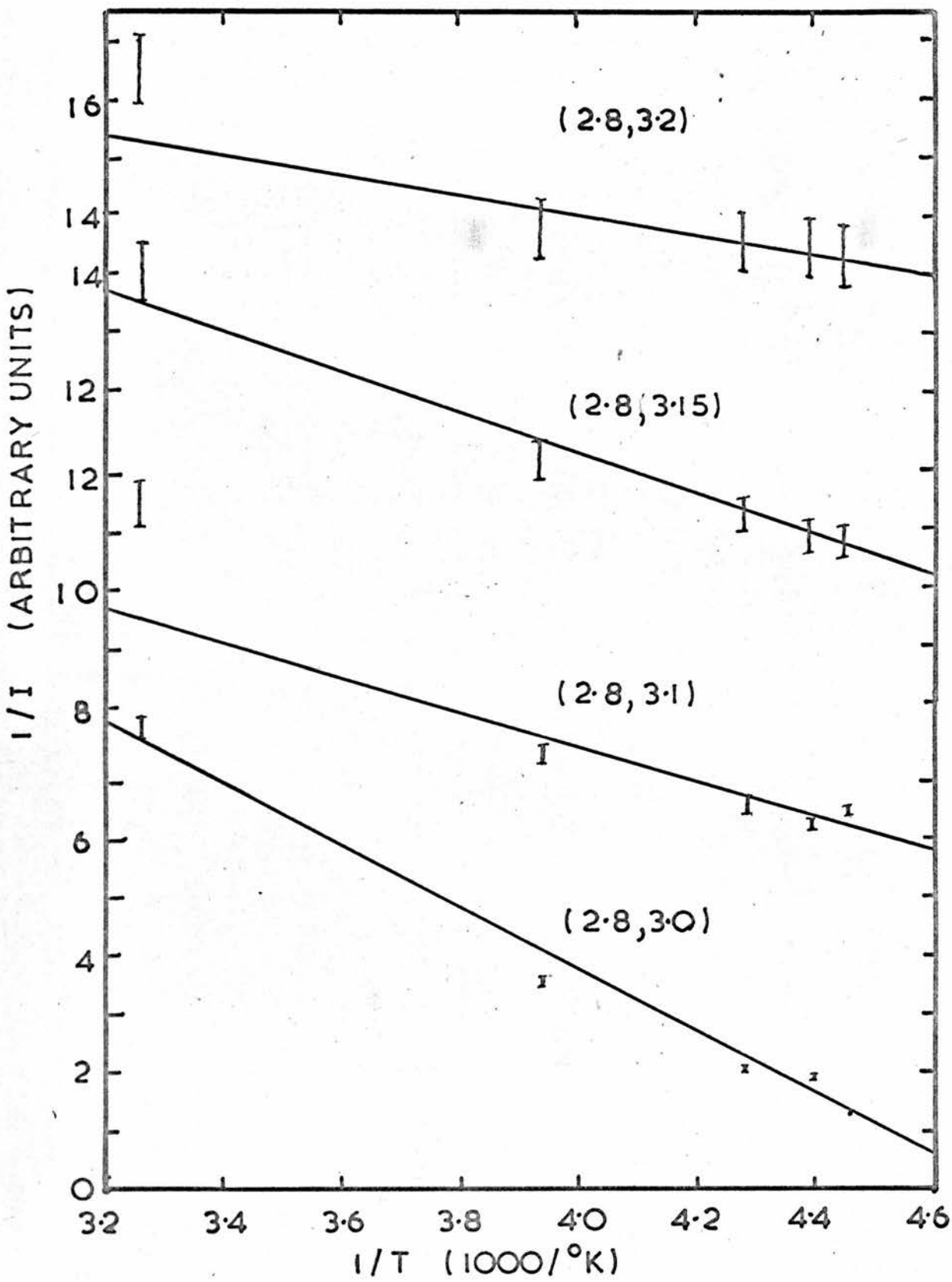
(2·8,3·2)
(2·8,3·15)
(2·8,3·1)
(2·8,3·0)
I/I (ARBITRARY UNITS)
1/T (1000/°K)
0
2
4
6
8
10
12
14
16
3·2
3·4
3·6
3·8
4·0
4·2
4·4
4·6

Figure 4.5

The interaction $J(\underline{q})$ and structure factor squared $N|F(\underline{Q})|^2$ along the line $(\zeta, 3)$. The solid curve for $J(\underline{q})$ uses only nearest neighbour interactions, while the dotted curve uses next nearest neighbours as well.

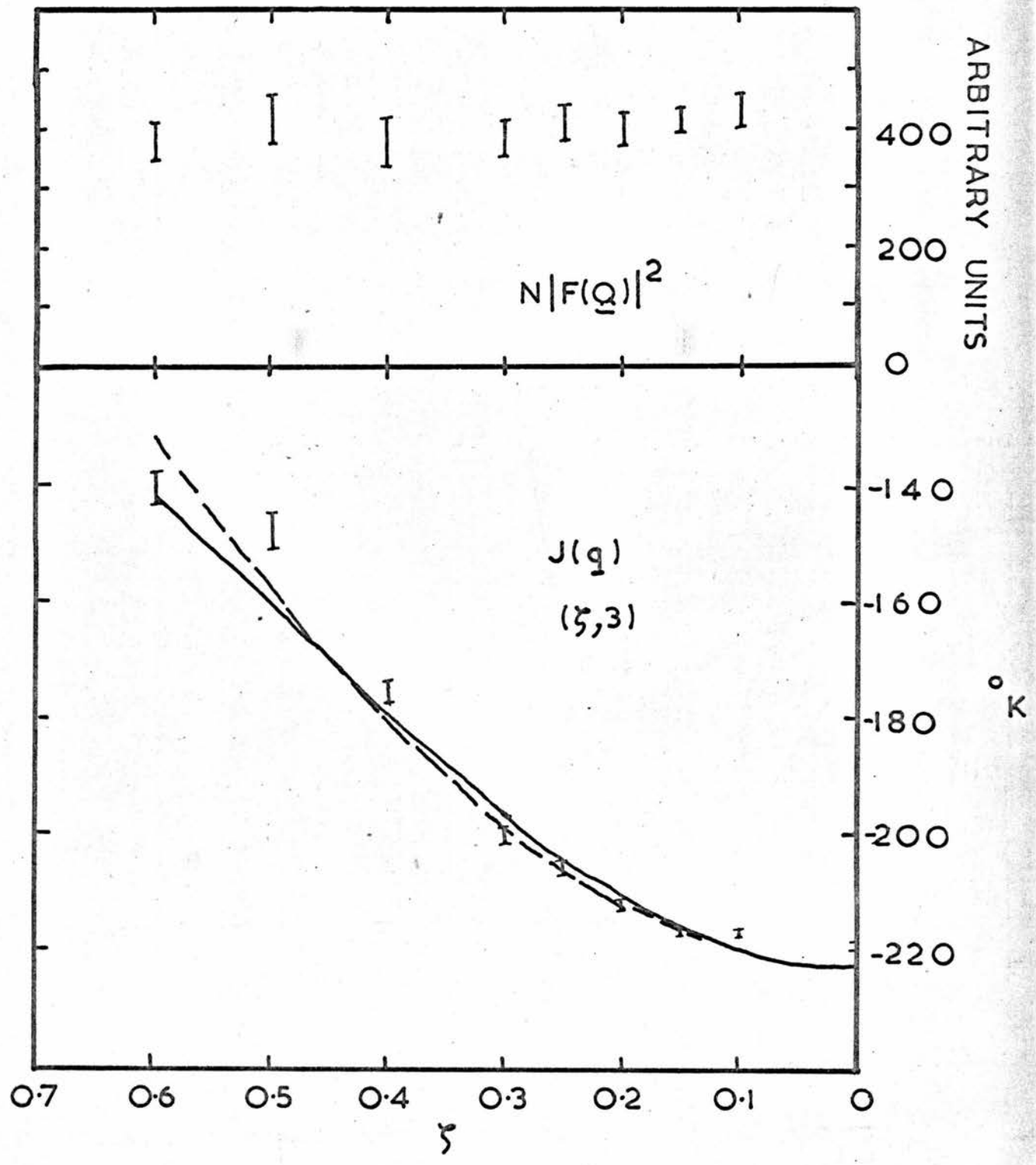
ARBITRARY UNITS
400
200
0
$N|F(Q)|^2$
-140
-160
-180
-200
-220
°K
J(q)
(ζ,3)
0·7
0·6
0·5
0·4
0·3
0·2
0·1
0
ζ

Figures 4.6

The interaction I(q) and structure factor squared $N|F(Q)|^2$ along the lines (2.4, η), (2.6, η), (2.8, η), (2.9, η) and (3.0, η). The solid curves for I(q) use only nearest neighbour interactions and a separate Coulomb interaction, V_c, for each line, while the dotted curves use next nearest neighbour interactions and one value for the Coulomb interaction.

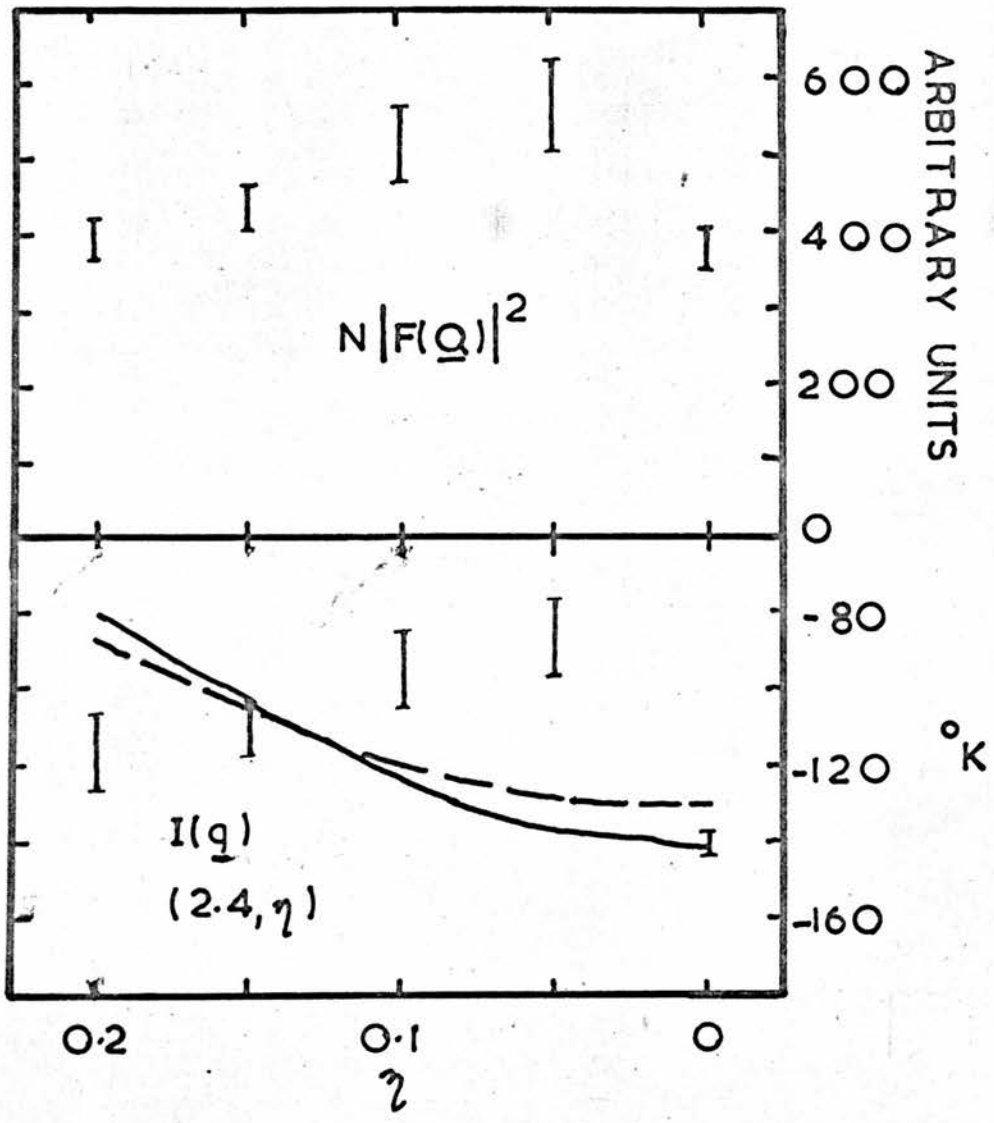
600
400
200
0
ARBITRARY UNITS
$N|F(Q)|^2$
-80
-120
-160
°K
I(q)
(2.4, η)
0·2
0·1
0
η

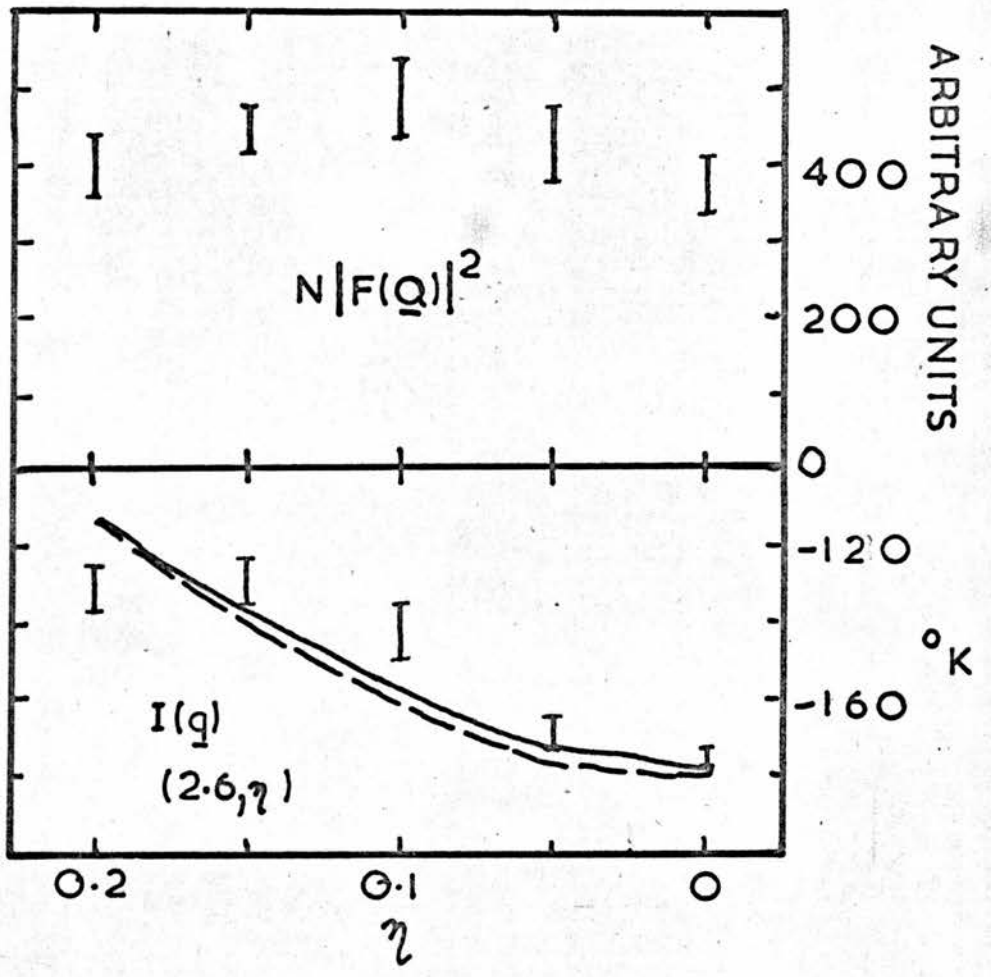
400
200
0
-120
-160
ARBITRARY UNITS
°K
N|F(Q)|²
I(q)
(2.6,η)
0·2
0·1
0
η

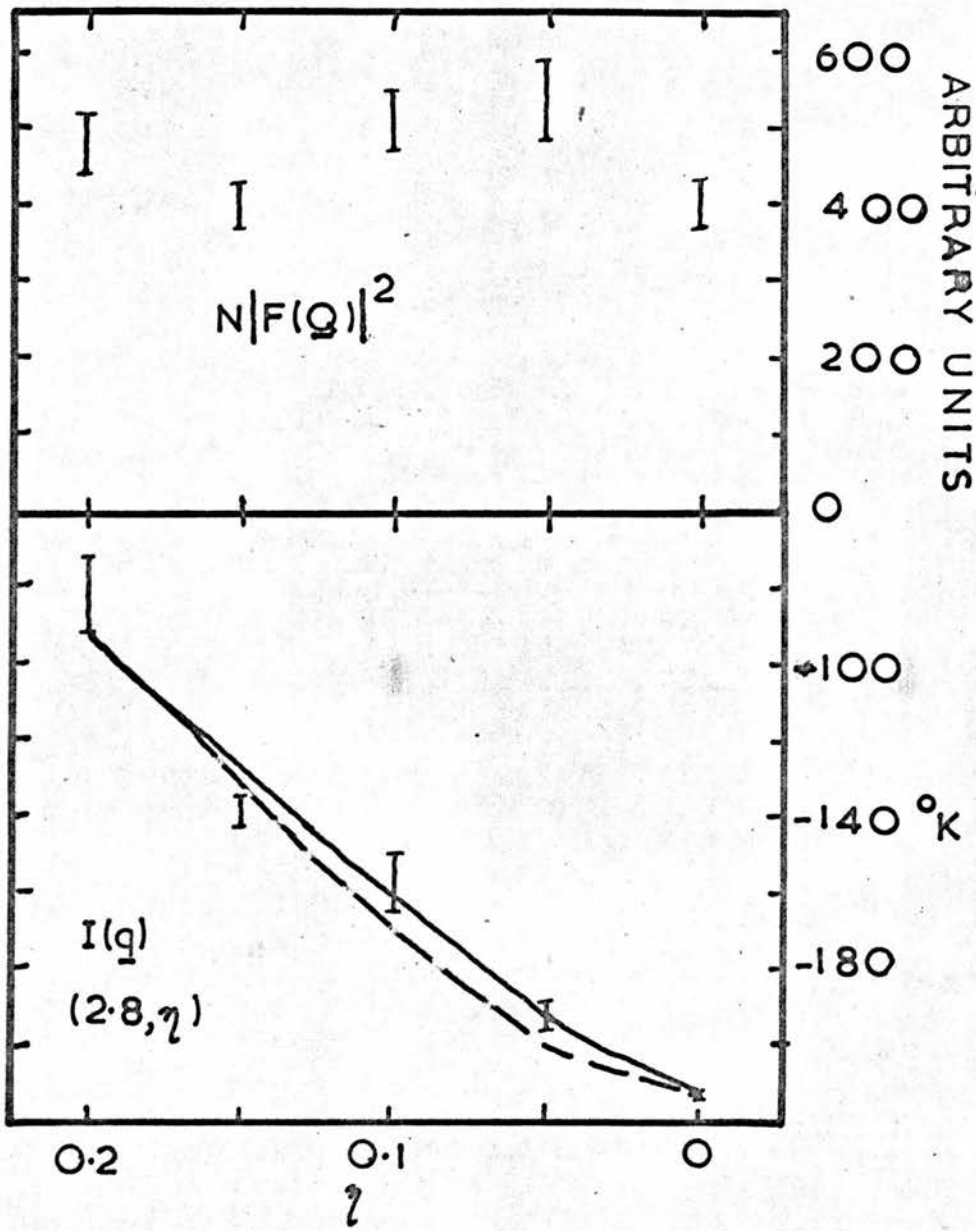
600
400
200
0
ARBITRARY UNITS
N|F(Q)|²
-100
-140 °K
-180
I(q)
(2·8,η)
0·2
0·1
0
η

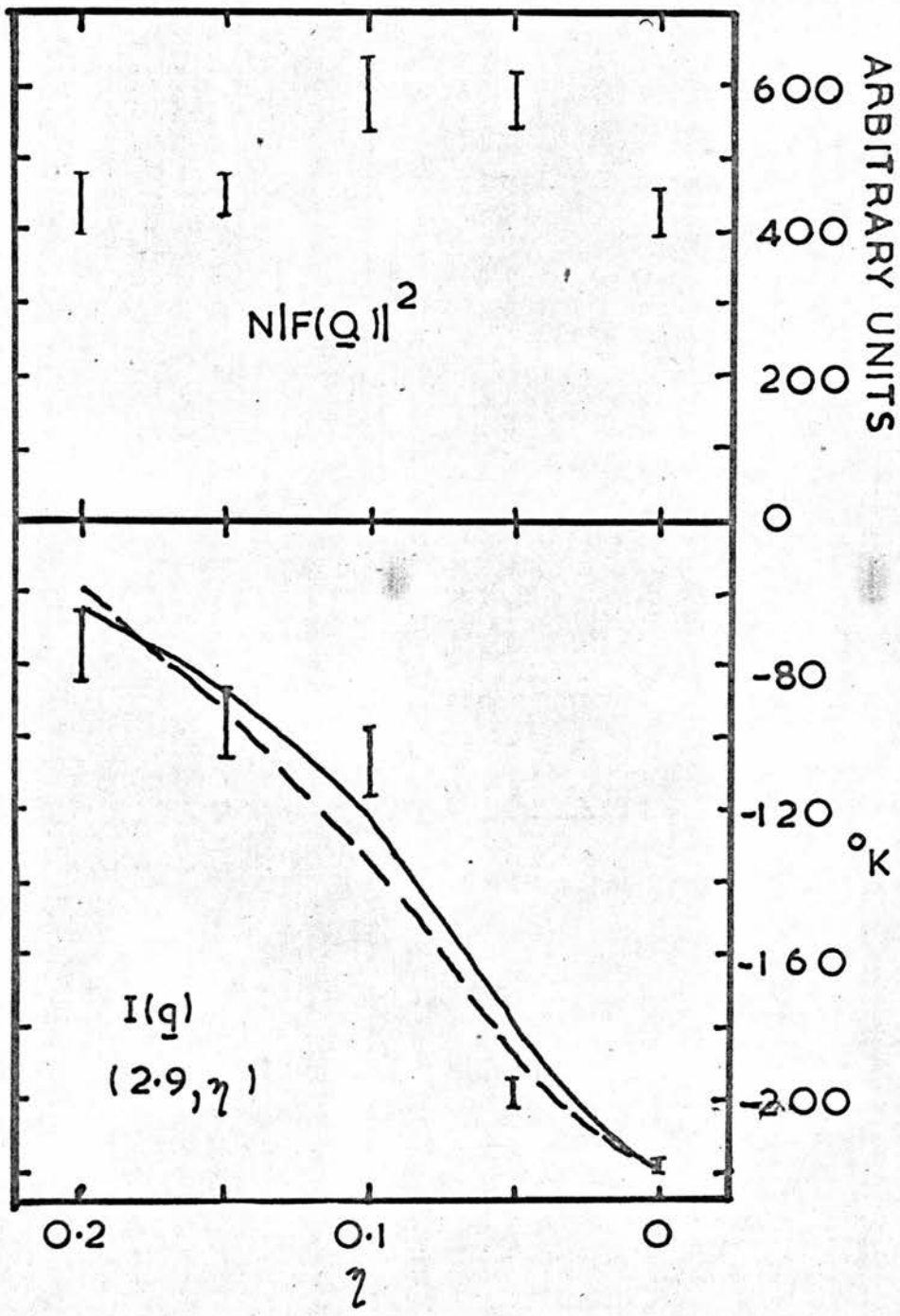
600
400
200
0
ARBITRARY UNITS
N|F(Q)|²
-80
-120
°K
-160
-200
I(q)
(2·9, η)
0·2
0·1
0
η

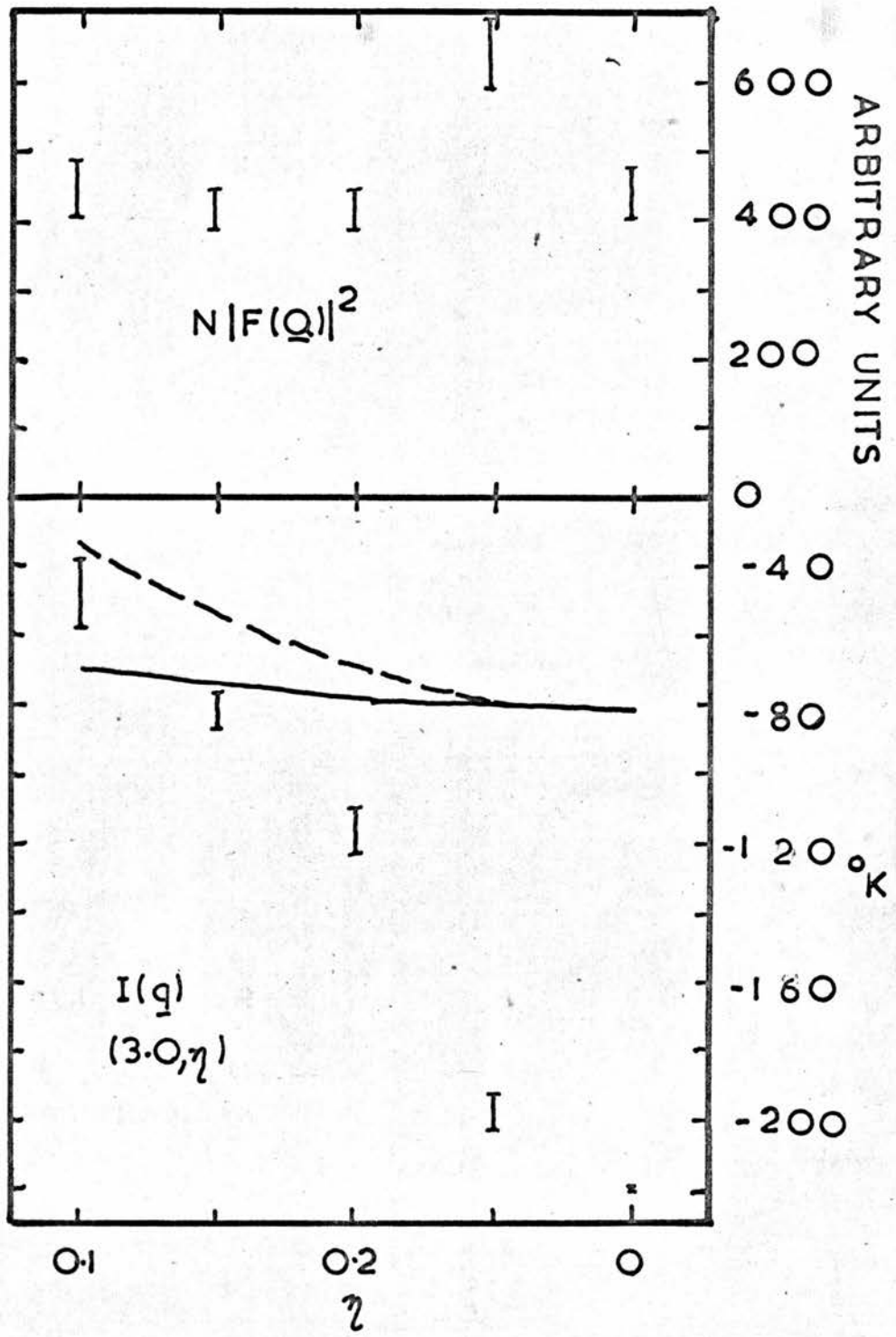
600
400
200
0
ARBITRARY UNITS
N|F(Q)|²
-40
-80
-120
°K
-160
-200
I(q)
(3.0,η)
0·1
0·2
0
η

5. Microscopic Model

5.1 The model

The most recent microscopic models for KDP, which are reviewed by Tokunaga (1966) and Tokunaga and Matsubara (1966), use de Gennes' (1963) fictitious spin formalism. The models are designed with a term which describes the proton tunnelling and is able to account for the isotope effect on the transition temperature. The quasielastic nature of the critical scattering described in chapter 2 shows that for DKDP the dynamical tunnelling term is indeed very small. The tunnelling is therefore considered to occur on a very long time scale compared with the displacements due to the phonons. The deuterons are thus regarded as tunnelling, in order to allow a mechanism for their transfer from one site to another in a hydrogen bond, but the dynamical nature of the tunnelling is disregarded. The model presented here is therefore applicable to DKDP, and to any other KDP type crystal in which the dynamical nature of the tunnelling may be disregarded. It is likely that all deuterium substituted KDP type crystals satisfy this condition.

The experimental results also indicate the importance of including the whole lattice in any model of the ferroelectric transition. The effects of the proton - lattice interaction on the excitations of the system were described in detail by Villain and Stamenkovic (1966) who

solved the equations of motion of the coupled system in the molecular field approximation. They considered the total system of four protons and the complete lattice, every proton moving in the one molecular field. The simplest case of their theory, an interaction between one spin and one lattice mode per unit cell, yielded an excitation with the soft mode temperature dependence. Exactly the same result for the simple case of one spin interacting with one lattice mode was derived independently by Kobayashi (1968), who discusses the form of the excitation in greater detail.

Novakovic (1966) preferred to consider the tunnelling to be of such a low frequency that the lattice vibrations are not effected by the proton-lattice interaction. In this adiabatic approximation the non-hydrogen atoms in the crystal are always in equilibrium sites relative to the position (or fictitious spin) of the hydrogen atoms. Above the transition temperature the equilibrium sites are those determined by Bacon and Pease (1953). The lattice spectrum is therefore unchanged by the presence of the protons. The excitations of the spin system (extended to four spins per cell by Novakovic, 1967), when determined in the molecular field approximation, have exactly the same form as without the proton - lattice interaction, but with a renormalised parameter. They therefore have the soft mode characteristics mentioned in chapter 1. This renormalisation of the proton-proton interaction was also realised by Blinc and Svetina (1966), who then discarded the term.

In the model described here the dynamical nature of the tunnelling is disregarded. It is then unnecessary to use the molecular field approximation, but the adiabatic approximation is used to include the proton-lattice interaction. An attempt is made to present a model which will not only qualitatively describe the results, but which is simple enough to enable reliable quantitative predictions to be made.

Each proton (or deuteron) (k) in the unit cell ℓ has two equilibrium sites. The fictitious spin $S(\ell k)$ is +1 if the proton is at site 1 and -1 if at site 2. The potential between the protons ℓk and $\ell' k'$ at sites i and j respectively is written $\phi^{ij}\left(\frac{\ell\ell'}{kk'}\right)$, abbreviated ϕ^{ij}. The potential between two protons is then

$$\tfrac{1}{4}(\phi^{11} + \phi^{12} + \phi^{21} + \phi^{22}) + \tfrac{1}{4}(\phi^{11} + \phi^{12} - \phi^{21} - \phi^{22})S(\ell k)$$

$$\tfrac{1}{4}(\phi^{11} - \phi^{12} + \phi^{21} - \phi^{22})S(\ell' k') + \tfrac{1}{4}(\phi^{11} - \phi^{12} - \phi^{21} + \phi^{22})S(\ell k)S(\ell' k')$$

The potential between a K, P, or O atom and a proton may be similarly written

$$\tfrac{1}{2}(\phi^{1} + \phi^{2}) + \tfrac{1}{2}(\phi^{1} - \phi^{2})S(\ell k)$$

These forms for the potential were suggested by R. A. Cowley (private communication). The model following from the potentials is described by Paul et al. (1969) and corresponds, with some points of different emphasis, to the discussion in this chapter from equation 5.7 onwards.

The potentials may be expanded in Taylor series as a function of the (small) displacements of the protons from their equilibrium positions at sites 1 or 2 in the hydrogen bond. The proton-proton interaction in the crystal, neglecting the dynamical part becomes (to second order only)

$$\sum_{\substack{\ell\ell' \\ kk'=H}} \tfrac{1}{2}\phi_{\alpha\beta}\left(\begin{matrix}\ell\ell' \\ kk'\end{matrix}\right) u_\alpha(\ell k)u_\beta(\ell' k') + \chi_\alpha\left(\begin{matrix}\ell\ell' \\ kk'\end{matrix}\right) u_\alpha(\ell k)S(\ell' k') + \tfrac{1}{2}\psi\left(\begin{matrix}\ell\ell' \\ kk'\end{matrix}\right) S(\ell k)S(\ell' k') \qquad \ldots\ldots\ldots\ldots\ldots 5.1$$

The proton-proton interaction is therefore composed of three parts, a lattice part ($\phi_{\alpha\beta}$), a spin-lattice part (χ_α) and a spin-spin part (ψ).

Equation 5.1 assumes that only two body interactions are important, whereas Slater's (1941) theory includes four body interactions. The microscopic model of Blinc and Svetina (1966) includes the term ψ for $\ell \neq \ell'$, only for long range interactions. They introduced a short range term (fourth order in $S(\ell k)$) into the description which takes account of the energy of the Slater-Takagi configurations of the protons surrounding one PO_4 group. The term ψ for $\ell = \ell'$ can however account for most of the short range Slater-Takagi configurations because the fourth order terms $S(\ell k)S(\ell k)S(\ell k')S(\ell k'')$ reduce to $S(\ell k')S(\ell k'')$. The remaining fourth order term will be neglected here. This term has been included in Novakovic's (1966) molecular field approximation model. Greens function techniques, again using a molecular field approximation (Errey, 1968), show that with this fourth order term the correlation function seen

by neutron scattering would not have the simple temperature dependence observed and discussed in chapter 4. The present model therefore includes only two body interactions.

The proton lattice interaction is written, again to second order

$$\sum_{\substack{\ell\ell' \\ k=K,P,O \\ k'=H}} \phi_{\alpha\beta}\left(\begin{matrix}\ell\ell' \\ kk'\end{matrix}\right) u_\alpha(\ell k)\, u_\beta(\ell' k') + \chi_\alpha\left(\begin{matrix}\ell\ell' \\ kk'\end{matrix}\right) u_\alpha(\ell k) S(\ell' k').$$

as in equation 5.1, this expression contains both a lattice and a spin-lattice part. The potential energy of the lattice is written

$$\sum_{\substack{\ell\ell' \\ kk'=K,P,O}} \tfrac{1}{2}\, \phi_{\alpha\beta}\left(\begin{matrix}\ell\ell' \\ kk'\end{matrix}\right) u_\alpha(\ell k)\, u_\beta(\ell' k')$$

The three Taylor series expansions for the proton-proton interaction, the proton-lattice interaction and the potential energy of the lattice are written omitting the constant term $\sum_{\substack{\ell\ell' \\ kk'}} \phi\left(\begin{matrix}\ell\ell' \\ kk'\end{matrix}\right)$ as it just defines the energy zero. The term χS is missing because, by symmetry

$$\sum_{\ell k} \chi\left(\begin{matrix}\ell\ell' \\ kk'\end{matrix}\right) = \sum_{\ell k}\left(\phi^1\left(\begin{matrix}\ell\ell' \\ kk'\end{matrix}\right) - \phi^2\left(\begin{matrix}\ell\ell' \\ kk'\end{matrix}\right)\right) = 0. \qquad \ldots\ldots\ldots\ldots\ldots 5.2$$

In the paraelectric phase,

$$\sum_{\ell' k'} \chi_\alpha\left(\begin{matrix}\ell\ell' \\ kk'\end{matrix}\right) S(\ell' k') = 0 \qquad \ldots\ldots\ldots\ldots\ldots 5.3$$

since the average value of $S(\ell'k')$ for each k', $\langle S \rangle = 0$.

The equilibrium condition

$$\sum_{\ell'k'} \phi_\alpha \begin{pmatrix} \ell\ell' \\ kk' \end{pmatrix} + \sum_{\ell'k'} \chi_\alpha \begin{pmatrix} \ell\ell' \\ kk' \end{pmatrix} S(\ell'k') = 0$$

therefore gives

$\sum_{\ell'k'} \phi_\alpha \begin{pmatrix} \ell\ell' \\ kk' \end{pmatrix} = 0$, which means that the term $\phi_\alpha u_\alpha$, linear in u in the Taylor series expansion is zero in the paraelectric phase.

Two further conditions may be established. Translational invariance of the potential and its derivative show that

$$\sum_{\ell k = K, P, O, H} \chi_\alpha \begin{pmatrix} \ell\ell' \\ kk' \end{pmatrix} = 0 \qquad \ldots\ldots\ldots\ldots\ldots 5.4$$

and

$$\sum_{\ell k = K, P, O, H} \phi_{\alpha\beta} \begin{pmatrix} \ell\ell' \\ kk' \end{pmatrix} = 0$$

Before developing the model it is useful to discuss the three matrixes ϕ, χ and ψ which appear in the description in order to give them some quantitative meaning. The matrixes $\phi_{\alpha\beta}$ are the second derivatives of the potentials ϕ, ϕ^i and ϕ^{ij}. The matrixes χ_α are defined in terms of the first derivatives of the potentials ϕ^i and ϕ^{ij}

$$\chi_\alpha \begin{pmatrix} \ell\ell' \\ kk' \end{pmatrix} = \tfrac{1}{2} \left(\phi^1 \begin{pmatrix} \ell\ell' \\ kk' \end{pmatrix} - \phi^2 \begin{pmatrix} \ell\ell' \\ kk' \end{pmatrix} \right)$$

and a similar definition for the term involving ϕ^{ij}. The matrixes ψ

are defined in terms of the potentials ^{ij} themselves

$$\psi\begin{pmatrix} \ell\ell' \\ kk' \end{pmatrix} = \frac{1}{4}\left(\phi^{11}\begin{pmatrix} \ell\ell' \\ kk' \end{pmatrix} - \phi^{12}\begin{pmatrix} \ell\ell' \\ kk' \end{pmatrix} - \phi^{21}\begin{pmatrix} \ell\ell' \\ kk' \end{pmatrix} + \phi^{21}\begin{pmatrix} \ell\ell' \\ kk' \end{pmatrix}\right.$$

The matrixes $\phi_{\alpha\beta}$ contain all the parameters required, for example, ionic charges and short range axially symmetric central force parameters, and these may be used in χ_α. Short range forces, however, are not required in due to the large distance between protons. The Coulomb potential is therefore the only contribution to ψ.

It remains only to use some simple potential functions to give the three unknown matrixes ϕ, χ and ψ the quantitative meaning desired. Following chapter 3 a short range axially symmetric central force, rigid ion model may be proposed. The matrixes $\phi_{\alpha\beta}$ are then determined in the same way as in chapter 3. The short range contributions to χ_α are (Born and Huang, 1954)

$$\chi_\alpha\begin{pmatrix} \ell\ell' \\ kk' \end{pmatrix} = \frac{e^2}{2v} \quad B_{kk'} \quad r_\alpha$$

with the notation of equation 3.1. The calculation of the Coulomb contributions to ϕ_α^{ij} and ϕ^{ij} for the χ_α and ψ matrixes would require the use of expressions for the Coulomb sums which have been derived from Born and Huang (1954). The expressions will not be given here, as they are fairly simply derived, rather long, and have not been used in calculations. Although the calculations have not been done, it can be

seen that this model does indeed give calculable meaning to the three unknown matrixes. Calculations could therefore be performed, not only for DKDP, but for all deuterated KDP type crystals, including DADP, which are expected to have very low frequency tunnelling modes.

In view of the uncertainty in the parameters of the model to fit the phonon dispersion relations for DKDP it was decided not to proceed with the full model calculation for the total system but to see whether any simplifying approximations could give a workable model. The approximation is made in the expression for the potentials ϕ^i and ϕ^{ij}.

The position of the ℓkth proton in the double minimum potential well is either $\underline{R}(\ell k) \pm \underline{a}(k)$ for sites 1 and 2 respectively. ($\underline{R}(\ell k) = \underline{R}(\ell) + \underline{R}(k)$ where $\underline{R}(\ell)$ is a vector to a point of the Bravais lattice.) The potentials ϕ^{ij} and ϕ^i may then be expanded in Taylor series

$$\phi^i\left(\begin{matrix}\ell\ell'\\ kk'\end{matrix}\right) = \phi\left(\begin{matrix}\ell\ell'\\ kk'\end{matrix}\right) \pm \sum_\alpha a_\alpha(k)\,\phi_\alpha\left(\begin{matrix}\ell\ell'\\ kk'\end{matrix}\right) + \tfrac{1}{2}\sum_{\alpha\beta} a_\alpha(k)a_\beta(k')\phi_{\alpha\beta}\left(\begin{matrix}\ell\ell'\\ kk'\end{matrix}\right) \pm \cdots$$

and similarly for ϕ^{ij}. $\chi_\alpha\left(\begin{matrix}\ell\ell'\\ kk'\end{matrix}\right)$ and $\psi\left(\begin{matrix}\ell\ell'\\ kk'\end{matrix}\right)$ then have $\phi_{\alpha\beta}\left(\begin{matrix}\ell\ell'\\ kk'\end{matrix}\right)$ as their lowest order terms and are composed of only even derivatives. The potential energy of the crystal may then be split into three parts, the lattice (including protons), the spin-lattice (including spin-proton) and the spin-spin contributions, the leading terms of which are expressed in the approximation for the potential

$$\tfrac{1}{2} \sum_{\alpha\beta} \sum_{\substack{ll' \\ kk'=K,P,O,H}} \phi_{\alpha\beta}\left(\begin{matrix} ll' \\ kk' \end{matrix}\right) u_\alpha(lk)\, u_\beta(l'k')$$

$$\sum_{\alpha\beta} \sum_{\substack{ll' \\ k=K,P,O,H \\ k'=H}} \phi_{\alpha\beta}\left(\begin{matrix} ll' \\ kk' \end{matrix}\right) u_\alpha(lk)\, a_\beta(k') S(l'k')$$

$$\tfrac{1}{2} \sum_{\alpha\beta} \sum_{\substack{ll' \\ kk'=H}} \phi_{\alpha\beta}\left(\begin{matrix} ll' \\ kk' \end{matrix}\right) a_\alpha(k)\, a_\beta(k') S(lk) S(l'k') \quad \ldots\ldots\ldots\ 5.5$$

These expressions have interesting implications for the Coulomb parts of the matrixes χ_α and ψ. The Madelung energy, when split into parts $\psi\left(\begin{matrix} ll' \\ kk' \end{matrix}\right)$ and taken into Fourier transformed form, has components corresponding to the macroscopic electric field term which are proportional to $1/|\underline{q}|^2$. These divergent terms sum to zero due to charge neutrality, but are required when the matrixes are divided into interatomic parts. The expressions 5.5 show that this divergent term does not arise, but that the first term appearing in ψ is the second derivative of the potential, which requires the normal Coulomb sums and does not diverge at $\underline{q} = 0$. The second derivative is also the first term appearing in χ_α.

The frequency of the O-H stretching vibrations in KDP (Lazarev et al., 1961; Blinc et al., 1958) show that the protons move in a double minimum potential well rather than a very flat bottomed potential well. The

approximation expressed by equation 5.5 is therefore not only very poor, but incorrect, having the wrong sign for the second derivative, and could not be expected to provide a good model calculation. The higher order terms in the Taylor series expansion are therefore required to give a good model.

The general model is now developed by introducing the Fourier transformed operators $u_\alpha(\underline{q}k)$ and $S(\underline{q}k)$ in the N cell system.

$$u_\alpha(\ell k) = \frac{1}{\sqrt{N\, m_k}} \sum_{\underline{q}} u_\alpha(\underline{q}k) \exp(i\underline{q}.\underline{R}(\ell k))$$

$$S(\ell k) = \frac{1}{\sqrt{N}} \sum_{\underline{q}} S(\underline{q}k) \exp(i\underline{q}.\underline{R}(\ell k)) \qquad \ldots\ldots\ldots\ldots\ldots 5.6$$

The Hamiltonian for the system, neglecting both the constant term and the kinetic term for the lattice may be written

$$\mathcal{H} = \mathcal{H}_L + \mathcal{H}_{SL} + \mathcal{H}_{SS}$$

$$\mathcal{H}_L = \tfrac{1}{2} \sum_{\substack{\alpha\beta \\ kk'}} \sum_{\underline{q}} C_{\alpha\beta}(\underline{q}kk')\, u_\alpha(-\underline{q}k) u_\beta(\underline{q}k')$$

$$\mathcal{H}_{SL} = \sum_{\substack{\alpha \\ kk'}} \sum_{\underline{q}} G_\alpha(\underline{q}kk')\, u_\alpha(-\underline{q}k)\, S(\underline{q}k')$$

$$\mathcal{H}_{SS} = \tfrac{1}{2} \sum_{kk'} \sum_{\underline{q}} I(\underline{q}kk')\, S(-\underline{q}k) S(\underline{q}k') \qquad \ldots\ldots\ldots\ldots\ldots 5.7$$

with the summations over appropriate atoms as given in the expression 5.5. From equation 5.1 and the following expressions, the Fourier transformed matrixes are defined

$$\sqrt{m_k m_{k'}}\; C_{\alpha\beta}(\underline{q}kk') = \sum_{l} \phi_{\alpha\beta}\begin{pmatrix} l\,l' \\ k\,k' \end{pmatrix} \exp(i\underline{q}.(\underline{R}(l'k') - \underline{R}(lk))). \qquad \ldots\ldots\ldots\ldots\ldots 5.8$$

The matrixes $\sqrt{m_k}\; G_\alpha(\underline{q}kk')$ and $I(\underline{q}kk')$ are defined identically by the Fourier transforms of $\chi_\alpha\begin{pmatrix} l\,l' \\ k\,k' \end{pmatrix}$ and $\psi\begin{pmatrix} l\,l' \\ k\,k' \end{pmatrix}$.

At this point the adiabatic approximation is introduced and equation 5.7 is minimised with respect to the atomic displacements. If is found that

$$u_\alpha(\underline{q}k) = - \sum_{\substack{\beta \\ k'=K,P,O,H \\ k''=H}} C^{-1}_{\alpha\beta}(\underline{q}kk')G_\beta(\underline{q}k'k'')S(\underline{q}k'') \qquad \ldots\ldots\ldots\ldots\ldots 5.9$$

Even though the matrix C is singular this equation has solutions by condition 5.3.

The cross terms in the Hamiltonian disappear in this approximation. $\mathcal{H}_L$ remains unchanged and yields the phonon frequencies $\omega(\underline{q}j)$ and eigenvectors $e_\alpha(k\underline{q}j)$

$$\omega^2(\underline{q}j) = \sum_{\substack{\alpha\beta \\ kk'}} C_{\alpha\beta}(\underline{q}kk')e_\alpha(k\text{-}\underline{q}j)e_\beta(k'\underline{q}j) \qquad \ldots\ldots\ldots\ldots\ldots 5.10$$

The remainder of the Hamiltonian becomes an Ising model Hamiltonian

$$\mathcal{H}_{SS} = \tfrac{1}{2} \sum_{kk'} \sum_{\underline{q}} J(\underline{q}kk')S(-\underline{q}k)S(\underline{q}k')$$

with a renormalised matrix

$$J(\underline{q}kk') = I(\underline{q}kk') - \sum_{\substack{\alpha\beta \\ k''k''' \\ j}} G_\alpha(-\underline{q}k''k)\frac{e_\alpha(k''\underline{q}j)e_\beta(k'''-\underline{q}j)}{\omega^2(\underline{q}j)} G_\beta(\underline{q}k'''k') \qquad \ldots\ldots\ldots\ldots\ldots 5.11$$

From this equation it would appear that the frequency of the acoustic modes as $\underline{q}\to 0$ would make the interaction matrix J diverge. However, for the acoustic modes all $e_\alpha(k\underline{q}j)/\sqrt{m_k}$ are the same for each atom K and so the sums of 5.11 include the term $\sum_k \sqrt{m_k}\, G_\alpha(0kk')$ which, by equation 5.4 is zero.

By expanding equation 5.8 in powers of $\underline{q}$ it can be shown that $\sum_k \sqrt{m_k}\, G_\alpha(\underline{q}kk')$ is proportional to $\underline{q}$. The acoustic mode therefore causes no anomalous interaction as $\underline{q}\to 0$. However, more importantly, equation 5.3 shows that the interaction tends to zero as $\underline{q}\to 0$. This point is perhaps intuitive, as expressed by Kobayashi (1968), but it should be stressed that there are two conditions required. The first condition is that the crystal is in the paraelectric phase. Equation 5.3 is then true. Secondly the translational invariance condition is required. The interaction of the fictitious spin with its own displacement must therefore be considered. Kobayashi's model, which does not include this interaction, should then have an anomaly as $\underline{q}\to 0$. It is interesting to note that the spin-lattice (one atom only)interaction for an Ising ferromagnet (Matsudaira, 1968) has only a 2% effect on the transition

temperature. In KDP the main effect of the interaction is expected to be via the non-spin atoms K, P and O. As these are the atoms which give the greatest contribution to the spontaneous polarisation, it is thought that the spin-lattice interaction causes considerably more than a 2% effect on the transition parameters in DKDP.

An Ising model Hamiltonian has therefore been set up to describe the fictitious spin system. The interaction matrix is defined by equation 5.11. Eigenvalues $J(\underline{q}\lambda)$ and eigenvectors $E(k\underline{q}\lambda)$ of the matrix $J(\underline{q}kk')$ may be found and these are the values of J which apply to the four tunnelling modes in KDP. The spin coordinates $S(\ell k)$ transform in the same way under the space group operations as the tunnelling vectors described in appendix 1 and so the eigenvectors, which are written in terms of the spin coordinates

$$S(\underline{q}k) = \sum_{\lambda} E(k\underline{q}^{\lambda})S(\underline{q}^{\lambda}), \qquad \ldots\ldots\ldots\ldots\ldots 5.12$$

lie in spaces irreducible under the representations given in appendix 1.4.

The clearest description of what the fictitious spin $S(\ell k)$ represents has, perhaps, been given earlier, where it was stated that $S(\ell k) = \pm 1$ depending upon the occupation of a site. The work of Blinc and Svetina (1966) does not use the fictitious spin formalism, but it may be seen that the operators $S(\ell k)$ are the difference between their number operators on sites 1 and 2

$$S(\ell k) = n(\ell k1) - n(\ell k2)$$

This is the mathematical way of putting the above statement. It is important to note that while the fictitious spin ± 1 is discussed, the model really involves a spin $\frac{1}{2}$ system which has only two energy levels, or states.

The degrees of freedom described by the fictitious spin coordinate are additional to the translational degrees of freedom enjoyed by each proton or deuteron. Remembering that there is some finite dynamic nature to these extra degrees of freedom, even in DKDP, they are called tunnelling modes. There are always four of them at any given wave vector in addition to the phonons. The group theory of appendix 1 (table A1.5) shows that no matter what model for the potentials is chosen, the tunnelling modes with symmetries $\Gamma_2 + \Gamma_4 + \Gamma_5$, $\Sigma_1 + 3\Sigma_2$, $\Lambda_1 + \Lambda_2 + \Lambda_{34}$ and $M_{34} + M_5$ can only interact with the lattice modes $5\Gamma_2$, $7\Gamma_4$, $13\Gamma_5$, $23\Sigma_1$, $25\Sigma_2$, $11\Lambda_1$, $11\Lambda_2$, $13\Lambda_{34}$ and $7M_{34}$, $11M_5$, respectively, if anharmonic interaction is neglected. The group theory also shows that the ferroelectric (c-axis) tunnelling mode Γ_4 can only interact with 6(optic) Γ_4 modes.

5.2 Neutron scattering

The neutron scattering cross section for the tunnelling modes may be calculated from the model. The scattering is quasi-elastic for DKDP and so only the scattering function $\mathcal{S}(\underline{Q})$ is required. The derivation of the scattering properties for an uncoupled fictitious spin

system has been given by Cochran (1969).

$$\mathcal{S}(\underline{Q},\omega) = \int \langle F_S(-\underline{Q},0)F_S(\underline{Q},t)\rangle \exp(-i\omega t)dt$$

where $F_S(\underline{Q},t)$ is the Fourier transform of the scattering density for the spin system, which is written

$$\sum_{\ell k} \tfrac{1}{2} b_k \left[\delta(\underline{R} - \underline{R}(\ell k) - \underline{a}(k) - \underline{u}(\ell k,t)) - \delta(\underline{R} - \underline{R}(\ell k) + \underline{a}(k) - \underline{u}(\ell k,t))\right] S(\ell k,t).$$

b_k is the scattering length of the ℓk th proton with displacement $\underline{u}(\ell k,t)$ and $S(\ell k,t)$ is the fictitious spin of the ℓk th proton at time t. Then

$$F_S(\underline{Q},t) = i \sum_{\ell k} b_k \exp(i\underline{Q}.(\underline{R}(\ell k) + \underline{u}(\ell k,t)))\sin(\underline{Q}.\underline{a}(k))S(\ell k,t)$$

The time dependence of this equation may be split into two parts, that of the displacements and that of the fictitious spins. In the adiabatic approximation the displacements do not depend on the fictitious spin, the operators commute, and so the average $\langle F_S(-\underline{Q},0)F_S(\underline{Q},t)\rangle$ may be factorised into the sum of products of two averages, one involving displacements $\underline{u}(\ell k,t)$ and the other involving fictitious spins $S(\ell k,t)$. The former may be treated as in phonon theory (Cochran and Cowley, 1967) and for the present purpose the constant term in the expansion of the exponential is taken. The scattering lengths are then written including a Debye-Waller factor $b_k(\underline{Q})$. Using equation 5.6 the Fourier transform of $S(\ell k,t)$ may be defined and

$$F_S(\underline{Q},t) = i\sqrt{N} \sum_k b_k(\underline{Q}) \exp(i\underline{\tau}.\underline{R}(k))\sin(\underline{Q}.\underline{a}(k))S(\underline{q}k,t)$$

where $\underline{\tau} = \underline{Q} + \underline{q}$ is a reciprocal lattice vector. For DKDP the quasi-

elastic nature of the critical scattering means that the time dependence of the fictitious spin and the structure factor is of no interest, so that a time independent structure factor is defined

$$F_S(\underline{Q}) = i\sqrt{N} \sum_k b_k(\underline{Q}) \exp(i\underline{\tau}.\underline{R}(k))\sin(\underline{Q}.\underline{a}(k))S(\underline{q}k).$$

The four tunnelling modes may now be separated using equation 5.12.

$$F_S(\underline{Q}) = \sum_\lambda F_S(\underline{Q}\lambda)$$

$$F_S(\underline{Q}) = i\sqrt{N} \sum_k b_k(\underline{Q}) \exp(i\underline{\tau}.\underline{R}(k)) \sin(\underline{Q}.\underline{a}(k))E(k\underline{q}\lambda)S(\underline{q}\lambda)$$

The above structure factors are for the scattering from deuterons only. The interaction of the lattice in the adiabatic approximation may now be considered. The other atoms in the crystal have displacements in the tunnelling modes governed by equation 5.9. The structure factor for scattering from these atoms has the form

$$F_L(\underline{Q}) = i\sqrt{N} \sum_k b_k(\underline{Q})(\sqrt{m_k}^{-1})\exp(i\underline{\tau}.\underline{R}(k))\underline{Q}.\underline{u}(\underline{q}k)$$

Here again the time dependence is so slow that it has been neglected. Rewriting equation 5.9 using 5.10 and 5.12

$$u_\alpha(\underline{q}k) = - \sum_{\substack{\beta j\lambda \\ k'=K,P,O,H \\ k''=H}} \frac{e_\alpha(k\underline{q}j)e_\beta(k'-\underline{q}j)}{\omega^2(\underline{q}j)} G_\beta(\underline{q}k'k'')E(k''\underline{q}\lambda)S(\underline{q}\lambda)$$

$$= - \sum_{k'j\lambda} e_\alpha(k\underline{q}j) \frac{H(k'\underline{q}j)}{\omega^2(\underline{q}j)} E(k'\underline{q}\lambda)S(\underline{q}\lambda)$$

defining H. The structure factor is then written

$$F_L(\underline{Q}) = -i\sqrt{N} \sum_{\substack{k=K,P,O,H \\ k'=H \\ j}} b_k(\underline{Q})\left(\sqrt{m_k}\right)^{-1} \exp(i\underline{\tau}.\underline{R}(k))\underline{Q}.\underline{e}(k\underline{q}j)$$

$$\times \frac{H(k'\underline{q}j)E(k'\underline{q}\lambda)S(\underline{q}\lambda)}{\omega^2(\underline{q}j)}$$

$$= -\sum_{\substack{j \\ k}} \mathcal{F}_L(\underline{Q}j) \frac{H(k\underline{q}j)}{\omega^2(\underline{q}j)} E(k\underline{q}\lambda)S(\underline{q}\lambda)$$

defining $\mathcal{F}_L$, the structure factor for scattering by the phonons. As equation 5.9 does have solutions the acoustic mode causes no anomaly in the structure factor. The total scattering function for the tunnelling modes may then be written

$$\mathcal{S}(\underline{Q}) = N \sum_{\lambda} |\mathcal{F}(\underline{Q}\lambda)|^2 \langle S(-\underline{q}\lambda)S(\underline{q}\lambda)\rangle$$

$$= N \sum_{\lambda} |\mathcal{F}(\underline{Q}\lambda)|^2 \Gamma(\underline{q}\lambda)$$

with $\mathcal{F}(\underline{Q}\lambda) = \sum_{k=H} \left\{ ib_k(\underline{Q})\exp(i\underline{\tau}.\underline{R}(k))\sin(\underline{Q}.\underline{a}(k)) \right.$

$$\left. - \sum_j \mathcal{F}_L(\underline{Q}j) \frac{H(k\underline{q}j)}{\omega^2(\underline{q}j)} \right\} E(k\underline{q}\lambda)$$

The correlation function $\Gamma(\underline{q}\lambda)$ may be determined in the random phase approximation (Brout, 1965)

$$\Gamma(\underline{q}\lambda) = (1 + \beta J(\underline{q}\lambda))^{-1}$$

As discussed in chapter 4 this function describes the neutron scattering in DKDP quite well so that a temperature $T_c(\underline{q}\lambda) = -J(\underline{q}\lambda)/k_B$ may be

defined.

Equation 5.11 may now be written more neatly using the definition

$$H(\lambda \underline{q} j) = \sum_{k} H(k\underline{q}j)E(k\underline{q}\lambda)$$

$$J(\underline{q}\lambda) = I(\underline{q}\lambda) - \sum_{j} \frac{H(\lambda\,-\underline{q}j)H(\lambda\,\underline{q}j)}{\omega^2(\underline{q}j)} \qquad \ldots\ldots\ldots\ldots\ldots\ldots 5.13$$

where j and λ belong to the same irreducible representation.

The scattering function just derived has several interesting features. In the 'polar' representations ($\lambda = \Gamma_4$, Γ_5, appendix 1) the values of $\omega(\underline{q}j)$, $H(\lambda \underline{q}j)$, $I(\underline{q}\lambda)$ as $\underline{q} \rightarrow 0$ depend on the direction of $\underline{q}$. The phonon frequencies $\omega(0j)$ always have a 'longitudinal' component at a higher frequency than the transverse component. Thus for the branches compatible with Γ_4, $\omega(0\Lambda_1) > \omega(0\Sigma_2)$ and for the doubly degenerate Γ_5, $\omega(0\Sigma_1) > \omega(0\Sigma_2) = \omega(0\Lambda_{34})$. A tetragonal crystal is different to a cubic crystal in which the zone centre polar representation is triply degenerate and the phonon frequency $\omega(0j)$ splits for any direction of $\underline{q}$ into a longitudinal and two transverse branches. In the tetragonal crystal, as Γ_4 and Γ_5 modes must polarise the crystal either perpendicular to or in the (001) plane respectively, the frequencies may be written in terms of the frequencies $\omega_e(0j)$ not involving the macroscopic electric field. The angle between the wave vector $\underline{q}$ and either the [001] direction or (001) plane is defined as α. The squares of the

required frequencies are then the eigenvalues of the matrix (Born and Huang, 1954)

$$\omega_e^2(0j)\,\delta_{jj'} + 4\pi v\,|\underline{P}(0j)|\,|\underline{P}(0j')|\cos^2\alpha$$

The polarisation $\underline{P}(0j)$ is set up by the mode j in the unit cell of volume v. From simple mathematical considerations it can be shown that the eigenvalues of the matrix are of the form

$$\omega_o^2(0j) + \omega_1^2(0j)\cos^2\alpha$$

where $\omega_o^2(0j)$ is a linear combination (with positive coefficients) of the $\omega_e^2(0j)$. The longitudinal modes must therefore have higher frequencies than the corresponding transverse modes. Similarly it is expected that

$$H(\lambda 0j) = H_o(\lambda 0j) + H_1(\lambda oj)\cos^2\alpha$$

$$I(0\lambda) = I_o(0\lambda) + I_1(0\lambda)\cos^2\alpha$$

and therefore from 5.13

$$J(0\lambda) = I_o(0\lambda) + I_1(0\lambda)\cos^2\alpha - \sum_j \frac{(H_o(\lambda 0j) + H_1(\lambda 0j)\cos^2\alpha)^2}{\omega_o^2(0j) + \omega_1^2(0j)\cos^2\alpha}$$

$$\simeq J_o(0\lambda) + J_1(0\lambda)\cos^2\alpha$$

It should be noted that with a large enough H_1 the longitudinal rather than transverse tunnelling mode would have the smaller $J(0\lambda)$ and would therefore cause a ferroelectric transition. The $\underline{q}$-dependence of the critical scattering discussed in chapter 4 showed that this was not the case for DKDP. Assuming that $J_1(0\lambda)$ is positive for both Γ_4 and Γ_5, the

knowledge of the symmetry of the tunnelling modes gives the form of $J(\underline{q}\lambda)$ as a function of $\underline{q}$ as shown in figure 5.1.

The neutron scattering function is dependent on the direction of $\underline{q}$ through the correlation function $\Gamma(\underline{q}\lambda)$ and as well through the interaction part of the structure factor. The interaction matrix $H_1(\lambda\,\underline{q}j)$ is expected to be very small for the Γ_4 modes as the proton tunnelling vector is almost perpendicular to the $\underline{c}$-axis and therefore the dipole moment produced along the $\underline{c}$-axis would be very small. The matrix H_1 for the Γ_5 modes is on the other hand expected to be quite important, implying that a large $J_1(0\ \Gamma_5)$ exists. As pointed out earlier there is always for any $\underline{q}\to 0$ a transverse Γ_5 mode, so that the scattering from this mode has a structure factor, including the spin part $\mathcal{F}_S$,

$$\mathcal{F}(\underline{\tau}\,\Gamma_5) = \mathcal{F}_S(\underline{\tau}\,\Gamma_5) - \sum_j \mathcal{F}_L(\underline{\tau}j)\,\frac{H_o(\Gamma_5 0j)}{\omega_o^2(0j)}$$

This scattering cannot be removed (as in a Raman scattering experiment) and will always be seen together with the scattering from the longitudinal component, whose structure factor is

$$\mathcal{F}(\underline{\tau}\,\Gamma_5) = \mathcal{F}_S(\underline{\tau}\,\Gamma_5) - \sum_j \mathcal{F}_L(\underline{\tau}j)\,\frac{(H_o(\Gamma_5 0j)+H_1(\Gamma_5 0j)\cos^2\alpha)}{\omega_o^2(0j)+\omega_1^2(0j)\cos^2\alpha}$$

which has its own $\Gamma(0\ \Gamma_5)$ involving $J_1(0\ \Gamma_5)$.

The frequencies $\omega(\underline{q}j)$ are known from the analysis of the phonon

dispersion relations in chapter 3. No estimates, however, have been made of the matrixes J or H, although it was pointed out in section 5.1 that the matrixes can be calculated. It is interesting to recall two results of the phonon calculations at this point. There were two low frequency modes of Γ_4 and Γ_5 symmetry with which a large electric polarisation was associated. It could be reasonably expected that the interaction matrixes H for these modes might dominate the spin - lattice interaction.

5.3 Dynamical model

The model described in this chapter is only applicable to a KDP type crystal with a very low tunnelling frequency for the protons. If the splitting between the two lowest proton energy levels in the double minimum potential well (2Ω) is included in the Hamiltonian then the additional term appearing is (de Gennes, 1963)

$$-2\Omega \sum_{\ell k} X(\ell k)$$

where $X(\ell k)$ is the x-component of the fictitious spin $\frac{1}{2}$ system whose z-component is $S(\ell k)/2$.

Neglecting the proton-lattice interaction, the molecular field approximation shows that the resultant tunnelling modes have an energy above the transition temperature (Brout et al., 1966)

$$\hbar^2 \Omega^2(\underline{q}\lambda) = 4\Omega(\Omega + I(\underline{q}\lambda)\tanh\beta\Omega) \qquad \ldots\ldots\ldots\ldots\ldots 5.14$$

$$\propto (T - T_c(\underline{q}\lambda))/T \text{ for } \beta\Omega \ll 1.$$

Applying the adiabatic approximation to the proton-lattice interaction $I(\underline{q}\lambda)$ becomes $J(\underline{q}\lambda)$ (Novakovic, 1967). Equation 5.14 is also obtained when the adiabatic approximation is applied to Kobayashi's (1968) one phonon coupled equations of motion result.

The effect of the proton-lattice interaction on the phonons is to raise their frequency (Kobayashi, 1968), but as $\Omega \to 0$, the change also becomes zero, as in the adiabatic approximation. This implies that for DKDP the lattice dynamical calculations of chapter 3 are valid.

For a large 2Ω, however, it must be remembered that the protons are in double minimum potential wells and it is therefore expected that their motion might be considerably damped. The neutron scattering function is

$$\mathcal{S}(\underline{Q},\omega) = N \sum_{\lambda} |\mathcal{F}(\underline{Q}\lambda)|^2 \int \langle S(-\underline{q}\lambda, 0)S(\underline{q}\lambda, t)\rangle \exp(-i\omega t)dt$$

In the molecular field and random phase approximations the integral in this equation, $\Gamma(\underline{q}\lambda,\omega)$, for a damped excitation is expected to be (Cochran, 1969)

$$\Gamma(\underline{q}\lambda,\omega) = \frac{8\Omega}{\hbar} \tanh\beta\Omega\,(\bar{n}(\omega) + 1)\,\frac{2\omega\gamma(\underline{q}\lambda)}{(\Omega^2(\underline{q}\lambda) - \omega^2)^2 + 4\omega^2\gamma^2(\underline{q}\lambda)}$$

where $\bar{n}(\omega) = (\exp(\beta\hbar\omega) - 1)^{-1}$ and $\gamma(\underline{q}\lambda)$ is a damping constant.

For an overdamped mode $\gamma(\underline{q}\lambda) >> \Omega(\underline{q}\lambda)$ and for low frequencies $\beta\hbar\omega << 1$, $\Gamma(\underline{q}\lambda, \omega)$ becomes Lorentzian in frequency

$$\Gamma(\underline{q}\lambda, \omega) = \frac{8\Omega^2}{\hbar^2 2\gamma(\underline{q}\lambda)} \quad \frac{1}{\omega^2 + \left(\frac{\Omega^2(\underline{q}\lambda)}{2\gamma(\underline{q}\lambda)}\right)^2} \qquad \ldots\ldots\ldots\ldots\ldots 5.15$$

and using 5.14

$$\Gamma(\underline{q}\lambda, \omega) = \frac{1}{1+\beta J(\underline{q}\lambda)} \quad \frac{2\tau(\underline{q}\lambda)}{1+\omega^2\tau^2(\underline{q}\lambda)} \qquad \ldots\ldots\ldots\ldots\ldots 5.16$$

with

$$\tau(\underline{q}\lambda) = \frac{2\gamma(\underline{q}\lambda)}{\Omega^2(\underline{q}\lambda)} = \frac{\hbar^2\gamma(\underline{q}\lambda)}{2\Omega^2(1+\beta J(\underline{q}\lambda))}$$

and when integrated over frequency

$$\Gamma(\underline{q}\lambda) = \int \Gamma(\underline{q}\lambda, \omega) \frac{d\omega}{2\pi} = (1 + \beta J(\underline{q}\lambda))^{-1}$$

which is the Ising model result. Equations 5.15 and 5.16 are identical with the integral $\Gamma(\underline{q}\lambda, \omega)$ describing the dynamical nature of the Ising model (Suzuki and Kubo, 1968) as discussed by Cochran (1969). The relaxation time $\tau(\underline{q}\lambda)$ for the tunnelling mode shows the 'critical slowing down' form.

The results for DKDP may therefore be described either by the Ising model formalism of by an overdamped tunnelling model with a definite

tunnelling integral 2Ω. However, as the effect of the transition on the phonons is experimentally negligible (chapter 2), while the frequencies should increase as the temperature is lowered (Kobayashi, 1968), it may be suggested that the tunnelling integral 2Ω in DKDP is rather small.

Figure 5.1

Interaction constants $J(\underline{q}\,\lambda)$ for DKDP

The splittings for Γ assume that the longitudinal tunnelling modes have a greater $J(O\Gamma)$ than the transverse modes. The Γ_2 and M_5 modes involve four protons approaching one PO_4 group.

DKDP

J(q λ)

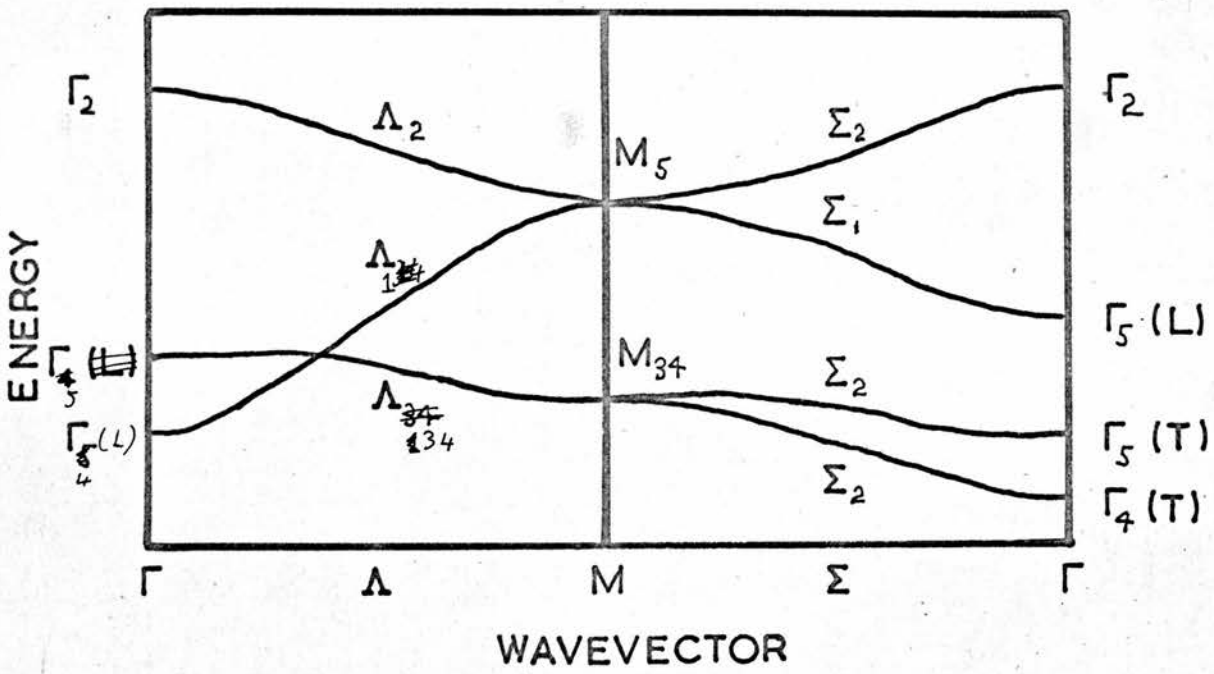
Γ2
Λ2
M5
Σ2
Γ2
Σ1
Λ
Γ5 (L)
ENERGY
M34
Σ2
Γ5 (T)
Γ5 (L)
Σ2
Γ4 (T)
Γ
Λ
M
Σ
Γ
WAVEVECTOR

6. Discussion

6.1 DKDP

In order to examine the implications of the model presented in the last chapter when applied to the experimental results for DKDP, it is necessary to extend the expression for the dielectric properties of the simple model of chapter 4 to the microscopic model. The formulae are given by Cochran (1969). The expression for the c-axis transverse dielectric constant is

$$\epsilon(0) = \epsilon_L + 4\pi v \left| \underline{P}(\Gamma_4) \right|^2 \beta \Gamma(0\ \Gamma_4)$$

In the same way as the structure factor for the neutron scattering is split into fictitious spin and lattice parts, the structure factor here

$$\underline{P}(\Gamma_4) = \sum_{k=H} \left\{ \frac{Z(k)}{v} \underline{a}(k) - \sum_j \underline{P}(0j) \frac{H(k0j)}{\omega^2(0j)} \right\} E(k0\ \Gamma_4)$$

where the terms are defined in chapter 5, and Z(k) is the apparent charge for the deuterium atoms. The lattice dielectric constant is composed of a high frequency part and a phonon part

$$\epsilon_L = \epsilon_\infty + 4\pi v \sum_j \left| \underline{P}(0j) \right|^2 / \omega^2(0j)$$

The summations over j in both of these expressions involve only Γ_4 terms.

A simple expression for the dielectric constant may be obtained when there is one dominant spin-lattice interaction and it is assumed that the deuterons do not contribute to the polarisation. Then, retaining the index j, and using equation 5.13

$$\epsilon(0) = \epsilon_\infty + 4\pi v \frac{|\underline{\underline{R}}(0j)|^2}{\omega^2(0j)} \left\{ 1 + (I(0\ \Gamma_4) - J(0\ \Gamma_4))\, \beta\, \Gamma(0\ \Gamma_4) \right\}$$

$$= \epsilon_\infty + (\epsilon_L - \epsilon_\infty) \left\{ 1 + \frac{T_c(0\ \Gamma_4) - T_o(0\ \Gamma_4)}{T - T_c(0\ \Gamma_4)} \right\}$$

where $T_o(0\ \Gamma_4) = -I(0\ \Gamma_4)/k_B$. Now remembering that the Curie constant $C = 4040^\circ K$ and $\epsilon_L - \epsilon_\infty = 4.1$ (chapter 4), it is found that, in abbreviated notation, $T_c - T_o \simeq 980^\circ K$, and therefore $T_o \simeq -760^\circ K$. This fact says that the deuterium system is stable and that the transition is caused by the interaction of the deuteron system with the lattice.

Using the adiabatic approximation to include the spin-lattice interaction (Novakovic, 1966), the transition temperature in the dynamic tunnelling model with a tunnelling integral 2Ω is given by

$$\tanh \beta_c \Omega = \Omega / J(0\ \Gamma_4)$$

The value for Ω determined by Kaminow and Damen (1968) for KDP is 1.5THz so that at $T_c = 123^\circ K$, $J(0\ \Gamma_4) = 136^\circ K$. The dielectric susceptibility of the dynamic tunnelling model may be reduced to the form given above in the limit $\tanh \beta\Omega \simeq \beta\Omega$ (Kobayashi, 1968). Then, for KDP, using $\epsilon_L - \epsilon_\infty = 5.7$ from the results of Barker and Tinkham (1963),

the difference $T_c - T_o$ may be calculated as 570°K from C = 3250°K (Jona and Shirane, 1962) so that T_o = -430°K. It should be mentioned that the difference between the results for $\epsilon_L - \epsilon_\infty$ for DKDP and KDP seemsrather large. It is however clear that the difference between the transition temperatures of KDP and DKDP is not described by the tunnelling of the protons, and further, that the proton-lattice interaction in the crystals is of different magnitude.

The neutron scattering properties can not be simplified by considering the interaction with only one mode, as the deuterium atoms do contribute to the scattering, except possibly along $\underline{c}^*$. In the analysis of chapter 4 it has been shown that the structure factor may be separated from the correlation function. The results not only gave a reasonable fit to the correlation function, but also indicated an anomaly in the structure factor, as predicted by the spin-lattice interaction.

The Raman scattering results of Kaminow and Damen (1968) on KDP show that the ferroelectric mode is a heavily damped excitation. They were able to extract both a damping constant and a frequency from the observations at each temperature, showing an excitation with the temperature dependence of equation 5.14 and a temperature independent damping constant. In view of the results of Hill and Ichiki (1963) on the dielectric susceptibility of DKDP (figure 4.1) it is reasonable to regard the Ising model formation used throughout as a simplification. The excitation

being discussed is really highly damped and the correlation function is given in section 5.3.

6.2 DADP

It is of interest to see what the microscopic model can predict when applied to other KDP type crystals. The ammonium compounds in the series, characterised by ADP have an antiferroelectric transition. The structure of the lowest temperature phase has not been determined, but its orthorhombic symmetry shows that its space group must be $\underline{P}2_12_12_1$ resulting from a condensation of an M_{34} mode rather than $\underline{P}\bar{4}$ symmetry resulting from an M5 mode (figure A1.3). For a crystal of DADP the tunnelling modes should be overdamped as in DKDP and therefore quasi-elastic critical scattering at the zone boundary point M would be expected. No electric polarisation is created in the crystal by an M_{34} mode so that the critical scattering would have a regular profile with $\bar{4}2m$ symmetry. The scattering results from a doubly degenerate mode so that, as in DKDP the pair correlation function can not be of the Ornstein-Zernike type. This convolution function is isotropic and therefore may only occur at Γ (for a non polar mode), or at the zone boundary, in cubic crystals with triply degenerate modes.

The critical scattering observed by Meister et al. (1969) for DADP had the above characteristics. They were also able to detect inelasticity

in the scattering and found that the inverse relaxation time of equation 5.16 was proportional to temperature. Section 5.3, however, shows that the inverse relaxation time should be proportional to inverse temperature and the results were found to fit this relation just as well with $2\Omega^2/\gamma^2(\underline{q}\, M_{34}) = 1.4$THz. It is interesting to compare this value with the 1.75THz of Kaminow and Damen (1968), and a value less than 0.07THz from Hill and Ichiki (1963) for DKDP. It should be remembered that for an overdamped excitation it is required that $\gamma >> \Omega$. It is generally assumed that the tunnelling is slower in deuterated crystals than in hydrogenated ones, and with the value of 1.5THz for Ω from the KDP results (Kaminow and Damen, 1968), this leads to an estimate of γ for DADP of between 0.7 and 3.0THz, compared with the value 2.6THz for KDP.

Apart from the scattering at the zone boundary, the model also predicts scattering at the zone centre. The a-axis dielectric constant of ADP (Kaminow, 1965) has the Curie-Weiss behaviour with an extrapolated Curie temperature of -55°K, well below the transition temperature of the crystal. As there is no phonon in KDP with an anomalous temperature dependence, this implies that the Γ_5 tunnelling modes in ADP should give some neutron scattering. The same dielectric constant in KH_2AsO_4 is anomalous implying that underneath the critical scattering for the Γ_4 mode there is also critical scattering from the ferroelectric Γ_5 mode.

It may also be seen that this change in dielectric constant with replacement of phosphorus by arsenic may only be explained by proton-lattice interaction, which is qualitatively described by the model.

As described in section 5.2, the neutron scattering from these modes has a contribution from one branch (transverse) which has no anomaly near Γ, in a similar way to the M_{34} scattering. The other Γ_5 branch has the same type of anomaly as the Γ_4 branch, in this case due to the electric field set up in the a-direction, and the scattering will be reduced in the a* - b* plane, producing a dumbbell along the c*-axis.

6.3 Elastic constants

As DKDP is a piezoelectric crystal in the paraelectric phase, the elastic constant c_{66} is expected to have anomalous temperature dependence. The effect arises through coupling of the acoustic modes and the polarisation in the crystal (Jona and Shirane, 1962).

The elastic constants may be measured with a plated or an unplated crystal. The former technique allows no charges to build up on the surface of the crystal so that the elastic constants are those at constant electric field. It is this constant which is anomalous. The difference between the elastic constants or their inverses is proportional to the clamped or free dielectric constants, which are measured by long wavelength excitations

with high and low frequency. The constant electric field elastic constants are also measured by Brillouin scattering (KDP, Brody and Cummins, 1968). The non anomalous piezoelectric and other constants for the crystal may be used to predict that the free Curie temperature, which is always greater than the clamped Curie temperature is $4^{\circ}K$ higher in KDP (Jona and Shirane, 1962), in agreement with the difference between the experiments of Brody and Cummins (1968) and the free dielectric Raman scattering measurements of Kaminow and Damen (1968).

The dielectric response of the DKDP crystal, as measured by neutron scattering is at frequencies less than the acoustic wave energies so that the elastic constants measured are the values at constant polarisation and they should not have an anomaly. It is therefore interesting that the intensity of the neutron group corresponding to the c_{66} elastic constant was temperature dependent, although its frequency remained constant.

This point also means that the free dielectric response of the crystal is measured in the neutron experiments, so that the calculated $T_c = 222 \pm 2^{\circ}K$ (chapter 4) is in good agreement with the transition temperature of $223.6^{\circ}K$. The results of Hill and Ichiki (1963) on an incompletely deuterated crystal showed the free and clamped transition temperatures as $218.5^{\circ}K$ and $211.8^{\circ}K$, a larger difference than in KDP.

Appendix 1

Crystallography and Group Theory of KDP

A1.1 Structure

The crystal structure of KDP was first determined by X-ray diffraction (West, 1930). Neutron diffraction studies by Bacon and Pease (1953, 1955) revealed that above the transition temperature the hydrogen atoms in the crystal were either dynamically or statically disordered between two sites in a hydrogen bond between PO_4 groups. Below the transition temperature the hydrogen atoms become ordered on one of the sites so that H_2PO_4 groups with dipole moments in the c-direction are formed and the crystal becomes polarised in the c-direction.

The space group above the transition temperature is the body centred tetragonal $I\bar{4}2d$. The crystal is piezoelectric, that is, it does not have a centre of symmetry and it is also non polar. The body centred tetragonal crystal may be described in terms of a face centred tetragonal cell of twice the volume with space group $F\bar{4}d2$. This cell is then more easily related to that of the low temperature phase whose space group is the polar $Fdd2$. There are four units of KH_2PO_4 in the body centred cell $I\bar{4}2d$ and therefore only two units in the primitive cell. The origin chosen by the International Tables, Vol. 1 (1965) for $I\bar{4}2d$ will be used here. The unit cell dimensions and coordinates of the atoms in the paraelectric and ferroelectric phases of KDP are given in table A1.1

The paraelectric structure of KDP is shown in figure A1.1 The potassium and phosphorus atoms are on sites of $\bar{4}$ point symmetry, the centres of the hydrogen bonds lie on two fold axes and the oxygen and hydrogen atom sites are in general positions of point symmetry 1. The almost regular PO_4 tetrahedra are linked by hydrogen bonds (which contain only one hydrogen atom, but two possible sites) to four other PO_4 tetrahedra. The potassium atoms are placed $\underline{c}/2$ from the phosphorus atoms in this framework.

A1.2 Group theory

High symmetry points in the Brillouin zone of KDP are shown in figure A1.2 The zone corresponds to the body centred tetragonal Bravais lattice of KDP which has a c/a ratio of 0.93. An incorrect zone had previously been used by Shur (1966). The point group of the crystal is $\bar{4}2m$ and there are eight point group elements: E, $\bar{4}$, 2_z, $\bar{4}^{-1}$, 2_x, m_d, 2_y, $m_{d'}$.

The elements of a space group may be written $(\gamma | \underline{v}_\gamma + \underline{n})$ where $\underline{n}$ is a lattice vector and $\underline{v}_\gamma$ is some non-primitive translation. In the non-symmorphic space group $I\bar{4}2d$ there is a non-primitive translation $\underline{v} = (0, \frac{1}{2}, \frac{1}{4})$ associated with the last four point group elements above. The only elements which require definition are $\bar{4}$, which operating in a fixed coordinate system, rotates and inverts the crystal so that what was at (x, y, z) moves to $(y, \bar{x}, \bar{z})$, and $m_{d'}$, which is the (110) plane.

Using the multiplier group techniques and notation described by Montgomery (1969) character tables for the multiplier group operators may be obtained for all the points in the Brillouin zone. These are shown in table A1.2. Also shown is the time reversal type. At Γ, the letters R and I-R indicate whether lattice vibrations with certain symmetries are Raman or infra-red active. The Γ_4 modes polarise the crystal in the z-direction and the Γ_5 modes polarise the crystal in the x-y plane.

The irreducible representations (IRs) for points inside the zone are just those for the point group of that wave vector $\underline{q}$ ($\Gamma, \Lambda, \Sigma, \Delta$, point groups $\bar{4}2m$, 2mm, 2, m). For points on the zone boundaries the multiplication table for the operators was set up and attempts were made to find one dimensional representations. For point groups of order 2 the matter is trivial (Y, N, point groups m, 2) as the multiplier group must be projective equivalent to the point group. The importance of projective equivalence is that the IRs of the multiplier group are some complex number (dependent only on γ) times the IRs of the point group. At X and W, point group 2mm, the multiplier group is not projective equivalent and there exists only one two dimensional IR, so that a one dimensional IR could not be found. At P and M ($\bar{4}2m$) some effort and assistance were required to determine the representations. M is projective equivalent, while P is not. Some matrixes for the two dimensional IRs which were found to be of use are given in table A1.3.

Time reversal symmetry has important effects on the IRs, particularly with regard to lattice vibrations. The star of $\underline{q}$ is defined as the set of wave vectors obtained by operating on $\underline{q}$ by each member of the point group of the crystal. There are now three cases to discuss. If $-\underline{q}$ is not in the star of $\underline{q}$ then time reversal makes each normal mode of wave vector $\underline{q}$ degenerate with a normal mode at $-\underline{q}$. When $-\underline{q}$ is in the star of $\underline{q}$ some restrictions are placed on the basis vectors for lattice vibrations in the space group $I\bar{4}2\underline{d}$. Time reversal degeneracy then may or may not exist, making two different IRs degenerate (the spaces which transform as the IRs become degenerate). The case in which no time reversal degeneracy exists is called type 1 and the other two cases are type 3 (Montgomery, 1969). The type and degeneracy of the IR's are given in table A1.2 with their labels. Matrixes for these time reversal degenerate IRs which were of some use are given in table A1.3.

For wave vectors in the plane containing Λ and Δ and the face containing W and Y the IRs are those of Δ and Y respectively. The IRs are not degenerate and are of type 3. The identity representation occurs for all other wave vectors, being type 3 except in the $\underline{a}^*$ - $\underline{c}^*$ and $\underline{a}^*$ - $\underline{b}^*$ planes where it is type 1. Some compatibility relations are given in table A1.4. It should be noted that time reversal types are not compatible.

A1.3 Lattice vibrations in KDP

The projection operator techniques described by Montgomery (1969)

(whose notation will be used here) were used to determine the basis vectors of the lattice vibrations for each representation. It is useful first to decompose the vibration space S_V for the crystal into its irreducible subspaces in order to find the number of occurrences of each IR. S_V is regarded as the product of a cell space S_C and a three dimensional complex Euclidean space S_E (Montgomery, 1969). The produce space concept is a particularly clear way of describing the intuitive application of projection operators to S_V.

The IRs of S_E are those of the point group of $\underline{q}$ and are therefore known. S_C must be decomposed by first separating it into invariant subspaces corresponding to each atomic species, or more specifically, each Wyckoff set, and then determining the character of each of these subspaces. The IRs of S_V are then derived from the product of the IRs of S_E and S_C.

In an initial analysis of KDP the protons may be omitted and the KPO_4 framework may be considered by itself. The oxygen atoms are all symmetry related and so there are only three types of atoms in the primitive cell which contains 2K, 2P and 8 oxygen atoms. S_C is therefore composed of S_K, S_P and S_O which are 2, 2 and 8 dimensional. If the high frequency lattice vibrations are of interest then the protons may be added to this system by assuming that they are in general positions. There are then two protons in the hydrogen bond and eight in the crystal instead of the actual number of four. They are in this case regarded by the group

theory in exactly the same manner as the oxygen atoms. A four dimensional space S_H in which the protons are considered to be at the centres of the hydrogen bonds may also be required. This space, however, is not involved in the determination of the tunnelling motion of the hydrogen atoms which is discussed in the next section.

S_O provides no problem as the atoms are on general positions (x, y, z). At Γ, S_O transforms as the regular representation, which contains all IRs and in which the number of occurrences of each IR is its dimensionality. At other wave vectors S_O transforms as the regular representation times 8 (the number of oxygen atoms) divided by the order of the point group of $\underline{q}$. The oxygen contribution to S_V then transforms as an integral number of regular representations (1, 2, 4 or 8) times three (from S_E). For this reason, in any IR the motion of the oxygen atoms is not restricted to any particular direction. This fact, which is probably so obvious that it should not be stressed, is true for atoms on general positions in any space group. The lattice vibrations in KDP may therefore only be classified as transverse and longitudinal with respect to the motion of the phosphorus and potassium atoms. The characters of S_K, S_P, S_O, S_H and the resultant character of S_V (excluding S_H) are given in table A1. 5. The restrictions on the motion of the phosphorus and potassium atoms are also given. The P and K atoms do not move in lattice vibrations which transform as Γ_1 and Γ_2. In every IR the restrictions placed on their motion are identical except at P where z

motion is not allowed for phosphorus and potassium atoms in P_1 and P_2 modes respectively.

The effect of the projection operator $\rho^{s}_{\lambda\mu}$ for the $\lambda\mu$ th component of the s th IR (Montgomery, 1969) on the vector ($|k\rangle \underline{i}_\beta$) in S_V may be written

$$\rho^{s}_{\lambda\mu}(|k\rangle \underline{i}_\beta) = \sum_\gamma (|\gamma k\rangle \gamma \underline{i}_\beta) N^{s}_{\lambda\mu}(\gamma, k) \quad \text{.....A1.1}$$

where ($|\gamma k\rangle \underline{i}_\beta$) is a vector in S_V; $|k\rangle$ and $|\gamma k\rangle$ are vectors in S_C, in particular, vectors in an invariant subspace of S_C, i. e. they refer to one type of atom only; and $\underline{i}_\beta$ and $\gamma \underline{i}_\beta$ are vectors in S_E. N is some complex number (defined by Montgomery (1969)). This equation links the simplicity of the product space concept ($|k\rangle \underline{i}_\beta$) with the intuitive application of projection operators, in which a set of three orthogonal vectors $\underline{i}_1$, $\underline{i}_2$, $\underline{i}_3$ is attached to an atom $|k\rangle$ and for each γ the whole set is taken to $|\gamma k\rangle$ (and becomes ($|\gamma k\rangle \gamma \underline{i}_\beta$)) and is multiplied by a number N. When the atom $|k\rangle$ is on a general position the picture built up by this process is the sum of three normalised basis vectors for the $\lambda\mu$ th component of the IR. The orthogonality of the original set $\underline{i}_\beta$ means that the basis vectors projected out are orthogonal.

The nonsymmorphic nature of the space group ($\underline{v}_\gamma$) does not enter explicitly into the projection operator. The picture described above may therefore be represented by the stereogram for the point group of the crystal with a vector $x\underline{i}_1 + y\underline{i}_2 + z\underline{i}_3$ representing the set $\underline{i}_\beta$ attached to

each atomic site. The stereogram plus vectors is shown in figure A1.3 The numbers N for each IR associated with each atom $|\delta\, k\rangle$ are then applied to the vectors and the picture of a basis vector is constructed. Each picture represents three basis vectors, corresponding to the three coordinates $\underline{i}_\beta$. The λ th basis vector (the IR may be two dimensional) of the p th occurrence (three for a one dimensional and six for a two dimensional IR) of the IR s at wave vector $\underline{q}$ is written $|pqs\lambda\rangle$.

The complete story is only told when time reversal has been considered. If the rotational part of the space group operator A transforms $\underline{q}$ into $-\underline{q}$ then the effect of the time reversal operator $\mathcal{R}$, which depends on the time reversal type, may be written (Montgomery, 1969).

$$\mathcal{R}|pqs\lambda\rangle = A\ |pqs\lambda\rangle \qquad \text{(type 1)} \qquad \ldots\ldots\ldots\ldots\text{A1.2}$$

$$\mathcal{R}|pqs\lambda\rangle = A\ |pqs'\lambda\rangle \qquad \text{(type 3)} \qquad \ldots\ldots\ldots\ldots\text{A1.3}$$

If $-\underline{q}$ is not in the star of $\underline{q}$ then

$$\mathcal{R}|pqs\lambda\rangle = |p\text{-}qs\lambda\rangle \qquad \text{(type 3)} \qquad \ldots\ldots\ldots\ldots\text{A1.4}$$

These equations depend on the choice of unimportant phase factors. When these equations are applied to the pictures for the basis vectors it is easily seen that only certain linear combinations of the basis vectors are allowed. The resultant basis vectors for Γ, Λ and Σ are shown in figure A1.3.

The basis vectors for atoms on special positions may be obtained quite simply from the basis vectors for atoms on general positions. In

some cases the basis vectors may be obtained more easily (by some) by inspection. Atoms at general positions will converge on a special position if one, two or all of the atomic coordinates are restricted to a special value. The projection operator of equation A1.1 operates on the vector $\underline{i}_\beta$ at $|k\rangle$. If $|k\rangle$ is now an atom at a special position then the projection operator will project out the same basis vector as for an atom at a general position, but the atoms $|\gamma k\rangle$ and their associated vectors $\gamma \underline{i}_\beta$ will converge onto the special positions. The vector addition of the $\gamma \underline{i}_\beta$'s may produce the zero vector, implying that an atom does not move in a particular IR (e.g. Γ_1 and Γ_2 for P and K atoms). This vector addition is also shown in figure A1.3. The basis vectors for Γ agree with those given by Shur (1966).

This group theory is of considerable use as the basis vectors block diagonalise the dynamical matrix defined in chapter 3; and using the dynamical operator $\mathcal{D}$ (Montgomery, 1969):

$$\langle \underline{pqs}\ \lambda | \mathcal{D} | p'\underline{qs}'\ \lambda' \rangle = D^{s}_{pp'}(\underline{q})\, \delta_{ss'}\, \delta_{\lambda\lambda'} \quad \text{.....A1.5}$$

where p runs over each basis vector of the λ th component of the IR s (Montgomery, 1969). The observation that the submatrixes $D_{pp'}$ are real for type 1 and complex conjugate for two degenerate type 3 IRs has been shown to be a completely general fact (H. Montgomery, private communication). This means that for a type 1 IR the eigenvalues and eigenvectors of a real matrix have to be found and this saves considerable computing time over a complex matrix routine.

The dynamical matrix for the KPO_4 problem is 36x36 dimensional. Group theory enables the matrix to be decomposed into submatrixes whose dimensions are given in the row for S_V in table A1.5. The calculation of eigenvalues for both partners of degenerate and time reversal degenerate IRs is avoided and also real matrix routines may be used in places. The Coulomb interaction part of the dynamical matrix is only calculated in the limit $\underline{q} \rightarrow 0$. Therefore for $q_x \rightarrow 0$, $q_y = q_z = 0$, the basis vectors for Σ must be used rather than those for Γ. The electric field which is set up in the crystal by the polar modes Γ_4 and Γ_5 causes the frequencies of these modes to depend on the direction of approach to $\underline{q} = 0$. This field is not taken into account by the group theory which cannot therefore be expected to predict splitting of the polar modes.

A1.4 Tunnelling of the protons in KDP

The two equilibrium sites for a proton in its hydrogen bond are related by a twofold axis (2_x or 2_y). The displacement of the proton which tunnels from one site to another in the bond is thus limited to a direction perpendicular to the two fold axis. There are four hydrogen bonds per primitive cell and therefore four tunnelling degrees of freedom for the proton. The four displacements or tunnelling vectors form a space and it is required to find the character of this space.

This problem cannot be solved by decomposing the space into S_C and

S_E as the tunnelling vectors depend on $|k\rangle$. The operators of the multiplier group must therefore be applied directly to the tunnelling vectors. The character of the space may then be determined for each $\underline{q}$:

Γ	$\Gamma_2 + \Gamma_4 + \Gamma_5$
M	$M_{34} + M_5$
P	$P_1 + P_2$
X	$2X_1$
Λ	$\Lambda_1 + \Lambda_2 + \Lambda_{34}$
Σ	$\Sigma_1 + 3\Sigma_2$

and others determined by compatibility.

The projection operator applied to one tunnelling vector yields the basis vectors of the irreducible subspaces. These basis vectors are shown schematically in figure A1.4 with the tunnelling vectors represented by arrows. It should be noted that these vectors are not displacements in lattice vibrations, but they represent a totally different degree of freedom discussed in chapter 5. The schematic pictures for $\underline{q} = 0$ were introduced by Kaminow (1965). Novakovic (1967) also used the pictures for $\underline{q} = 0$, however, labelling the M_{34} modes Γ_5.

Table A1.1

The unit cells of paraelectric and ferroelectric KDP

Fractional coordinates are given (Bacon and Pease, 1955).

The paraelectric cell dimensions are from Sliker and Burlage (1963).

	paraelectric			ferroelectric		
space group	$I\bar{4}2d$			Fdd2		
cell dimensions	(296°K)			(77°K)		
a	7.453			10.458		
b	7.453			10.54		
c	6.975			6.918		
coordinates	(132°K)			(77°K)		
	x	y	z	x	y	z
P	0	0	0	0	0	0
K	0	0	0.5	0	0	0.516
OH	0.149	0.0827	0.126	0.1158	-0.0339	0.139
O				0.0339	0.1164	-0.117
D	0.147	0.227	0.123	0.187	0.037	0.138

Table A1.2

Character tables for the space group $I\bar{4}2d$

γ	E	$\bar{4}$	2_z	$\bar{4}^{-1}$	2_x	m_d	2_y	$m_{d'}$	Time reversal
$\underline{v}_\gamma$	0	0	0	0	v	v	v	v	type
Γ_1	1	1	1	1	1	1	1	1	R
Γ_2	1	1	1	1	-1	-1	-1	-1	
Γ_3	1	-1	1	-1	1	-1	1	-1	R
Γ_4	1	-1	1	-1	-1	1	-1	1	R, I-R(z)
Γ_5	2	0	-2	0	0	0	0	0	R, I-R(x, y)
Λ_1	1		1			1		1	1
Λ_2	1		1			-1		-1	1
Λ_3	1		-1			-1		1	Λ_{34}, 3
Λ_4	1		-1			1		-1	
Σ_1	1				1				1
Σ_2	1				-1				1
M_1	1	i	-1	-i	1	-i	-1	i	M_{12}, 3
M_2	1	-i	-1	i	1	i	-1	-i	
M_3	1	i	-1	-i	-1	i	1	-i	M_{34}, 3
M_4	1	-i	-1	i	-1	-i	1	i	
M_5	2	0	2	0	0	0	0	0	1

γ	E	$\bar{4}$	2_z	$\bar{4}^{-1}$	2_x	m_d	2_y	$m_{d'}$	Time reversal type
Δ_1	1					1			1
Δ_2	1					-1			1
Y_1	1							i	Y_{12}, 3
Y_2	1							-i	
W_1, X_1	2		0			0		0	3, 1
P_1	2	(1-i)	0	(1+i)	0	0	0	0	3
P_2	2	-(1-i)	0	-(1+i)	0	0	0	0	3
N_1', N_1	1						$\frac{1}{\sqrt{2}}(1+i)$		3, 1
N_2', N_2	1						$-\frac{1}{\sqrt{2}}(1+i)$		3, 1

Table A1.3

Representations for the space group $I\bar{4}2d$.

γ	E	$\bar{4}$	2_z	$\bar{4}^{-1}$	2_x	m_d	2_y	$m_{d'}$
Γ_5	$\begin{pmatrix}1 & \\ & 1\end{pmatrix}$	$\begin{pmatrix} & 1\\ -1 & \end{pmatrix}$	$\begin{pmatrix}-1 & \\ & -1\end{pmatrix}$	$\begin{pmatrix} & -1\\ 1 & \end{pmatrix}$	$\begin{pmatrix} & 1\\ 1 & \end{pmatrix}$	$\begin{pmatrix}1 & \\ & -1\end{pmatrix}$	$\begin{pmatrix} & -1\\ -1 & \end{pmatrix}$	$\begin{pmatrix}-1 & \\ & 1\end{pmatrix}$
M_{12}	$\begin{pmatrix}1 & \\ & 1\end{pmatrix}$	$\begin{pmatrix} & 1\\ -1 & \end{pmatrix}$	$\begin{pmatrix}-1 & \\ & -1\end{pmatrix}$	$\begin{pmatrix} & -1\\ 1 & \end{pmatrix}$	$\begin{pmatrix}1 & \\ & 1\end{pmatrix}$	$\begin{pmatrix} & -1\\ 1 & \end{pmatrix}$	$\begin{pmatrix}-1 & \\ & -1\end{pmatrix}$	$\begin{pmatrix} & 1\\ -1 & \end{pmatrix}$
M_{34}	$\begin{pmatrix}1 & \\ & 1\end{pmatrix}$	$\begin{pmatrix} & 1\\ -1 & \end{pmatrix}$	$\begin{pmatrix}-1 & \\ & -1\end{pmatrix}$	$\begin{pmatrix} & -1\\ 1 & \end{pmatrix}$	$\begin{pmatrix}-1 & \\ & -1\end{pmatrix}$	$\begin{pmatrix} & 1\\ -1 & \end{pmatrix}$	$\begin{pmatrix}1 & \\ & 1\end{pmatrix}$	$\begin{pmatrix} & -1\\ 1 & \end{pmatrix}$
M_5	$\begin{pmatrix}1 & \\ & 1\end{pmatrix}$	$\begin{pmatrix}1 & \\ & -1\end{pmatrix}$	$\begin{pmatrix}1 & \\ & 1\end{pmatrix}$	$\begin{pmatrix}1 & \\ & -1\end{pmatrix}$	$\begin{pmatrix} & 1\\ 1 & \end{pmatrix}$	$\begin{pmatrix} & -1\\ 1 & \end{pmatrix}$	$\begin{pmatrix} & 1\\ 1 & \end{pmatrix}$	$\begin{pmatrix} & -1\\ 1 & \end{pmatrix}$
X_1, W_1	$\begin{pmatrix}1 & \\ & 1\end{pmatrix}$		$\begin{pmatrix}1 & \\ & -1\end{pmatrix}$			$\begin{pmatrix} & 1\\ 1 & \end{pmatrix}$		$\begin{pmatrix} & -1\\ 1 & \end{pmatrix}$
P_1	$\begin{pmatrix}1 & \\ & 1\end{pmatrix}$	$\begin{pmatrix}1 & \\ & -i\end{pmatrix}$	$\begin{pmatrix}1 & \\ & -1\end{pmatrix}$	$\begin{pmatrix}1 & \\ & i\end{pmatrix}$	$\begin{pmatrix} & -i\\ 1 & \end{pmatrix}$	$\begin{pmatrix} & 1\\ 1 & \end{pmatrix}$	$\begin{pmatrix} & i\\ 1 & \end{pmatrix}$	$\begin{pmatrix} & -1\\ 1 & \end{pmatrix}$
P_2	$\begin{pmatrix}1 & \\ & 1\end{pmatrix}$	$\begin{pmatrix}-1 & \\ & i\end{pmatrix}$	$\begin{pmatrix}1 & \\ & -1\end{pmatrix}$	$\begin{pmatrix}-1 & \\ & -i\end{pmatrix}$	$\begin{pmatrix} & i\\ -1 & \end{pmatrix}$	$\begin{pmatrix} & 1\\ 1 & \end{pmatrix}$	$\begin{pmatrix} & -i\\ -1 & \end{pmatrix}$	$\begin{pmatrix} & -1\\ 1 & \end{pmatrix}$

Table A1.4

Compatibility relations

Γ_1	$\Lambda_1 \cdot$	$\Sigma_1 \cdot$	Δ_1
Γ_2	$\Lambda_2 \cdot$	$\Sigma_2 \cdot$	Δ_2
Γ_3	$\Lambda_2 \cdot$	$\Sigma_1 \cdot$	Δ_2
Γ_4	$\Lambda_1 \cdot$	$\Sigma_2 \cdot$	Δ_1
Γ_5	Λ_{34},	$\Sigma_1 + \Sigma_2$,	$\Delta_1 + \Delta_2$
M_{12}	Λ_{34},	$2\Sigma_1 \cdot$	Y_{12}
M_{34}	Λ_{34},	$2\Sigma_2 \cdot$	Y_{12}
M_5	$\Lambda_1 + \Lambda_2$,	$\Sigma_1 + \Sigma_2$,	Y_{12}
P_1	$N'_1 + N'_2$,	W_1	
P_2	$N'_1 + N'_2$,	W_1	
X_1	$\Delta_1 + \Delta_2$,	Y_{12}, W_1	

Table A1.5

Characters of Spaces

space	Γ_1	Γ_2	Γ_3	Γ_4	Γ_5	Λ_1	Λ_2	Λ_{34}	Σ_1	Σ_2	M_{12}	M_{34}	M_5	Δ_1	Δ_2	Y_{12}	X_1	P_1	P_2	N_1	N_2
S_P	1	1				1	1		1	1			1	1	1	1	1	1		1	1
S_K	1	1				1	1		1	1			1	1	1	1	1		1	1	1
S_O	1	1	1	1	2	2	2	2	4	4	1	1	2	4	4	4	4	2	2	4	4
S_V	3	3	5	5	10	8	8	10	18	18	5	5	8	18	18	18	18	9	9	18	18
S_H	1		1		1	1	1	1	3	1	1		1	2	2	2	2	1	1	2	2
$S_V(H)$	1	2	1	2	3	3	3	3	5	7	1	2	3	6	6	6	6	3	3	6	6
restrictions																					
P	O		z	z	x,y	z	z	x,y			x,y	x,y	z					x,y			
K	only		z	z	x,y	z	z	x,y			x,y	x,y	z						x,y		

Figure A1.1

The crystal structure of KDP. Space group $I\bar{4}2d$.

KD_2PO_4

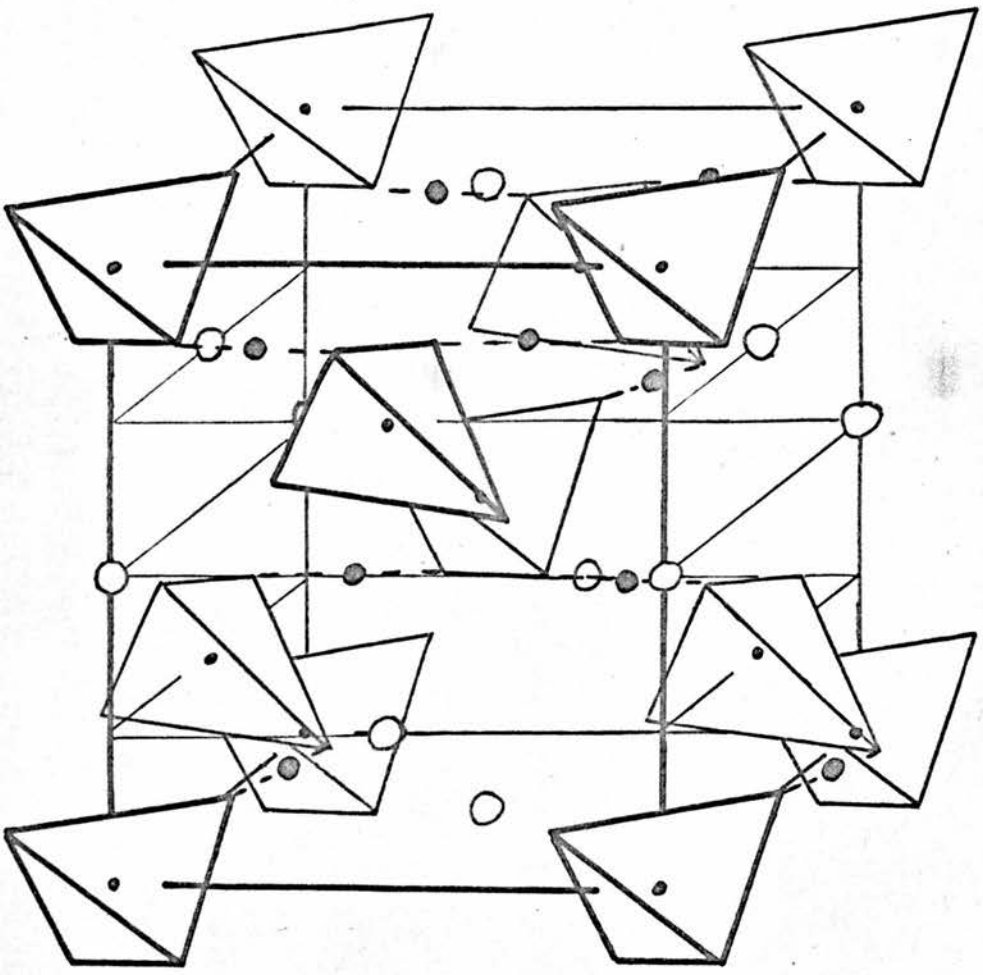

Figure A1.2

Points of high symmetry in the Brillouin zone of KDP.

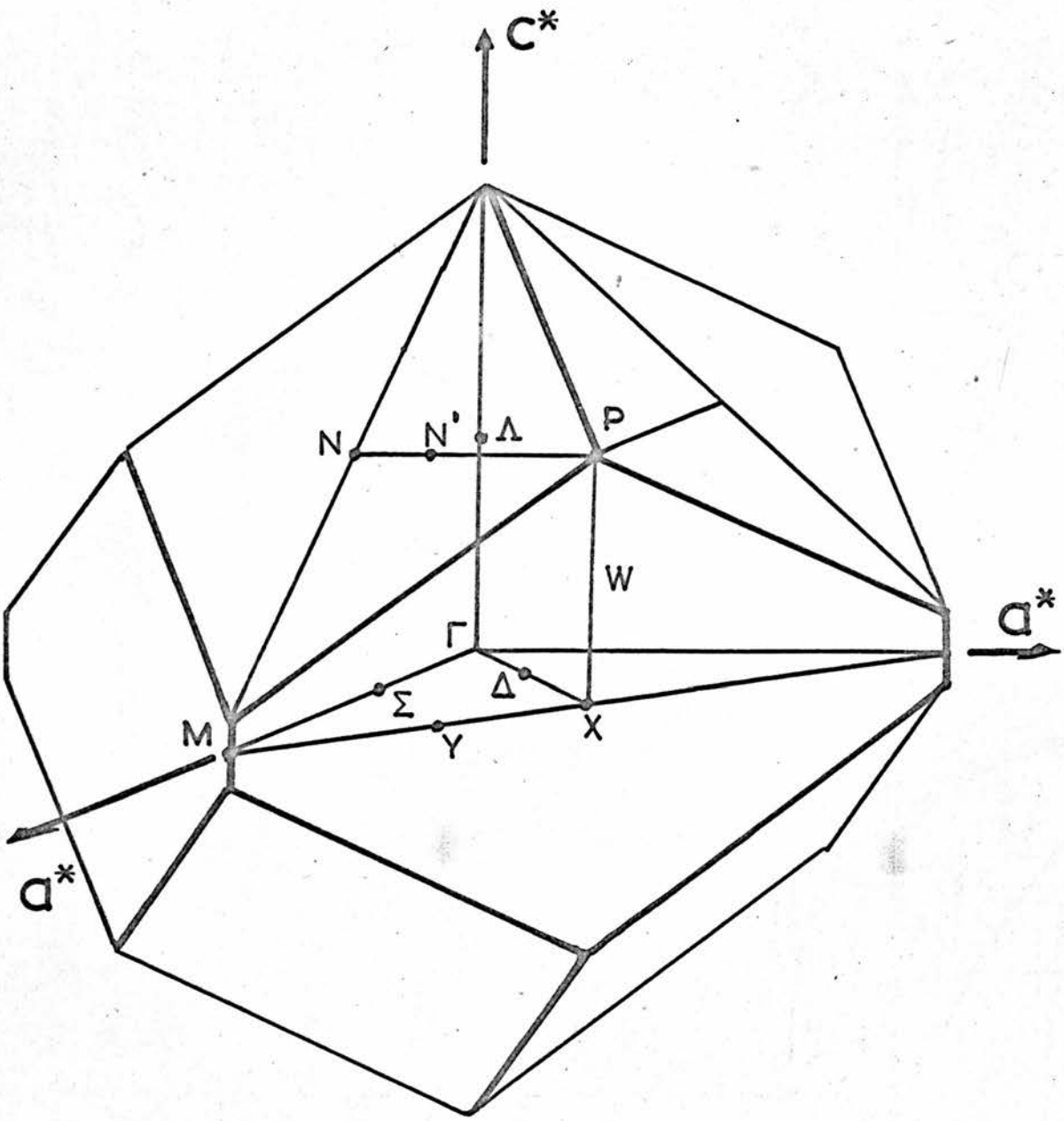
C*
N
N'
Λ
P
W
Γ
a*
Σ
Δ
M
Y
X
a*

Figure A1.3

Basis vectors for Γ, Λ and Σ. For Γ_1 the numbers N in equation A1.1 are all unity and so the picture for Γ_1 is the stereogram plus vectors to which the numbers $N^{s}_{\lambda\mu}(\gamma, k)$ are applied. The circles represent atoms. The filled vectors and circles denote +z and the open vectors and circles -z. The numbers a are complex and the real and imaginary parts represent separate basis vectors which must be normalised. The atoms in special positions (P and K) denoted by x are separated by $\underline{v}$. The + and - mean vectors $\pm$ z and the other vectors are in the x-y plane. For these vectors the components are either purely real or purely imaginary.

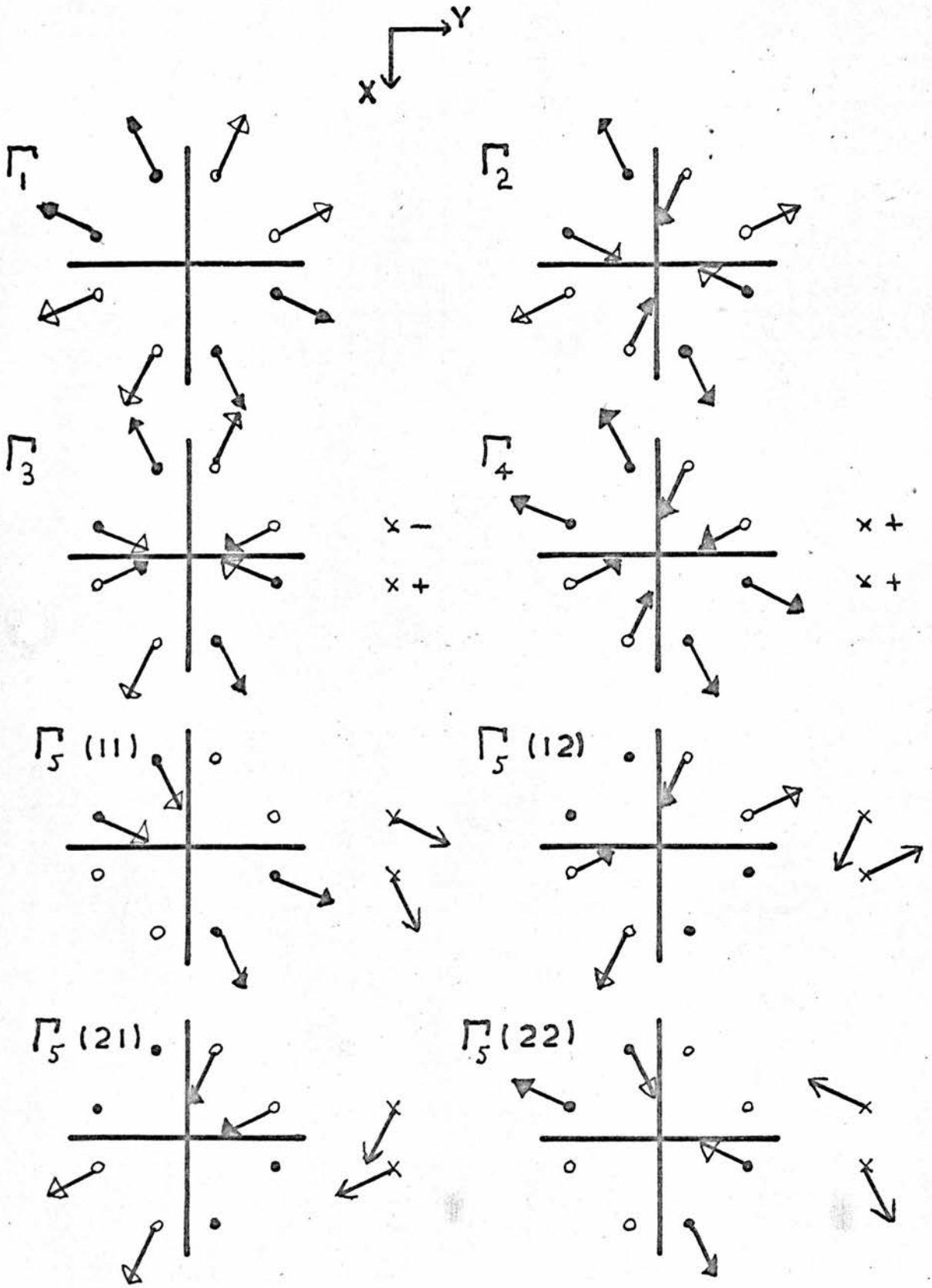
Y
X
Γ1
Γ2
Γ3
× −
× +
Γ4
× +
× +
Γ5 (11)
Γ5 (12)
Γ5 (21)
Γ5 (22)

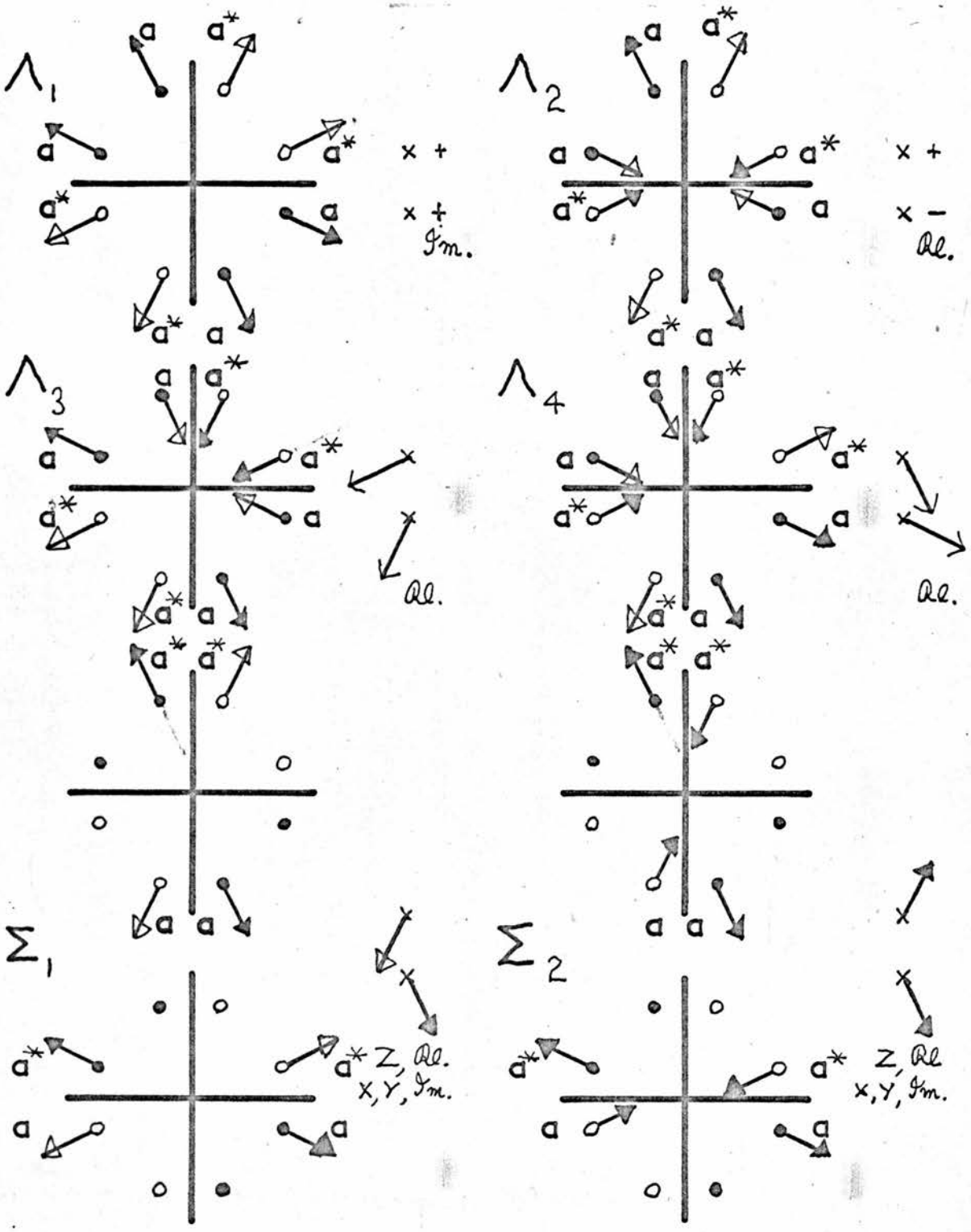
Λ1
a
a*
× +
× +
Im.
Λ2
× +
× −
Re.
Λ3
Re.
Λ4
Re.
Σ1
Z, Re.
X, Y, Im.
Σ2
Z, Re
X, Y, Im.

Figure A1.4

Basis vectors for tunnelling modes in KDP.

KDP TUNNELLING MODES

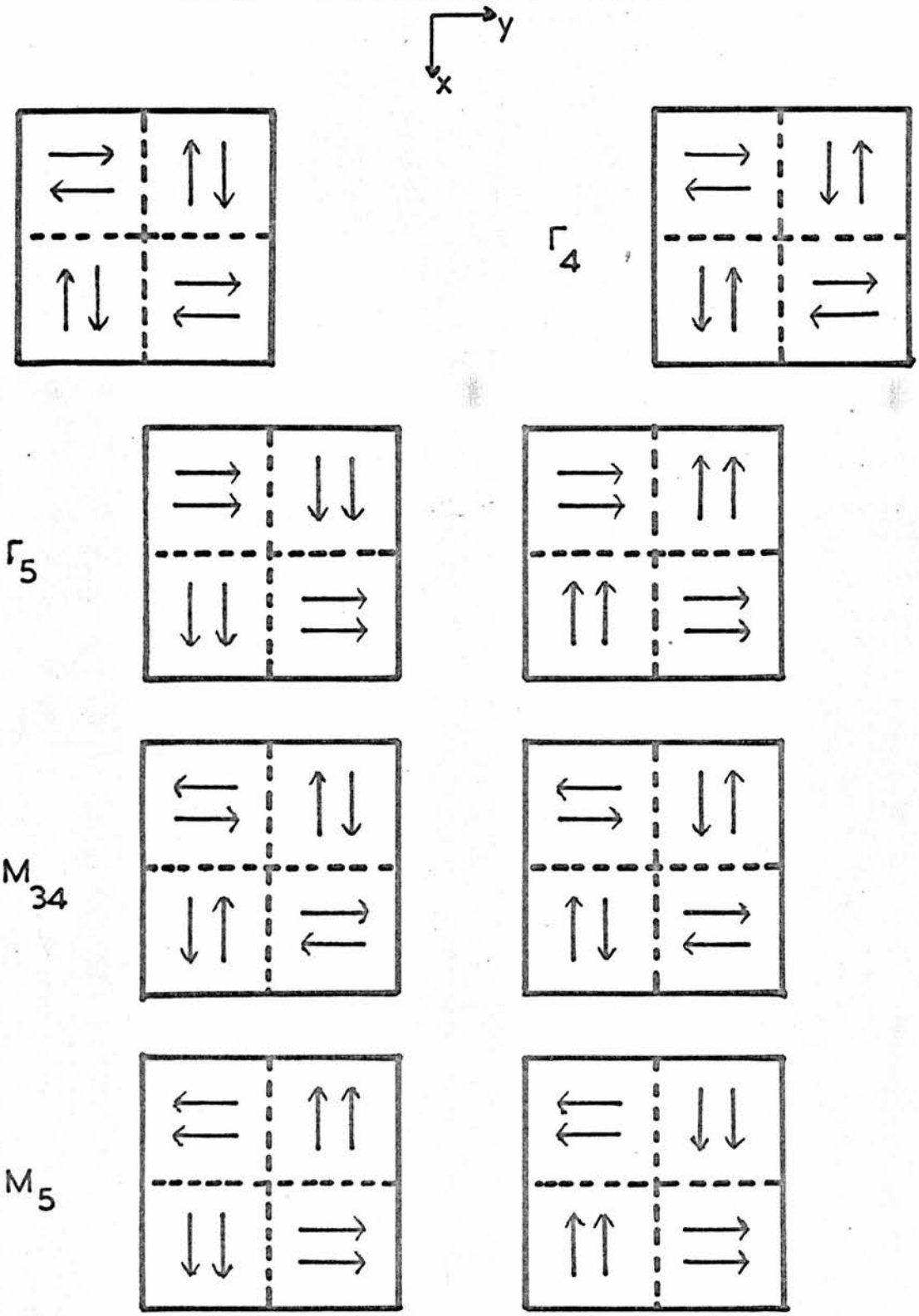

Appendix 2

Experimental Study of (Ge, Sn)Te

A1.1 Introduction

Alloys in the pseudo-binary system $Ge_xSn_{1-x}Te$, written (Ge, Sn)Te, undergo a phase transition from a face centred cubic (NaCl) structure to a face centred rhombohedral (Bi) structure at a temperature which is nearly linearly dependent on the germanium content (Bierly et al., 1963). The transition temperature of a 30% GeTe, 70% SnTe crystal is approximately 280°K and the extrapolated transition temperature for SnTe is 0°K.

A study of the lattice dynamics of the pure SnTe crystal revealed that the transverse optic (TO) branch in the [001] direction is very temperature dependent. The crystal almost becomes ferroelectric, the lowest temperature measured being 6°K (Pawley et al., 1966). A shell model to describe the lattice dynamics, which also takes into account the natural non-stoichiometric character of the semiconducting (p-type) crystals and the resultant screening of the LO (longitudinal) mode (Cowley et al., 1969) shows that the crystal may possibly be regarded as ionic. SnTe may therefore almost be a diatomic ionic ferroelectric the possibility of which was discussed by Cochran (1960).

It is thought that the ferroelectric phase transition in the (Ge, Sn)Te

alloys results from the instability of the TO mode at long wavelengths and is therefore of the displacive type (Pawley et al., 1966). Crystals with a GeTe content of less than 30% are cubic at room temperature. They may therefore be grown from the melt without going through a phase transition and may be studied with ease above the transition temperature. The simplicity of the experiment on the ferroelectric mode in SnTe indicated that it should not be too difficult to observe the soft mode in an alloy crystal of (Ge, Sn)Te and this was the proposed experiment. The research did not achieve any positive results, but the results which were obtained are recorded in this appendix.

In the next section is a description of the attempts to grow a single crystal and in the following sections the neutron inelastic scattering experiments on the commercially obtained crystals are described and discussed.

A2.2 Preparative experiments

It was planned to prepare single crystal specimens of composition $Ge_{0.2}\ Sn_{0.8}\ Te$ from the elements. The material was obtained from Koch-Light Laboratories. The furnace in which the crystals were to be grown was designed for use up to 1000°C. It had a 13 cm. long cylindrical filament arranged to allow the vertical Bridgman technique to be used to grow single crystals. The sample could be lowered at rates down to 1 mm. per hour. The capsules in which the crystals were

to be grown were cylinders of fused silica, 1.8 cm. internal diameter and 1.4 cm. in length, topped by a tube to allow the introduction of the elements. For nucleation of the crystal a sealed extension was attached to the bottom of the cylinder by a narrow neck so that growth of only one crystal would proceed. The equilibrium diagram for (Ge, Sn)Te (Abrikosov et al., 1958) indicated that a homogeneous crystal would be difficult to produce because of the large temperature differences between the liquidus and solidus curves. The crystal formed in a Bridgman experiment, in which a volume of melt is cooled slowly from one end, would have a lower concentration of Ge near the nucleation end. In a crystal pulled from a large volume of melt (Czokralski technique) this imperfection would not be as great.

Three experiments were performed, in each of which a total of 20g. of the elements in the desired proportions was added to the capsule. The capsule was then heated, evacuated and sealed. In the first two experiments the material became solid after the preliminary heating, and upon reheating, shattered the capsule. The third experiment was performed with more care. The system was heated with a constant current. The recorded temperature registered both the melting of Sn (232°C) and, at the melting point of Te (450°C), an exothermal reaction, presumably between Sn and Te. After the melting of SnTe (805°C) a highly exothermal reaction on the melting of Ge (937°C) was detected. This final reaction again shattered the capsule. The various

transitions were recognised from the work of Weller (1966) on SnTe and GeTe. In view of the disastrous effects of capsule shattering and as a commercial crystal had been obtained it was decided to discontinue the crystal growth experiments.

An 18g. crystal (called crystal A) was grown by Semi-elements Inc. using the Bridgman technique. The composition was claimed as 20% GeTe. Density measurements showed that it was 24 $\pm$ 2% GeTe. The crystal was a 1.8 cm. diameter 1.2 cm. long cylinder chamfered at one end. The cut surfaces of the crystal indicated that it was not single and this was confirmed by X-ray Laue photographs of these surfaces. The unit cell length was determined using a small chip as 6.24 $\pm$ 0.01 Å in good agreement with the results of Bierly et al. (1963). Elastic neutron diffraction experiments at AERE Harwell were used to determine the mass of each part of the crystal (assuming equal extinction effects) and their mosaic spreads. The crystal was composed of four parts. The integrated intensity of the 220 reflection from each part showed that their masses were 2.4, 4.5, 6.2 and 4.6 g. A stereogram of the orientations of the components showed that the first three parts were similarly oriented, their axes being from 2° to 5° apart. The fourth part was in a totally different orientation, such that, with knowledge of the orientation of the other crystallites, a neutron inelastic scattering experiment could be performed considering this part as the specimen. The mosaic spreads of the crystals were respectively 0.53°, 0.56°, 0.72°, and 0.87°, FWHM

measured against the (111) planes of an unsqueezed germanium monochromator crystal.

An X-ray scattering experiment was performed using a chip from the crystal to try to detect the ferroelectric phase transition in a single crystal. An 800 reflection was observed on an oscillation camera at room temperature and near liquid nitrogen temperature. The low temperature was maintained for short periods by about 2 $cm.^3$ of liquid nitrogen beneath the crystal. The time was long enough to obtain observable intensity on a film by manual oscillation of the crystal so that the desired reciprocal lattice point crossed the sphere of reflection about twenty times. Each reciprocal lattice point could be expected to split into four, corresponding to the reciprocal lattice points from the four rhombohedral lattices derivable by compressing the cubic lattice along each of the four [111] directions. With the crystal mounted about [001] on an oscillation camera the spot from to the 800 reflection would be expected to split into two spots with the same Bragg angle. These two spots were observed and it was shown that they became one spot above the transition point indicating that the transition is reversible and that at least a small crystal does not shatter at the transition. The order of the transition however could not be determined as this would require better temperature control.

A second crystal (B) whose composition was claimed as 30% GeTe,

weighing 7g. and grown by the Czokralski technique was supplied by Dr. I. Lefkowitz. The unit cell dimension, using the data of Bierly et al. (1963) was 6.23 Å. The crystal was approximately cylindrical, 3 cm. long and 0.8 cm. in diameter. X-ray Laue photographs of the uncut surfaces of crystal B indicated that it was not a single crystal. This is not a reliable conclusion as the X-rays may not have penetrated the amorphous surface due to the large absorption cross-section in this material. A neutron elastic scattering experiment showed that the crystal was single and that its mosaic spread was 1.1° FWHM measured against the (111) planes of an aluminium monochromator of unknown mosaic spread. This crystal could therefore also be used in a neutron inelastic scattering experiment.

A2.3 Neutron inelastic scattering experiments

It was anticipated that the experiments would not be easy due both to the small mass of the crystals and to their mosaic spreads and non-uniform nature.

The experiments with both crystals at room temperature were carried out on the triple axis spectrometers at the C4 and C5 facilities of the NRU reactor at Chalk River. The method of operation of the C5 spectrometer is discussed in chapter 2. The C4 spectrometer differs from the C5 spectrometer in its design and requires a different method of operation. It was constructed with a fixed $2\theta_M$ (54°) so that E_o and $\underline{k}_o$ are fixed.

The spectrometer may be used in both the constant $\underline{Q}$ and constant energy modes of operation.

The resolution of the C4 spectrometer was chosen with the (111) planes of an aluminium monochromator crystal and the (111) planes of a squeezed germanium analyser crystal. The collimations α_1 and α_2 (see table 2.2) were 0.7°. The resultant width of the vanadium scattering was 1.8° in $2\theta_M$ or 0.4 THz FWHM at $2\theta_A$ of 37.8°. The resolution of the C5 spectrometer was chosen with the same collimation and crystals described in chapter 2 with $2\theta_A$ of 43°. The vanadium scattering was then 0.26 THz FWHM.

The $(1\bar{1}0)$ plane was the scattering plane for all the experiments. This plane contains the three principal symmetry directions [001], [110] and [111] of the f.c.c. lattice. The reciprocal lattice points in the body centred reciprocal cell have Miller indexes all even or all odd. The one phonon structure factor shows that long wavelength optical branches are best observed near odd points and acoustic branches near even points. Previous experiments on SnTe had demonstrated the effects of focussing and were used to indicate the regions of strongest scattering (Pawley, G.S., private communication). One complication was that the almost equal scattering lengths of Sn and Te produced very weak scattering around optic reciprocal lattice points. An effective null matrix could not be formed, however, as the addition of Ge increases the difference in

scattering lengths. (Ge, Sn, Te, b = 0.84, 0.61, 0.56 x 10^{-12}cm. (8.4 etc. fm.)). Experiments were not performed at wave vectors $\underline{q}$ along the 111 direction in reciprocal space.

The experiment on the C4 spectrometer using crystal B showed the TA branches in the [001] and [110] directions from the zone centre to reduced wave vectors of 0.5 and 0.3 respectively. The $[1\bar{1}0]$ polarised transverse phonons propagating in the [110] direction cannot be seen in the $(1\bar{1}0)$ scattering plane. The [110] transverse modes seen are therefore polarised in the [001] direction. The TO branch whose detection was the object of the experiment was not seen in any direction.

In crystal A the TA branches in the [001] and [110] directions were again observed and there were indications of a TO branch in the [110] direction at approximately the same energies as the room temperature TO branch in SnTe (Cowley et al., 1968).

The experiments on C5 were performed in order to make use of the higher flux of this facility to find the TO branches. Two very poor neutron groups were seen from crystal B at approximately the expected frequencies. They were not, however, regarded as significant observations. The experiments on crystal A were only slightly more successful. The [001] TA branch was observed at wave vectors out to the zone boundary and some badly defined neutron groups approximately 1THz wide were observed at frequencies 0.2 THz less than the [001] TO

branch in SnTe. These results together with those from the C4 spectrometer are shown uncorrected in figure A2.1.

A2.4 Discussion

It could be claimed that the TA branches were seen in the crystals. It is probable that the higher frequency branch seen in crystal A was the TO branch, but its weakness and width, due in part to the crystal size, mosaic spread and uniformity, indicated that it would be studied better in a good crystal.

It is possible that in crystal B (30% GeTe) the TO branch at room temperature had a very low frequency at long wavelengths because of its composition. This fact combined with the nature of the crystal and the proximity of the acoustic branches may have made the TO branch difficult to find. Apart from these points there was a considerable amount of incoherent background scattering from the crystal. This scattering arises from the disordered array of Ge and Sn atoms. An experiment at higher temperatures may have yielded a resolved TO mode, but it was decided to discontinue the experiments.

Lefkowitz et al. (1969) were also restricted to poor crystals and their experiments gave no strong evidence for a TO branch. The temperature dependence of a Bragg reflection in the 15% GeTe alloy, however, indicated that a transition did occur.

Apart from their ferroelectric nature (Ge, Sn)Te crystals are interesting to study experimentally as disordered crystals. For a dilute alloy, perturbation theory led Cowley et al. (1968) to conclude that a localised mode would not occur in (Ge, Sn)Te. For a 33% GeTe alloy, however, calculations on a disordered linear chain model of (Ge, Sn)Te (J. K. Darby, private communication) showed that broadened and shifted SnTe and GeTe like modes would be observed, especially for long wavelength optic modes. The broadening of the possible TO mode in the above experiments is more likely due to the non-uniform nature of the crystal. The interesting effects of disorder would also be studied better in good (Ge, Sn)Te crystals.

Figure A2.1

Experimental results for (Ge, Sn)Te

The solid lines are from the experiments on SnTe (Cowley et al., 1968). The neutron groups were particularly poor in some cases giving large estimated errors.

(Ge Sn)Te

Crystal A X
Crystal B O

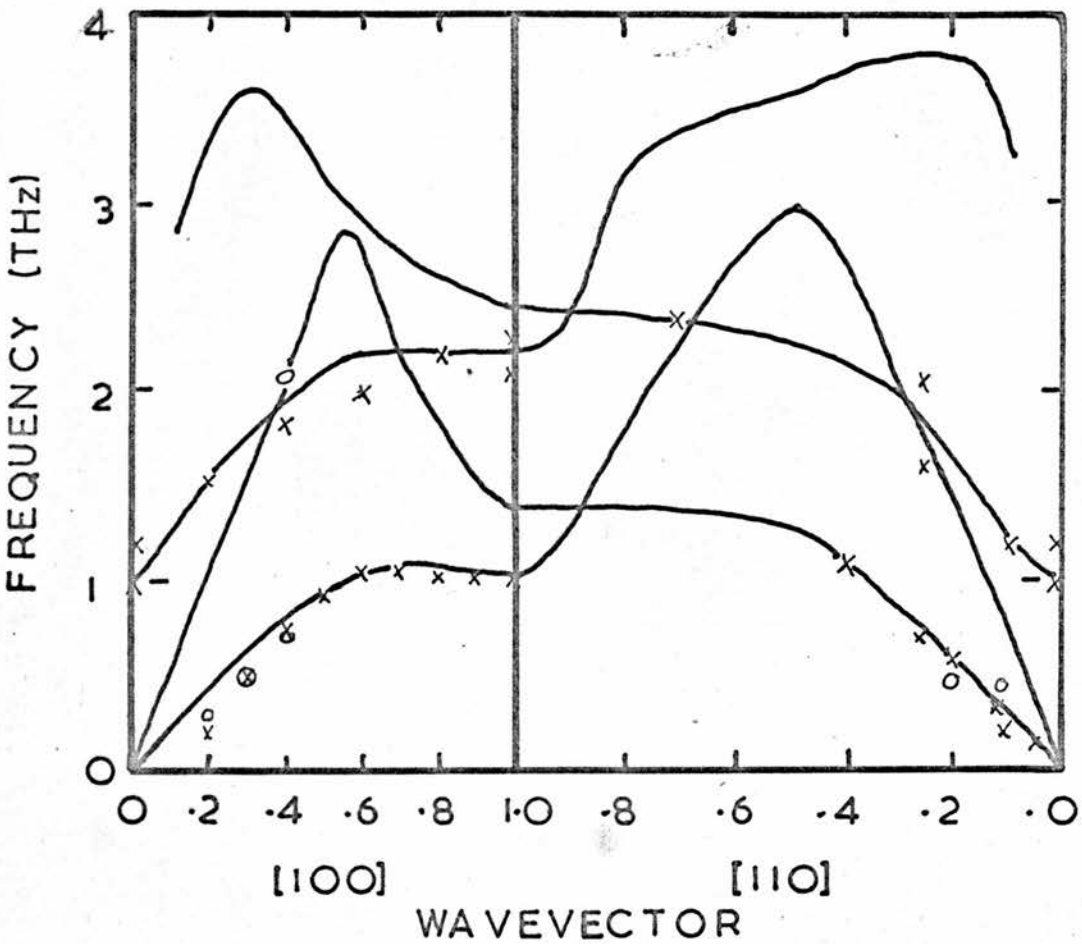

References

Abrikosov, N. Kh., Vasserman, A.M. and Poretskaia, L.V., 1958, Doklady Acad. Nauk.SSSR, 123, 279.

Als-Nielsen, J. and Dietrich, O.W., 1967, Phys. Rev., 153, 706, 711.

Bacon, G.E., 1962, Neutron Diffraction, Oxford U.P., London.

Bacon, G.E. and Pease, R.S., 1953, Proc. Roy. Soc., A220, 397.

Bacon, G.E. and Pease, R.S., 1955, Proc. Roy. Soc., A230, 359.

Baker, A.N., 1956, J. Chem. Phys., 25, 381.

Bantle, W., 1942, Helv. Phys. Acta, 15, 373.

Barker, A.S. and Tinkham, M., 1963, Phys. Rev., 38, 2257.

Bierly, J.N., Muldawer, L. and Beckman, O., 1963, Acta Met., 11, 447.

Bjorkstam, J.L., 1967, Phys. Rev., 153, 599.

Blinc, R., 1960, J. Phys. Chem. Solids, 13, 204.

Blinc, R., Cevc, P. and Schara, M., 1967, Phys. Rev., 159, 411.

Blinc, R., Dimic, V., Petkovsek, J. and Pirkmajer, E., 1967, Phys. Lett., 26A, 8.

Blinc, R. and Hadzi, D., 1958, Mol. Phys., 1, 391.

Blinc, R. and Ribaric, M., 1963, Phys. Rev., 130, 1816.

Blinc, R. and Svetina, S., 1965, Phys. Lett., 15, 119.

Blinc, R. and Svetina, S., 1966, Phys. Rev., 147, 423, 430.

Born, M. and Huang, K., 1954, Dynamical Theory of Crystal Lattices, Clarendon, Oxford.

Brockhouse, B.N., 1961, in Inelastic Scattering of Neutrons in Solids and Liquids, IAEA, Vienna, p. 113.

Brody, E.M. and Cummins, H.Z., 1968, Phys. Rev. Lett., 21, 1263.

Brout, R., 1965, Phase Transitions, Benjamin, N.Y.

Brout, R., Muller, K.A. and Thomas, H., 1966, Sol. State Comm., 4, 507.

Cochran, W., 1960, Adv. Phys., 9, 387.

Cochran, W., 1961, Adv. Phys., 10, 401.

Cochran, W., 1968, Neutron Inelastic Scattering, Vol. 1, I.A.E.A., Vienna, 275.

Cochran, W., 1969, to be published, Adv. Phys.

Cochran, W. and Cowley, R.A., 1967, Handbuch der Physik., 35/2a, 59.

Cooper, M.J. and Nathans, R., 1967, Acta Cryst., 23, 357.

Cowley, E.R., Darby, J.K. and Pawley, G.S., 1969, to be published.

Cowley, R.A., 1964, Phys. Rev. 134, A981.

de Gennes, P.G., 1963, Sol. State Comm., 1, 132.

Elliott, R.J. and Thorpe, M.F., 1967, Proc. Phys. Soc., 91, 903.

Errey, J.R., 1968, Phys. Rev., 174, 568.

Evrard, R., 1962, Bull. Soc. Roy. Sci. Liege, 31, 290.

Grindlay, J. and ter Haar, D., 1959, Proc. Roy. Soc., 250, 266.

Hill, R.M. and Ichiki, S.K., 1963, Phys. Rev., 130, 150.

Imry, Y., Pelah, I., Wiener (Avnear), E., and Zafrir, H., 1967, Sol. State Comm., 5, 41.

Imry, Y., Pelah, I. and Wiener, E., 1965, J. Chem. Phys. 43, 2332.

International Tables for X-ray Crystallography, Vol. 1, (1965), Kynoch Press, Birmingham.

Jona, F. and Shirane, G., 1962, Ferroelectric Crystals, Pergamon Press Inc., London.

Kaminow, I.P., 1965, Phys. Rev., 138, A1539.

Kaminow, I.P., and Damen, T.C., 1968, Phys. Rev. Lett., 20, 1105.

Kobayashi, K.K., 1968, J. Phys. Soc. Jap., 24, 497.

Kubo, R., 1966, Rep. Prog. Phys., 29, 255.

Lazarev, A.N., and Zaitseva, A.S., 1961, Soviet Physics - Solid State, 2, 2688.

Lefkowitz, I., Shields, M., Dolling, G., Buyers, W.J.L. and Cowley, R.A., 1969, to be published.

Lehman, G.W., Wolfram, T. and de Wames, R.E., 1962, Phys. Rev., 128, 1593.

Martin, D.H. and Stone, C.D., 1963, Phys. Lett., 5, 26.

Matsubara, T. and Yoshimitsu, K., 1967, Prog. Theor. Phys., 37, 634.

Matsudaira, N., 1968, J. Phys. Soc. Jap., 25, 1225.

Megaw, H.D., 1957, Ferroelectricity in Crystals, Methuen, London.

Meister, H., Skalyo, J., Fraser, B.C. and Shirane, G., 1969, to be published.

Montgomery, H., 1969, Proc. Roy. Soc., A.309, 521.

Novakovic, L., 1966, J. Phys. Chem. Solids, 27, 1469.

Novakovic, L., 1967, Bull. Boris Kidric Inst. Nuclear Sciences, 18, 23.

Paul, G.L., Cochran, W., Buyers, W.J.L. and Cowley, R.A., 1969,

to be published.

Pawley, G.S., Cochran, W., Cowley, R.A. and Dolling, G., 1966, Phys. Rev. Letts., 17, 753.

Pirenne, J., 1949, Physica, 15, 1019.

Pirenne, J., 1955, Physica, 21, 219.

Plesser, Th. and Stiller, H., 1968, to be published.

Powell, B.M., 1968, in Neutron Inelastic Scattering, Vol. II, I.A.E.A., Vienna, p. 185 and private communication.

Reese, W. and May, L.F., 1967, Phys. Rev., 162, 510.

Reese, W. and May, L.F., 1968, Phys. Rev., 167, 504.

Samara, G.A., 1967, Phys. Lett., 25A, 664.

Schenk, Ch., Wiener, E., Weckermann, B. and Kley, W., 1968, Phys. Rev., 172, 576.

Schmidt, V.H. and Uehling, E.A., 1962, Phys. Rev., 126, 447.

Senko, M.E., 1961, Phys. Rev., 121, 1599.

Shur, M.S., 1966, Soviet Physics - Crystallography, 11, 394 (translation).

Shuvalov, L.A. and Mnatsakanyan, A.V., 1966, Soviet Physics - Crystallography, 11, 210.

Silsbee, H.B., Uehling, E.A. and Schmidt, V.H., 1964, Phys. Rev., 133, A165.

Slater, J.C., 1941, J. Chem. Phys., 9, 16.

Sliker, T.R. and Burlage, S.R., 1963, J. Appl. Phys., 34, 1837.

Stekhanov, A.I. and Popova, E.A., 1966, Soviet Physics - Solid State,

7, 2849.

Suzuki, M. and Kubo, R., 1968, J. Phys. Soc. Japan, 24, 51.

Takagi, Y., 1948, J. Phys. Soc. Jap., 3, 271.

Tenzer, L., Fraser, B.C. and Pepinsky, R., 1958, Acta Cryst. 11, 505.

Tokunaga, M., 1966, Prog. Theor. Phys., 36, 857.

Tokunaga, M. and Matsubara, T., 1966, Prog. Theor. Phys., 35, 581.

Umebayashi, H., Fraser, B.C., Shirane, G. and Daniels, W.B., 1967, Sol. State Comm., 5, 591.

Villain, J. and Stamenkovic, S., 1966, Phys. Stat. Sol., 15, 585.

Weller, 1966, J. Electrochem. Soc. 113, 90.

West, J., 1930, Z. Krist. 74, 306.

Yamada, Y., Fujii, Y. and Hatta, I., 1968, J. Phys. Soc. Jap., 24, 1053.

Yamada, Y. and Yamada, T., 1966, J. Phys. Soc. Jap., 21, 2167.

Addendum

Litov, E. and Uehling, E.A., 1968, Phys. Rev. Lett., 21, 809.